Interrogating the molecular mechanisms of breast cancer metastasis: the contributions of RhoC GTPase and p38γ MAPK

by

Devin Thomas Rosenthal

A dissertation submitted in partial fulfillment
of the requirements for the degree of
Doctor of Philosophy
(Cellular and Molecular Biology)
in The University of Michigan
2011

Doctoral Committee:

Professor Sofia D. Merajver, Chair
Professor Eric R. Fearon
Professor Benjamin L. Margolis
Associate Professor Gary D. Hammer
Associate Professor Celina G. Kleer

Acknowledgments

First and foremost I would like to thank my mentor, Sofia Merajver, for her sense of adventure in being willing to take a chance on a mid-semester transfer student; for her encouragement for me to discover and explore my scientific curiosity; for the countless travel opportunities; for her insight, direction, and guidance; and for her patience in allowing me to take months to realize and conclude on my own things that she had told me months before. For all of this and more I am eternally indebted and grateful.

I am thankful for the experiences I have had the opportunity to share with everyone who has passed through the Merajver lab, but there are several people that I must acknowledge separately. I owe an enormous debt of gratitude to Zhifen Wu and Liwei Bao for all of the experiments they have performed for me – if I am earning a PhD then they each deserve one as well. They have taught me everything I know about experimental design, troubleshooting, Chinese (xiexie), and what a proper lunch should be. Even if I spent another 50 years in graduate school I would still be learning from them. Thank you to my fellow graduate students Lauren van Wassenhove and Michelle Wynn for their friendship, gossip, baking, and camaraderie. Thank you to Silvia Escudero for all of her help with the p38γ project, for her patience with my continual evolution as a mentor, and for all

the lessons she taught me as I taught her. Thank you also to Lian Zhu for her help with the breast cancer stem cell project and for the book recommendations. And thank you to Jie Zhang for laying the groundwork for the breast cancer stem cell project.

I thank all the members of my dissertation committee for their advice, guidance, and assistance throughout my graduate career and postdoctoral applications. I would especially like to thank Gary Hammer for all of his advising, which began even before I transferred to the University of Michigan, and for his contagious enthusiasm and passion. I would like to thank Celina Kleer for teaching me how to read normal and cancer breast tissue under the microscope, and for all of the help on our numerous collaborations. I also would like to thank Jessica Schwartz for the opportunity to become part of the CMB Program, and for the chance to have an active role within it.

I would like to thank my parents, Scott and Susan Rosenthal, for their unwavering love and support from day one, for growing with me as cancer biologists, and for their infinite patience and understanding when I would disappear beneath my work for long periods of time. I would also like to thank my brothers, Ethan and Benjamin Rosenthal, for always being the successes that I try to measure up to, and for never hesitating to let me know if I am becoming too much of a "square".

Table of Contents

List of Figures

Figure

List of Tables

Table

ABSTRACT

Interrogating the molecular mechanisms of breast cancer metastasis: the contributions of RhoC GTPase and p38γ MAPK

by

Devin Thomas Rosenthal

Chair: Sofia D. Merajver

Breast cancer lethality is primarily due to cancer cell metastasis away from the primary tumor to vital organs. Understanding and targeting the molecular mechanisms contributing to metastasis is therefore essential to combating the disease. Here we focus on two main mechanisms by which molecules contribute to metastasis—as either metastatic initiators (genes that can catalyze the shift from tumorigenic to metastatic) or metastatic perpetuators (genes that maintain, but cannot independently initiate, the metastatic state).

We discovered that RhoC GTPase is both necessary and sufficient for breast cancer stem cell metastasis. Surprisingly, RhoC was capable of initiating metastasis independent of primary tumor formation, which attests to its strength as a metastatic initiator. In addition to governing breast cancer stem cell metastatic potential, we also found that RhoC affects the abundance of breast

cancer stem cells within a population. Together these data establish RhoC as the first identified initiator of breast cancer stem cell metastasis.

In separate studies, we discovered that p38γ MAPK perpetuates breast cancer metastasis and specifically impacts the mesenchymal-like behaviors of aggressive breast cancer cells. Interestingly, we found that p38γ is connected to RhoC, as changes in p38γ expression concurrently alter RhoC expression by affecting RhoC ubiquitination and lysosomal degradation. These findings are clinically relevant, as high p38γ expression was associated with both the basal-like breast cancer subtype as well as poorer overall patient survival.

Using computational modeling alongside cell biology we revealed that p38γ modulates cell motility by regulating actin stress fiber organization. In doing so we also discovered a novel physical behavior of motile cells—leading edge protrusion oscillations—which we verified both experimentally and computationally. Through *in silico* modeling we were able to deduce a likely sequence of events leading from p38γ knockdown to the observed motility phenotype.

Taken together, this body of work defines a new subset of breast cancer stem cells that act as metastatic initiators—metastatic breast cancer stem cells, driven by RhoC expression—and characterizes a novel metastatic perpetuator in p38γ.

This work opens many new research avenues which we discuss and elaborate on through several proposed directions for future investigation.

Chapter I

Introduction

The normal mammary gland undergoes dramatic remodeling throughout a woman's life: invasive expansion through adipose tissue during puberty, widespread proliferation of lobules during pregnancy, and subsequent apoptosis during involution. Precise temporal and spatial control of these processes is essential for proper growth and development of the mammary gland. Deviation from this developmental blueprint leads to aberrant breast epithelial cell growth—which may be the beginnings of breast cancer.

Breast cancer presents as a dysplastic disease of mammary epithelial cells, which can grow abnormally for years yet remain confined within mammary ducts or lobules. Confinement of malignant epithelial cells within the ductolobular network is an important barrier to breast cancer progression. As long as malignant cells remain contained within the ducts or lobules, patient survival remains relatively high; approximately 98% of patients diagnosed with localized breast cancer will not suffer from cancer recurrence within 5 years (1).

Breast cancer prognosis dramatically worsens once cells invade out of the ductolobular network and into the surrounding stroma. The 5-year probability of

survival for regionally invasive breast cancer (breast cancer that has spread to regional lymph nodes) is only 83%—a 15% decrease from localized breast cancer (1). After exiting the ducts or lobules, cancer cells can metastasize via the blood or lymphatic systems to distant organs such as the lungs, liver, or bones. The presence of distant metastases at the time of diagnosis carries the worst prognosis: a mere 23% of patients will survive 5 years post-diagnosis (1). Targeting this final, lethal stage of breast cancer progression is therefore paramount for improving patient outcome.

*   *   *

The metastatic process begins with malignant epithelial cells breaking through the myoepithelial cell and basement membrane layers that enclose the ducts and lobules. Although the specifics of the interactions between breast carcinoma and myoepithelial cells during breast cancer progression remains poorly understood (2, 3), the overall effect is clear: once carcinoma cells traverse the myoepithelial cell barrier, patient outcome worsens (2).

In addition to crossing the myoepithelial cell barrier, a metastasizing cell must also break through the proteinaceous basement membrane enveloping the mammary ductolobular network. In the mammary gland, the basement membrane is primarily composed of collagens, laminins, and heparin sulfate proteoglycans that are secreted by the myoepithelial cells (4). The pores formed

by these matrix proteins are too small for cells to fit through; therefore, metastasizing cells must cleave these protein fibers in order to traverse the basement membrane. This is accomplished by expressing and secreting proteases, such as MMP-2, -9, and -14, which degrade the basement membrane and allow the metastasizing cell to pass through and enter the adipose-rich breast stroma (5).

Details of the steps in metastatic progression between initial escape from the primary tumor and colonization of a distant metastatic site are currently poorly understood. In general, after escaping from the mammary ducts or lobules, the metastasizing cell follows chemotactic signals from the blood or lymphatic system to locate vessels (6). Upon reaching the vasculature, the metastasizing cell enters the blood or lymphatic system by the process of intravasation (6, 7).

Early reports revealed clinically relevant links between the numbers of circulating tumor cells and patient survival (8-10), however little is known about the actual behavior of cancer cells in circulation. Metastatic circulating breast cancer most commonly manifests clinically in the bone, brain, lungs, and liver. Upon reaching one of these sites, a successful metastasizing breast cancer cell exits the vasculature through the process of extravasation. Once it has entered the metastatic site, the metastasizing cell shifts its cellular program from the invasive, motile behavior that allowed it to escape the confines of the primary tumor back

to a stationary, proliferative profile that enables it to colonize its new environment.

A similar plasticity in behavior occurs during normal development through a process known as the epithelial-mesenchymal transition (EMT). The EMT is a hallmark of normal developmental processes, such as mesoderm formation during gastrulation and wound healing. As the name implies, the EMT involves epithelial cells acquiring properties characteristic of mesenchymal cells—namely cell differentiation markers such as vimentin intermediate filaments, a shift from stationary to motile and invasive, and an accompanying change in cell shape from rounded to elongated (11). The EMT is reversible through a process known as mesenchymal-to-epithelial transition (MET), and epithelial cells that undergo an EMT may undergo a MET upon completion of their designated task (11, 12).

Cancer cells appear to harness the EMT to facilitate local invasion and ultimately metastasis (11, 13, 14); for example, cells at the invasive front of a tumor express mesenchymal markers, such as vimentin and smooth muscle actin. Accordingly, master regulators of the EMT, such as Twist, have been shown to induce breast cancer metastasis (15). Inhibition of twist specifically prevents breast cancer metastasis, while ectopic expression in non-tumorigenic mammary epithelial cells induces an EMT and increases cell motility. As expected based on the association between mesenchymal differentiation and metastatic properties,

the most aggressive breast cancer molecular subtypes are those that are the most mesenchymal-, or basal-, like (16).

Recently, the potential contribution of EMT to cancer has been shown to have some possible relation to cancer stem cells. The cancer stem cell hypothesis postulates that many cancers are maintained by a small population of variably pluripotent cells within the tumor, termed cancer stem cells (CSCs), which possess unlimited replication potential as well as the ability to self renew. The CSC hypothesis further postulates that cancers are hierarchically organized, with CSCs residing at the top of the hierarchy. Pioneering work by Michael Clarke and Max Wicha demonstrated that breast CSCs (BCSCs) can be identified by specific cell surface markers or enzymatic activity (17, 18) and that the BCSC population is the tumorigenic population in xenografted mice. Recent work has also suggested that CSCs may be resistant to conventional therapies (19); therefore, standard chemotherapy may eliminate the bulk population of non-CSCs but leave behind the minority CSC population, which is then capable of repopulating the tumor. Taken together, these properties of CSCs have led researchers to hypothesize that BCSCs drive breast cancer and are the major cause of cancer recurrence (20).

Elegant work by Mani *et al.* uncovered a link between EMT and CSCs (21). The group demonstrated that inducing EMT in human mammary epithelial cells (HMECs) causes these cells to express stem cell markers and behave like stem

cells. Inducing EMT in transformed HMECs generates CSCs and increases transformed HMEC tumorigenicity. They also discovered that breast stem cells and CSCs express EMT markers, suggesting that EMT may play a contributing role in the CSC phenotype. This convergence of concepts—CSCs in tumor growth, EMT in cancer metastasis, and the interrelatedness of the two—opens the possibility that CSCs, like EMT, are involved in cancer metastasis.

Early work on CSCs and metastasis uncovered circumstantial links, such as the connection between CSCs and EMT reported by Mani et al. (21), and prior work identifying an invasiveness gene signature in the BCSC population that predicted shorter metastasis-free survival (22). Recent studies have provided stronger correlative evidence linking CSCs and metastasis. Liu et al. revealed that the relative abundance of BCSCs is increased in spontaneous breast cancer metastases in an orthotopic xenograft model (23), and Charafe-Jauffret et al. found that BCSCs mediate metastasis of the most aggressive subset of breast cancer, inflammatory breast cancer (IBC) (24). In line with these studies, subpopulations within the CSC population, delineated by specific surface marker expression, have been identified that are required for metastasis of several types of cancer (25, 26). This correlative evidence provides solid support for CSCs functioning in metastasis, however to date there is no functional molecular link between BCSCs and metastasis.

*　　　*　　　*

Understanding the switch from tumorigenesis to metastasis—and subsequently elucidating the genes that empower metastatic cells—is fundamental to controlling breast cancer. The body of work presented here interrogates breast cancer metastasis by focusing on two essential questions: which genes cause a cell to metastasize, and which genes contribute to the metastatic properties of a metastasizing cell?

The distinction between these two questions is subtle, yet highly pertinent. From tumor inception a cancer cell functions as a proliferative machine; multiplying within the tissue of origin, resistant to normal growth-inhibitory signals. By contrast, a metastasizing cell is programmed for movement; escape from the primary tumor, travel through the vasculature to distant organs, and ultimately colonization of a new environment. Certain genes drive the fundamental behaviors associated with each of these cell programs, yet most of these genes alone are not sufficient to induce a programmatic switch—from tumorigenesis to metastasis, or vice versa.

Viewing metastasis from this perspective reveals two principle points for therapeutic intervention: either preventing metastasis by targeting the transition from tumorigenesis to metastasis, or impairing the progress of already metastatic cells. Each of these approaches holds potential, but each is important for a different clinical course. Take, for example, two hypothetical breast cancer cases:

Case 1: A 32 year-old woman presents with DCIS with microinvasion and 2/40 positive lymph nodes. She is treated with aggressive chemotherapy and hormonal therapy, which causes her tumor to regress. Shortly after ending therapy, however, her tumor recurs, spreads to 12/40 lymph nodes, and metastasizes to her lungs.

Case 2: A 42 year-old woman presents with widely invasive, metastatic triple-negative breast cancer and 10/40 positive lymph nodes.

In Case 1, the patient presents with locally invasive breast cancer—aggressive cancer, but not yet fully metastatic. Treatment with chemotherapy and hormonal therapy successfully eliminates the disease in the short term; however, the cancer later recurs as highly metastatic, aggressive breast cancer.

Case 1 is an example of a patient that would benefit from targeting the transition from tumorigenesis to metastasis. Although her cancer is locally invasive, the cells have not yet become fully metastatic. While the majority of the patient's tumor was eliminated by the combination of chemotherapy and hormonal therapy, a few cancer cells likely resisted treatment and remained dormant in her breast. Once these cells became active again they switched programs, from tumorigenic to metastatic, and disseminated throughout her body. Such a case is consistent with the CSC hypothesis (accounting for the few resistant cancer cells

capable of regenerating the disease), and the concept of a switch between tumorigenic and metastatic CSCs.

In Case 2, the patient presents with metastatic breast cancer. These cancer cells have already undergone the transition from tumorigenic to metastatic, so preventing this transition would minimally benefit the patient. Case 2 is an example of a patient that would benefit from impairing the progress of already metastatic cells. By elucidating and targeting the molecular perpetuators of these already metastatic breast cancer cells, the clinician could hope to restrict the metastatic, and ultimately lethal, spread of the patient's tumor—thus opening the possibility of surgical or chemotherapeutic intervention to effectively combat the disease.

*   *   *

Referring to our earlier description of the metastatic process, there is one property of metastasizing cells that persists throughout most stages of metastatic progression: cell motility. Mammary epithelial cells in the developing mammary gland are sessile, save for invasive outgrowth during puberty. The same holds true in a primary tumor, as cell energy is instead directed towards rapid and uncontrolled proliferation. Although many other abilities are needed for a cell to metastasize (invasion to traverse the basement membrane, anchorage-independent growth to survive in the circulation, and so forth), all stages of

metastatic progression, save for final colonization, require a stationary cell to acquire the ability to move.

Such a transition between stationary and motile occurs throughout development by the aforementioned EMT—the same process involved in breast cancer progression. In agreement with their having undergone an EMT, metastasizing breast cancer cells are able to rapidly move through diverse stroma and tissues using a mesenchymal-like mode of motility.

Mesenchymal cell motility is broadly characterized by repeated cycles of contractile-based motion. The process can be broken into four key phases: 1) leading edge protrusion leading to cell elongation, 2) formation of focal adhesions at the leading edge, 3) initiation of actomyosin contraction, and 4) dissolution of focal adhesions at the trailing edge, resulting in retraction of the trailing edge and rapid whole cell movement. It is interesting to note the parallels between mesenchymal motility and muscle contraction; namely, the use of actomyosin-based contractility to generate productive movement, whether of a muscle or a cell. We will return to and elaborate on this point later in the chapter, as this fundamental similarity serves as the basis for our hypothesis regarding breast cancer metastasis in chapters 3 and 4.

The four-step motility cycle outlined above repeats cyclically to generate productive, directed cell movement. Because of its cyclic nature, any step of this

cycle could be designated the initial step; for the purpose of the data to be presented here we will begin with leading edge protrusion. Below we elaborate on each phase of motion:

Leading edge protrusion and focal adhesion formation

Forward protrusion of a cell's leading edge is driven by actin polymerization in the form of either lamellipodial or pseudopodial structures. Underlying both structures is the requisite of focal adhesions anchored to the extracellular substratum. For reference, these components, as well as many of their regulatory proteins, are outlined in Figure 1.1. Once bound to the substratum, the immobilized focal adhesions bind and anchor existing actin filaments, providing a stable foundation against which polymerizing actin filaments are able to generate protrusive force (Figure 1.2). Conversely, detachment of focal adhesions from either the actin filaments or the substrate permits leading edge retraction by retrograde flow (Figure 1.2).

In general, cells will first extend small, finger-like pseudopodial protrusions, termed filopodia, to probe the surrounding environment. Filopodia are composed of parallel actin filaments tightly bundled together, with the barbed ends (the ends onto which actin monomers can be added) of the filaments facing towards the cell membrane (27). Filopodia are responsible for detecting chemo- and mechanotactic environmental cues and for forming focal adhesions, and thus guide cell movement in a given direction (27, 28).

The lamellipodium, by contrast, is composed of a thin, branched actin meshwork that, along with the lamella, generates protrusion across the entire leading edge of a cell (29, 30). Despite this morphologic difference, the underlying mechanism of protrusion remains the same; actin polymerization against focal adhesions generates protrusions, while retrograde flow permits retraction (31).

Focal adhesion composition

As described in the previous section, focal adhesion formation is essential for cell movement. Focal adhesions are the physical and biochemical links between the cell and its environment. They are large, macromolecular structures composed of up to 100 different proteins, depending on the nature of the focal adhesion (32). In general, though, focal adhesions consist of three principle components: integrins, adaptor proteins, and intracellular signaling proteins.

Integrins are heterodimeric transmembrane proteins that bind to the extracellular matrix, linking it to the intracellular environment (33). There are many different forms of integrins, each of which is specific for a particular extracellular matrix component (i.e. fibronectin, collagen, and others). Adaptor proteins, such as talin and vinculin, bind to the intracellular domain of an integrin and link it to the cytoskeleton. The integrin-adaptor protein-cytoskeleton complex then recruits and binds to various intracellular signaling proteins, such as focal adhesion kinase, which activate an array of signaling pathways within the cell (34).

Actomyosin contraction and focal adhesion dissolution

Once the leading edge of a cell has been extended by actin protrusion and anchored by the formation of new focal adhesions, the trailing edge of the cell must detach and retract in order for the cell to complete its movement. Myosin contained within the stress fibers generates the contractile forces that initiate this process. The contraction mechanism functions similarly to the protrusion mechanism in that actomyosin contractile force is generated by pulling (rather than pushing, in the case of protrusion) against stable focal adhesions at the leading and trailing regions of the cell (31).

Detachment of focal adhesions at the trailing edge can occur by one of two mechanisms. Trailing edge focal adhesions can be dissolved by releasing their attachment to the microenvironment, uncoupling from the cytoskeleton, and ultimately being broken down within the cell into their component proteins (35, 36). Alternatively, in some cell types integrins permanently adhere to the substratum; therefore they instead detach from the cytoskeleton and are ultimately left behind, adhered to the substratum, as the cell moves on (37, 38).

*   *   *

These phases of cell motility are regulated at many levels by hundreds of different proteins (39, 40); however, the majority of these processes are

regulated by members the <u>Ra</u>s <u>ho</u>mologous (Rho) protein family. Rho family GTPases comprise the largest subfamily cluster of the Ras-homology superfamily of small GTPases (~21 kDa). Currently, 22 Rho family entries are annotated in the ENTREZ database, which can be divided into 10 different groups on the basis of their sequence homology to either Cdc42, Rac1, RhoA, RhoD, Rif/RhoF, Rnd3/RhoE, TTF/RhoH, Chp/RhoV or RhoBTB.

Like most Ras homology proteins, Rho GTPases function as molecular switches – GTP-bound Rho proteins are active, GDP bound Rho proteins are inactive. Thus, Rho-GTP binds and activates downstream effectors leading to a variety of signaling cascades, while Rho-GDP does not.

Cycling between GTP- and GDP-bound states is tightly controlled by three different classes of Rho regulatory proteins: GTPase-activating proteins (GAPs), guanine nucleotide dissociation inhibitors (GDIs), and guanine nucleotide exchange factors (GEFs). GAPs and GDIs inhibit Rho activity - GAPs by accelerating Rho protein hydrolysis of GTP into GDP, and GDIs by sequestering Rho proteins to the cytoplasm and blocking GDP dissociation – while GEFs activate Rho proteins by triggering the release of GDP from Rho-GDP, thereby permitting the Rho protein to bind GTP.

The activation of Rho-family proteins is mediated through a wide array of mechanisms including interactions with G-protein-coupled receptors (GPCRs)

14

and other cell surface receptors, such as cytokine, tyrosine kinase, and adhesion receptors. Once initiated, Rho signaling leads to the activation of several different pathways depending on the precursor signal, the cellular context, and the crosstalk with other activated or repressed pathways. In fact, when Rho-family proteins were first brought into the limelight following landmark publications by Ridley, Hall, and their coworkers in 1992, the number of publications on the diversity of functions of Rho proteins rose exponentially (41, 42). In these papers, Ridley and Hall related the assembly of focal adhesions and actin stress fibers to growth factor signaling through Rho GTPase. Since then, Rho proteins have also been shown to play roles in adhesion, migration, phagocytosis, cytokinesis, neurite extension and retraction, cell morphogenesis and polarization, growth and cell survival (43-46). Additionally, aberrant overexpression of some Rho-family proteins, such as RhoC, has been shown to promote malignant transformation and metastasis.

RhoC is responsible for coordinating cell motility by regulating actomyosin contractility and focal adhesion turnover (40, 47, 48). Although highly homologous to RhoA, RhoC has distinct contributions to cell motility and cancer, such as playing a larger role in stress fiber formation and contraction than RhoA (49). RhoC expression also increases post-EMT and was required for post-EMT motility of colon carcinoma cells, whereas RhoA expression decreased and inhibited post-EMT motility (50).

In cancer, RhoC is a potent metastatic driver of many cancer types (51-54), and RhoC knockout selectively inhibits metastasis—independent from primary tumor formation—in a transgenic breast cancer model (55). In agreement with these previous findings, unpublished data from our lab suggests that RhoC overexpression also affects breast cancer metastasis. Specifically, crossing mice expressing mouse mammary tumor virus (MMTV)-driven RhoC in the mammary gland with either of two tumorigenic and metastatic transgenic mouse models— the Her2/neu and polyoma middle-T models—increases the incidence of lung metastasis and the number of metastases present without appreciably affecting tumor incidence or growth (unpublished observations)..

Earlier work from our lab sought to identify signaling pathways involved in mediating RhoC-induced metastatic behavior. This analysis revealed that the p38 mitogen activated protein kinase (MAPK) pathway was involved in RhoC-mediated motility, invasion, and angiogenesis (56).

The MAPK pathway consists of three branches – ERK, JNK, and p38 – which are responsible for integrating extracellular stimuli and translating them into cellular responses by phosphorylating a network of downstream effector proteins (57). The canonical MAPK signaling cascade consists of three levels. The MAPKs (ERK, JNK, and p38) are at the end of the cascade, preceded by the MAPK kinases (MAP2Ks) and the MAPK kinase kinases (MAPK3Ks), respectively. Signals from various extracellular stimuli are transmitted to the MAPK3Ks, which

phosphorylate (and thus activate) the MAPK2Ks, which subsequently phosphorylate the MAPKs, which then proceed to phosphorylate a plethora of downstream effectors to enact behaviors as diverse as proliferation, motility, apoptosis, and differentiation (58).

Despite the nomenclature, ERK is the only member of the MAPK family that responds to mitogenic signals. JNK and p38, by comparison, are activated by genotoxic and environmental stresses as well as inflammation, and accordingly are also referred to as stress activated protein kinases (SAPKs) (58, 59).

The p38 arm of the MAPK pathway is effected by four closely related isoforms: p38 α, β, γ and δ. Based on protein sequence homology p38 α and β cluster together, as do p38 γ and δ. Despite their sequence similarity and shared upstream kinases, the p38 isoforms can have unrelated, and even antagonistic, roles in development and disease (59-63). These disparate results appear to be due to both context dependence (cell type, signal specificity, and others), as well as oft-ignored isoform-specific functions.

The vast majority of studies focusing on the p38 pathway utilize pyridinyl imidazole inhibitors such as SB203580, which act as competitive inhibitors by binding to the ATP pocket of p38 (64). Though highly effective and easily administered *in vitro*, this class of inhibitors only targets the α and β isoforms;

thus most knowledge about p38 signaling focuses on these two isoforms, often without differentiating between them.

With the advent of RNA interference technologies, isoform-specific p38 studies emerged. Interestingly, the non-canonical p38 isoforms, specifically p38δ, have been shown to promote and regulate tumorigenic and metastatic properties (65-67). Cancer research focused on p38γ has still remained quite limited however, despite studies implicating it in cancer-related properties such as maintenance of intercellular junctions (68) and progenitor cell expansion (69).

p38γ (also referred to as MAPK12, ERK6, or SAPK3) is a 42 kDa member of the p38 MAPK family that is activated by cytokines, such as IL-1 and TNFα, and cellular stresses, such as osmotic shock and inhibition of protein synthesis (70). Unlike the other p38 isoforms, which are ubiquitously expressed, p38γ expression is restricted to muscle tissue, where its primary function is to promote myoblast differentiation into myogenic precursor cells and myotubes (69, 71-74). Though highly homologous to the other three p38 isoforms, p38γ has a unique c-terminal –ETXL sequence that enables binding to PDZ domains within PDZ domain-containing proteins such as human discs large (hDlg), SAP90, and SAP97 (68, 75-77). PDZ domains serve to localize PDZ domain-containing proteins to specific subcellular sites, where they often function as connections between transmembrane proteins and the cytoskeleton (75), suggesting that p38γ may interact with the cytoskeleton. Based on its developmental roles in

18

muscle cell differentiation and its suggested association with the cytoskeleton, it is tempting to speculate that p38γ may function in regulating mesenchymal-like cellular motility, such as that used by metastasizing breast cancer cells.

Indeed, p38γ has been shown to have oncogenic functions. On a correlative level, p38γ mRNA is overexpressed in several types of cancer (78, 79). p38γ has been shown to bind the PDZ domain of the phosphatase PTPH1, and their binding and interaction facilitates Ras-induced oncogenesis (80). Additionally, p38γ is the only member of the p38 family that is induced by Ras activation (78, 81), and its expression helps increase Ras-induced cancer invasion (81, 82).

*   *   *

As discussed earlier, we view the overarching questions regarding breast cancer metastasis as: which genes cause a cancer cell to metastasize, and which genes contribute to the metastatic properties of a metastasizing cell? Based on the body of work surrounding the signaling molecules discussed in the previous section, we proposed two hypotheses aimed at addressing these two questions.

As discussed earlier in this chapter, the EMT is required for stationary epithelial cells to acquire mesenchymal-like motility properties. Additionally, the EMT can induce epithelial cells to acquire stem cell-like properties, and carcinoma cells to become cancer stem cells (21). As stated in the previous section, RhoC is a

19

potent inducer of cell motility, invasion, and metastasis—all hallmark behaviors of mesenchymal cells, and accordingly of carcinoma cells that have undergone EMT. Additionally, RhoC expression was shown to increase post-EMT and promote post-EMT motility of colon carcinoma cells. In light of these established functions for RhoC, the link between RhoC and the EMT, and the recently identified interrelationship between the EMT and cancer stem cells, we hypothesized that RhoC might contribute to the metastatic properties of breast cancer stem cells.

As implied by the name, under normal developmental conditions the EMT is utilized to change an epithelial cell into a mesenchymal cell. Interestingly, the behavior of mesenchymal cells—particularly their contractility-based mode of locomotion—shares many similarities with the contractile behavior of muscles. Indeed, the mesoderm layer formed by the EMT and subsequent invagination of the ectoderm layer during gastrulation eventually gives rise to muscles in the body. It is therefore a logical prediction to reason that genes which mediate muscle differentiation may also function in establishing muscle-like, or mesenchymal-like, behavior in other cell types. Based on this reasoning, we hypothesized that p38γ may promote mesenchymal-like cell behavior in breast carcinoma cells and thus promote metastasis.

We address these hypotheses in the following three chapters:

Chapter 2: RhoC determines the metastatic potential and affects the abundance of breast cancer stem cells

In this chapter we address the question "which genes allow a cancer cell to metastasize?" By specifically inhibiting RhoC in a metastatic breast cancer cell line and overexpressing RhoC in a non-tumorigenic, non-metastatic mammary epithelial cell line we were able to determine that RhoC is both necessary for and sufficient to induce metastasis of breast cancer stem cells—making RhoC the first identified molecular initiator of BCSC metastasis. Surprisingly, we also discovered that RhoC expression and activity of the BCSC marker ALDH1 are tightly intertwined, as changes in RhoC expression directly influence the abundance of BCSCs, and conversely RhoC expression is primarily restricted to the ALDH (+) BCSC population. Furthermore, expression of RhoC and ALDH1 was tightly correlated in breast cancer patient tissue samples, suggesting that the relationship between these two proteins may indeed hold clinical relevance.

Chapter 3: p38γ regulates breast cancer cell motility and metastasis through modulation of RhoC GTPase

Here we address the question "which genes contribute to the metastatic properties of a metastasizing cell?" We observed that p38γ is overactivated in a panel of basal (or mesenchymal-like) breast cancer cell lines. By inhibiting p38γ using two types of RNA interference and by overexpression of a dominant negative construct, we determined that p38γ contributes to the metastatic abilities of basal breast cancer cells, both *in vitro* and *in vivo*. Surprisingly, we

discovered that p38γ modulates RhoC expression by a novel mechanism—regulation of RhoC ubiquitination, and consequently lysosomal degradation. We extended this research into the clinical setting and revealed that the relationship between RhoC and p38γ persists in human breast cancer patients, and that p38γ is associated with the basal breast cancer subtype and lower overall patient survival.

Chapter 4: Computational mechanical modeling reveals the role of p38γ in shaping the cytoskeleton and controlling locomotion of aggressive breast cancer cells

Here we extend the work of the previous chapter and take an alternative approach to the traditional "mechanistic" study by exploring the physical behaviors, rather than signaling molecules, underlying the relationship between p38γ, the actin cytoskeleton, and cell motility. By computationally modeling basal breast cancer cell motility we were able to determine that p38γ-mediated cytoskeletal changes are central to the motility defects observed following p38γ knockdown. In the course of our study the computational models predicted, and biological experiments subsequently verified, a novel behavior at the leading edge of motile cells: leading edge protrusion oscillations. Subsequent *in silico* analysis revealed a likely sequence of events leading from p38γ knockdown to the observed motility defects, thereby mechanistically linking p38γ to the cytoskeletal remodeling necessary for mesenchymal-like cell motility.
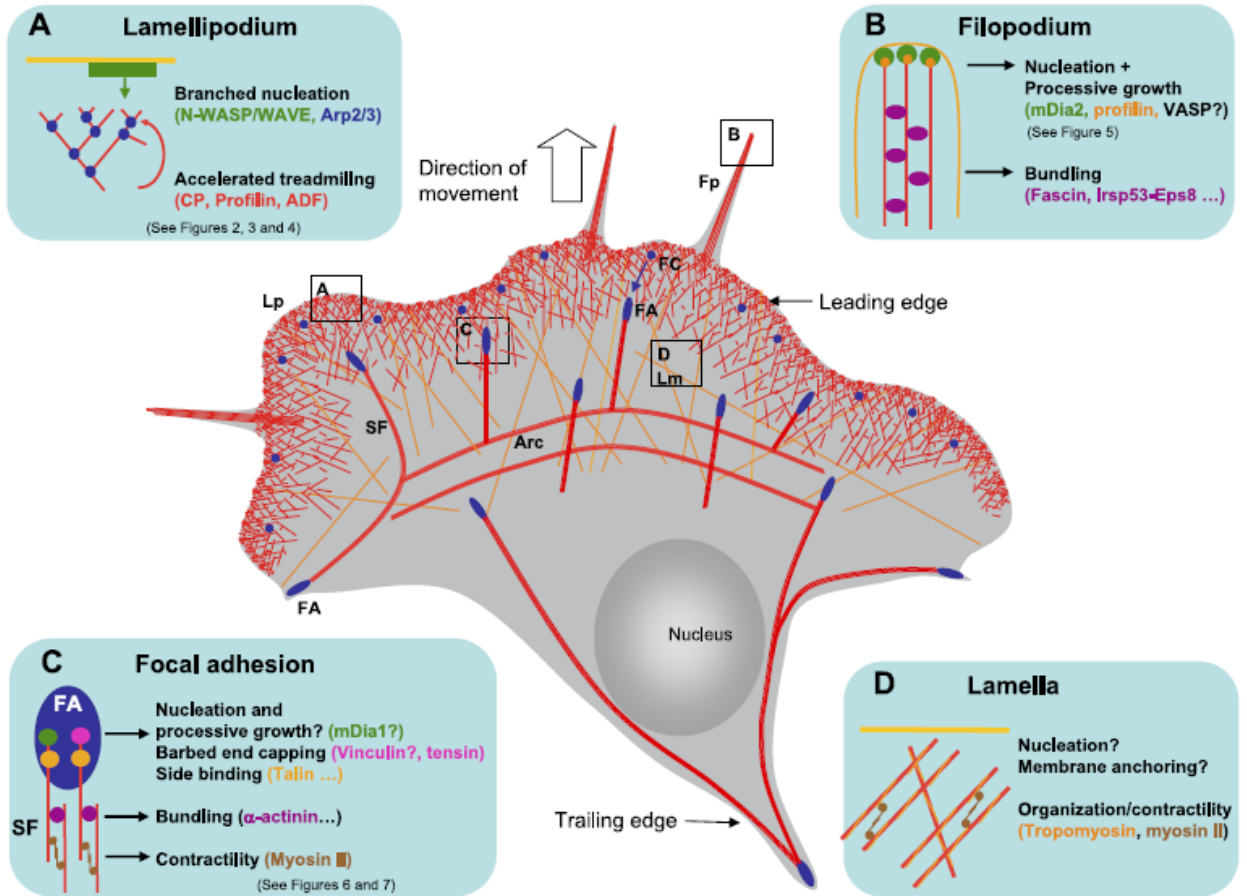
Figure 1.1 – Overview of the cytoskeletal components of a motile cell and the corresponding regulatory proteins (from Le Clainche and Carlier, Physiological Reviews 2008 (Am Physiol Soc, used with permission)).
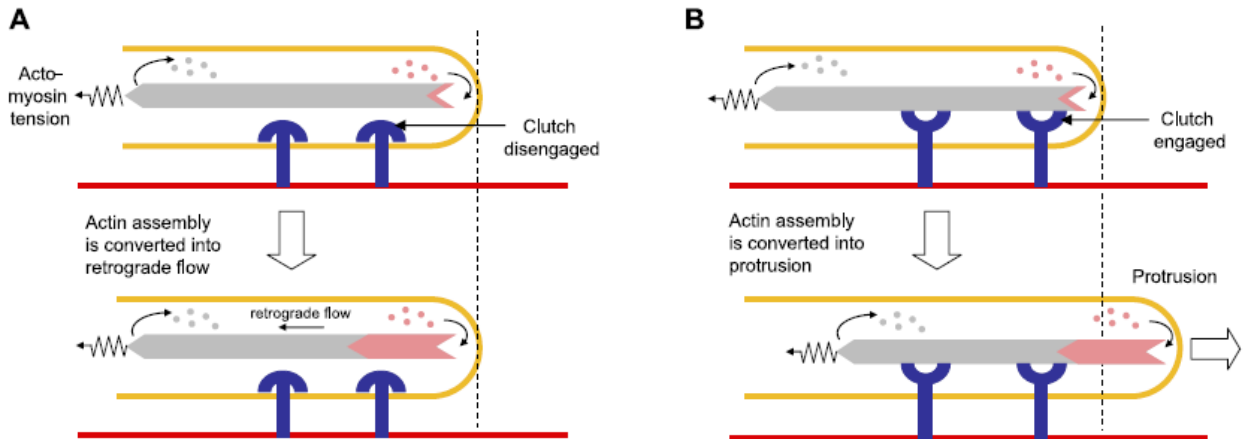
Figure 1.2 – Focal adhesions act as a "molecular clutch". Using this clutch mechanism focal adhesions direct either (A) retrograde actin flow or (B) protrusion (or alternatively trailing edge retraction, as mediated by myosin-based contractility) (from Le Clainche and Carlier, Physiological Reviews 2008 (Am Physiol Soc, used with permission)).

Portions of Chapter 1 are found in my book chapter on Rho GTPase signaling

published in *The Rho GTPases in Cancer* (2010), pp. 29-42, under the title "Rho

Proteins in Cancer" by Devin T. Rosenthal, J. Chadwick Brenner, and Sofia D.

Merajver.

References

1.   Howlader N NA, Krapcho M, Neyman N, Aminou R, Waldron W, Altekruse SF, Kosary CL, Ruhl J, Tatalovich Z, Cho H, Mariotto A, Eisner MP, Lewis DR, Chen HS, Feuer EJ, Cronin KA, Edwards BK. SEER Cancer Statistics Review, 1975-2008. Bethesda, MD: National Cancer Institute; 2011.
2.   Pandey PR, Saidou J, Watabe K. Role of myoepithelial cells in breast tumor progression. Front Biosci. 2010;15:226-36.
3.   Polyak K, Hu M. Do myoepithelial cells hold the key for breast tumor progression? J Mammary Gland Biol Neoplasia. 2005;10:231-47.
4.   Martin GR, Timpl R. Laminin and other basement membrane components. Annu Rev Cell Biol. 1987;3:57-85.
5.   Wiseman BS, Werb Z. Stromal effects on mammary gland development and breast cancer. Science. 2002;296:1046-9.
6.   Condeelis J, Pollard JW. Macrophages: obligate partners for tumor cell migration, invasion, and metastasis. Cell. 2006;124:263-6.
7.   Bockhorn M, Jain RK, Munn LL. Active versus passive mechanisms in metastasis: do cancer cells crawl into vessels, or are they pushed? Lancet Oncol. 2007;8:444-8.
8.   Racila E, Euhus D, Weiss AJ, Rao C, McConnell J, Terstappen LW, et al. Detection and characterization of carcinoma cells in the blood. Proc Natl Acad Sci U S A. 1998;95:4589-94.
9.   Gaforio JJ, Serrano MJ, Sanchez-Rovira P, Sirvent A, Delgado-Rodriguez M, Campos M, et al. Detection of breast cancer cells in the peripheral blood is positively correlated with estrogen-receptor status and predicts for poor prognosis. Int J Cancer. 2003;107:984-90.
10.   Cristofanilli M, Budd GT, Ellis MJ, Stopeck A, Matera J, Miller MC, et al. Circulating tumor cells, disease progression, and survival in metastatic breast cancer. N Engl J Med. 2004;351:781-91.
11.   Yang J, Weinberg RA. Epithelial-mesenchymal transition: at the crossroads of development and tumor metastasis. Dev Cell. 2008;14:818-29.
12.   Thiery JP, Acloque H, Huang RY, Nieto MA. Epithelial-mesenchymal transitions in development and disease. Cell. 2009;139:871-90.
13.   Thiery JP. Epithelial-mesenchymal transitions in tumour progression. Nat Rev Cancer. 2002;2:442-54.
14.   Lee JM, Dedhar S, Kalluri R, Thompson EW. The epithelial-mesenchymal transition: new insights in signaling, development, and disease. J Cell Biol. 2006;172:973-81.
15.   Yang J, Mani SA, Donaher JL, Ramaswamy S, Itzykson RA, Come C, et al. Twist, a master regulator of morphogenesis, plays an essential role in tumor metastasis. Cell. 2004;117:927-39.
16.   Perou CM, Sorlie T, Eisen MB, van de Rijn M, Jeffrey SS, Rees CA, et al. Molecular portraits of human breast tumours. Nature. 2000;406:747-52.
17.   Al-Hajj M, Wicha MS, Benito-Hernandez A, Morrison SJ, Clarke MF. Prospective identification of tumorigenic breast cancer cells. Proc Natl Acad Sci U S A. 2003;100:3983-8.

18.   Ginestier C, Hur MH, Charafe-Jauffret E, Monville F, Dutcher J, Brown M, et al. ALDH1 is a marker of normal and malignant human mammary stem cells and a predictor of poor clinical outcome. Cell Stem Cell. 2007;1:555-67.
19.   Dean M, Fojo T, Bates S. Tumour stem cells and drug resistance. Nat Rev Cancer. 2005;5:275-84.
20.   McDermott SP, Wicha MS. Targeting breast cancer stem cells. Mol Oncol. 2010;4:404-19.
21.   Mani SA, Guo W, Liao MJ, Eaton EN, Ayyanan A, Zhou AY, et al. The epithelial-mesenchymal transition generates cells with properties of stem cells. Cell. 2008;133:704-15.
22.   Liu R, Wang X, Chen GY, Dalerba P, Gurney A, Hoey T, et al. The prognostic role of a gene signature from tumorigenic breast-cancer cells. N Engl J Med. 2007;356:217-26.
23.   Liu H, Patel MR, Prescher JA, Patsialou A, Qian D, Lin J, et al. Cancer stem cells from human breast tumors are involved in spontaneous metastases in orthotopic mouse models. Proc Natl Acad Sci U S A. 2010;107:18115-20.
24.   Charafe-Jauffret E, Ginestier C, Iovino F, Tarpin C, Diebel M, Esterni B, et al. Aldehyde dehydrogenase 1-positive cancer stem cells mediate metastasis and poor clinical outcome in inflammatory breast cancer. Clin Cancer Res. 2010;16:45-55.
25.   Hermann PC, Huber SL, Herrler T, Aicher A, Ellwart JW, Guba M, et al. Distinct populations of cancer stem cells determine tumor growth and metastatic activity in human pancreatic cancer. Cell Stem Cell. 2007;1:313-23.
26.   Pang R, Law WL, Chu AC, Poon JT, Lam CS, Chow AK, et al. A subpopulation of CD26+ cancer stem cells with metastatic capacity in human colorectal cancer. Cell Stem Cell. 2010;6:603-15.
27.   Lewis AK, Bridgman PC. Nerve growth cone lamellipodia contain two populations of actin filaments that differ in organization and polarity. J Cell Biol. 1992;119:1219-43.
28.   Machesky LM. Lamellipodia and filopodia in metastasis and invasion. FEBS Lett. 2008;582:2102-11.
29.   Ponti A, Machacek M, Gupton SL, Waterman-Storer CM, Danuser G. Two distinct actin networks drive the protrusion of migrating cells. Science. 2004;305:1782-6.
30.   Gupton SL, Anderson KL, Kole TP, Fischer RS, Ponti A, Hitchcock-DeGregori SE, et al. Cell migration without a lamellipodium: translation of actin dynamics into cell movement mediated by tropomyosin. J Cell Biol. 2005;168:619-31.
31.   Le Clainche C, Carlier MF. Regulation of actin assembly associated with protrusion and adhesion in cell migration. Physiol Rev. 2008;88:489-513.
32.   Zamir E, Geiger B. Components of cell-matrix adhesions. J Cell Sci. 2001;114:3577-9.
33.   Burridge K, Fath K, Kelly T, Nuckolls G, Turner C. Focal adhesions: transmembrane junctions between the extracellular matrix and the cytoskeleton. Annu Rev Cell Biol. 1988;4:487-525.

34.   Burridge K, Chrzanowska-Wodnicka M. Focal adhesions, contractility, and signaling. Annu Rev Cell Dev Biol. 1996;12:463-518.

35.   Webb DJ, Parsons JT, Horwitz AF. Adhesion assembly, disassembly and turnover in migrating cells -- over and over and over again. Nat Cell Biol. 2002;4:E97-100.

36.   Ezratty EJ, Partridge MA, Gundersen GG. Microtubule-induced focal adhesion disassembly is mediated by dynamin and focal adhesion kinase. Nat Cell Biol. 2005;7:581-90.

37.   Ridley AJ, Schwartz MA, Burridge K, Firtel RA, Ginsberg MH, Borisy G, et al. Cell migration: integrating signals from front to back. Science. 2003;302:1704-9.

38.   Lauffenburger DA, Horwitz AF. Cell migration: a physically integrated molecular process. Cell. 1996;84:359-69.

39.   Ridley AJ. Rho GTPases and cell migration. J Cell Sci. 2001;114:2713-22.

40.   Rosenthal DT, Brenner JC, Merajver SD. Rho Proteins in Cancer. In: van Golen KL, editor. The Rho GTPases in Cancer. New York: Springer New York; 2010. p. 29-42.

41.   Ridley AJ, Paterson HF, Johnston CL, Diekmann D, Hall A. The small GTP-binding protein rac regulates growth factor-induced membrane ruffling. Cell. 1992;70:401-10.

42.   Ridley AJ, Hall A. The small GTP-binding protein rho regulates the assembly of focal adhesions and actin stress fibers in response to growth factors. Cell. 1992;70:389-99.

43.   Chimini G, Chavrier P. Function of Rho family proteins in actin dynamics during phagocytosis and engulfment. Nat Cell Biol. 2000;2:E191-6.

44.   Etienne-Manneville S, Hall A. Rho GTPases in cell biology. Nature. 2002;420:629-35.

45.   Evers EE, Zondag GC, Malliri A, Price LS, ten Klooster JP, van der Kammen RA, et al. Rho family proteins in cell adhesion and cell migration. Eur J Cancer. 2000;36:1269-74.

46.   Raftopoulou M, Hall A. Cell migration: Rho GTPases lead the way. Dev Biol. 2004;265:23-32.

47.   Wheeler AP, Ridley AJ. Why three Rho proteins? RhoA, RhoB, RhoC, and cell motility. Exp Cell Res. 2004;301:43-9.

48.   Ridley AJ. The GTP-binding protein Rho. Int J Biochem Cell Biol. 1997;29:1225-9.

49.   Wu M, Wu ZF, Rosenthal DT, Rhee EM, Merajver SD. Characterization of the roles of RhoC and RhoA GTPases in invasion, motility, and matrix adhesion in inflammatory and aggressive breast cancers. Cancer. 2010;116:2768-82.

50.   Bellovin DI, Simpson KJ, Danilov T, Maynard E, Rimm DL, Oettgen P, et al. Reciprocal regulation of RhoA and RhoC characterizes the EMT and identifies RhoC as a prognostic marker of colon carcinoma. Oncogene. 2006;25:6959-67.

51.   van Golen KL, Wu ZF, Qiao XT, Bao LW, Merajver SD. RhoC GTPase, a novel transforming oncogene for human mammary epithelial cells that partially recapitulates the inflammatory breast cancer phenotype. Cancer Res. 2000;60:5832-8.

52.   Clark EA, Golub TR, Lander ES, Hynes RO. Genomic analysis of metastasis reveals an essential role for RhoC. Nature. 2000;406:532-5.
53.   Ikoma T, Takahashi T, Nagano S, Li YM, Ohno Y, Ando K, et al. A definitive role of RhoC in metastasis of orthotopic lung cancer in mice. Clin Cancer Res. 2004;10:1192-200.
54.   Islam M, Lin G, Brenner JC, Pan Q, Merajver SD, Hou Y, et al. RhoC expression and head and neck cancer metastasis. Mol Cancer Res. 2009;7:1771-80.
55.   Hakem A, Sanchez-Sweatman O, You-Ten A, Duncan G, Wakeham A, Khokha R, et al. RhoC is dispensable for embryogenesis and tumor initiation but essential for metastasis. Genes Dev. 2005;19:1974-9.
56.   van Golen KL, Bao LW, Pan Q, Miller FR, Wu ZF, Merajver SD. Mitogen activated protein kinase pathway is involved in RhoC GTPase induced motility, invasion and angiogenesis in inflammatory breast cancer. Clin Exp Metastasis. 2002;19:301-11.
57.   Chang L, Karin M. Mammalian MAP kinase signalling cascades. Nature. 2001;410:37-40.
58.   Raman M, Chen W, Cobb MH. Differential regulation and properties of MAPKs. Oncogene. 2007;26:3100-12.
59.   Wagner EF, Nebreda AR. Signal integration by JNK and p38 MAPK pathways in cancer development. Nat Rev Cancer. 2009;9:537-49.
60.   Cuenda A, Rousseau S. p38 MAP-kinases pathway regulation, function and role in human diseases. Biochim Biophys Acta. 2007;1773:1358-75.
61.   Wang Y, Huang S, Sah VP, Ross J, Jr., Brown JH, Han J, et al. Cardiac muscle cell hypertrophy and apoptosis induced by distinct members of the p38 mitogen-activated protein kinase family. J Biol Chem. 1998;273:2161-8.
62.   Platanias LC. Map kinase signaling pathways and hematologic malignancies. Blood. 2003;101:4667-79.
63.   Qi X, Pohl NM, Loesch M, Hou S, Li R, Qin JZ, et al. p38alpha antagonizes p38gamma activity through c-Jun-dependent ubiquitin-proteasome pathways in regulating Ras transformation and stress response. J Biol Chem. 2007;282:31398-408.
64.   English JM, Cobb MH. Pharmacological inhibitors of MAPK pathways. Trends Pharmacol Sci. 2002;23:40-5.
65.   Schindler EM, Hindes A, Gribben EL, Burns CJ, Yin Y, Lin MH, et al. p38delta Mitogen-activated protein kinase is essential for skin tumor development in mice. Cancer Res. 2009;69:4648-55.
66.   Junttila MR, Ala-Aho R, Jokilehto T, Peltonen J, Kallajoki M, Grenman R, et al. p38alpha and p38delta mitogen-activated protein kinase isoforms regulate invasion and growth of head and neck squamous carcinoma cells. Oncogene. 2007;26:5267-79.
67.   Efimova T. p38delta mitogen-activated protein kinase regulates skin homeostasis and tumorigenesis. Cell Cycle. 2010;9:498-05.
68.   Sabio G, Arthur JS, Kuma Y, Peggie M, Carr J, Murray-Tait V, et al. p38gamma regulates the localisation of SAP97 in the cytoskeleton by modulating its interaction with GKAP. EMBO J. 2005;24:1134-45.

69.   Gillespie MA, Le Grand F, Scime A, Kuang S, von Maltzahn J, Seale V, et al. p38-{gamma}-dependent gene silencing restricts entry into the myogenic differentiation program. J Cell Biol. 2009;187:991-1005.

70.   Cuenda A, Cohen P, Buee-Scherrer V, Goedert M. Activation of stress-activated protein kinase-3 (SAPK3) by cytokines and cellular stresses is mediated via SAPKK3 (MKK6); comparison of the specificities of SAPK3 and SAPK2 (RK/p38). EMBO J. 1997;16:295-305.

71.   Tortorella LL, Lin CB, Pilch PF. ERK6 is expressed in a developmentally regulated manner in rodent skeletal muscle. Biochem Biophys Res Commun. 2003;306:163-8.

72.   Cuenda A, Cohen P. Stress-activated protein kinase-2/p38 and a rapamycin-sensitive pathway are required for C2C12 myogenesis. J Biol Chem. 1999;274:4341-6.

73.   Wang XS, Diener K, Manthey CL, Wang S, Rosenzweig B, Bray J, et al. Molecular cloning and characterization of a novel p38 mitogen-activated protein kinase. J Biol Chem. 1997;272:23668-74.

74.   Li Z, Jiang Y, Ulevitch RJ, Han J. The primary structure of p38 gamma: a new member of p38 group of MAP kinases. Biochem Biophys Res Commun. 1996;228:334-40.

75.   Sabio G, Reuver S, Feijoo C, Hasegawa M, Thomas GM, Centeno F, et al. Stress- and mitogen-induced phosphorylation of the synapse-associated protein SAP90/PSD-95 by activation of SAPK3/p38gamma and ERK1/ERK2. Biochem J. 2004;380:19-30.

76.   Sabio G, Cerezo-Guisado MI, Del Reino P, Inesta-Vaquera FA, Rousseau S, Arthur JS, et al. p38gamma regulates interaction of nuclear PSF and RNA with the tumour-suppressor hDlg in response to osmotic shock. J Cell Sci. 2010;123:2596-604.

77.   Hasegawa M, Cuenda A, Spillantini MG, Thomas GM, Buee-Scherrer V, Cohen P, et al. Stress-activated protein kinase-3 interacts with the PDZ domain of alpha1-syntrophin. A mechanism for specific substrate recognition. J Biol Chem. 1999;274:12626-31.

78.   Tang J, Qi X, Mercola D, Han J, Chen G. Essential role of p38gamma in K-Ras transformation independent of phosphorylation. J Biol Chem. 2005;280:23910-7.

79.   Loesch M, Chen G. The p38 MAPK stress pathway as a tumor suppressor or more? Front Biosci. 2008;13:3581-93.

80.   Hou SW, Zhi HY, Pohl N, Loesch M, Qi XM, Li RS, et al. PTPH1 dephosphorylates and cooperates with p38gamma MAPK to increase ras oncogenesis through PDZ-mediated interaction. Cancer Res. 2010;70:2901-10.

81.   Qi X, Tang J, Loesch M, Pohl N, Alkan S, Chen G. p38gamma mitogen-activated protein kinase integrates signaling crosstalk between Ras and estrogen receptor to increase breast cancer invasion. Cancer Res. 2006;66:7540-7.

82.   Loesch M, Zhi HY, Hou SW, Qi XM, Li RS, Basir Z, et al. p38{gamma} MAPK cooperates with c-Jun in trans-activating matrix metalloproteinase 9. J Biol Chem. 2010.

Chapter II

RhoC determines the metastatic potential and affects the abundance of breast cancer stem cells

Abstract

Cancer stem cells have been shown to promote tumorigenesis of many tumor types, including breast, although their relevance to cancer metastasis remains unclear. While subpopulations of cancer stem cells that are required for metastasis have been identified, to date there are no known molecular regulators of breast cancer stem cell metastasis. Here we identify RhoC GTPase as an essential regulator of breast cancer stem cell metastasis, and present evidence that RhoC also modulates the frequency of breast cancer stem cells within a population. Using an orthotopic xenograft model of spontaneous metastasis we discover that RhoC is both necessary and sufficient to promote breast cancer stem cell metastasis, often independent from primary tumor formation. The relationship between RhoC and breast cancer stem cells persists in breast cancer patients as well, as expression of RhoC and the breast cancer stem cell marker ALDH1 are highly correlated in clinical breast cancer specimens. These results open new avenues to combating the deadliest cells driving the most lethal stage of breast cancer progression.

Introduction

The cancer stem cell (CSC) hypothesis posits that a small subset of cells within a tumor is responsible for maintaining the growth and survival of the cancer. The minority CSC population retains a relatively undifferentiated state and possesses unlimited replication potential, as well as the ability to both self-renew and produce differentiated progeny, and thus aid in generating heterogeneity within a tumor (83). Although constituting only a small proportion of total tumor mass, CSCs are thought to be the only cells within a tumor capable of sustaining tumor growth. CSCs are presumed to be more adept at resisting conventional therapies than non-CSCs, and therefore are thought to be the cause of recurrence in many patients (19). The presumption that CSCs are resistant to conventional therapies and capable of regenerating a tumor thought to be in remission makes targeting CSCs of paramount clinical importance.

Despite the local effects of a primary tumor, the actual lethality of many cancers, such as breast cancer, is due to metastasis of cells away from the primary tumor to vital organs. Intriguingly, recent work has revealed an emerging role for CSCs in cancer metastasis. Initial work uncovered circumstantial links between CSCs and metastasis, including the presence of an invasiveness gene signature in the breast CSC ("BCSC") population that predicted shorter metastasis-free survival (22), and an association between BCSCs and the metastasis-associated epithelial-to-mesenchymal transition (21).

Recent studies have demonstrated more causative links between BCSCs and metastasis. A recent publication from Liu et al. revealed that BCSCs are enriched within spontaneous breast cancer metastases in an orthotopic xenograft model (23), and Charafe-Jauffret et al. found that BCSCs mediate metastasis of the most aggressive subset of breast cancer, inflammatory breast cancer (IBC) (24). In line with these studies, subpopulations within the CSC population have been identified, based on surface marker expression, that selectively enable metastasis of several types of cancer (25, 26). While evidence for CSCs having an important role in metastasis exists and markers identifying metastatic CSC populations are emerging, a functional molecular link between BCSCs and metastasis has not yet been identified (84). Here we demonstrate that RhoC GTPase promotes BCSC metastasis, and is capable of initiating metastasis independent of primary tumor formation.

RhoC is a member of the Rho family of GTPases and is responsible for coordinating cell motility by regulating actomyosin contractility and focal adhesion turnover (40, 47, 48). In cancer, RhoC has been shown to be a potent metastatic driver of many cancer types (51-54), and RhoC knockout selectively inhibits metastasis—independent from primary tumor formation—in a transgenic breast cancer model (55).

The metastatic influence of RhoC is exemplified by IBC. IBC is the most lethal form of breast cancer, and is metastatic from its inception. RhoC was found to be

overexpressed in 90% of IBC cases (85), and RhoC overexpression is capable of partially recapitulating the IBC phenotype *in vitro* (51). As mentioned previously, BCSCs play an important role in IBC metastasis and are associated with poor clinical outcome (24). Based on the strong association between RhoC, BCSCs, and metastasis in IBC, we used the IBC-derived SUM149 cell line to address RhoC functionality in BCSC metastasis.

Here we discover that RhoC plays an essential role in mediating BCSC metastasis. Inhibiting RhoC revealed that it is necessary for BCSC metastasis in the highly metastatic SUM149 cell line, and conversely overexpressing RhoC alone was sufficient to enable metastasis of BCSCs from the otherwise non-tumorigenic, non-metastatic MCF-10A cell line. Surprisingly, RhoC often promoted spontaneous BCSC metastasis independent from primary tumor formation – speaking to RhoC potency as a metastasis-promoting gene. RhoC also appears to directly influence the BCSC population size, as the percent of BCSCs within each cell line varied concurrent with changes in RhoC expression. Expression of RhoC and the BCSC marker ALDH1 strongly correlate in clinical breast cancer specimens, suggesting that the link between RhoC and BCSCs has therapeutic relevance. To the best of our knowledge RhoC is therefore the first identified molecular promoter of BCSC metastasis – one which holds therapeutic promise for the most lethal form of breast cancer.

Results

RhoC expression is enriched in the ALDH (+) population

To address the question of whether RhoC functions in the pathogenesis of BCSCs, we first asked whether RhoC expression was associated with BCSCs. Using the highly aggressive RhoC-overexpressing SUM149 cell line we discovered that, after sorting for aldehyde dehydrogenase (ALDH) activity using the ALDEFLUOR assay (18), RhoC expression was primarily confined to the ALDH (+) BCSC population (Figure 2.1A), introducing the possibility that RhoC is preferentially utilized by BCSCs.

To empirically determine whether RhoC functionally contributes to BCSC aggressiveness we generated genetically modified cell lines to test the effects of inhibiting RhoC in SUM149 cells ("SUM149 shRhoC") or overexpressing constitutively active RhoC in the non-tumorigenic mammary epithelial cell line MCF-10A ("MCF-10A G14V") (Figure 2.1B). Importantly, neither modification affected expression of the close RhoC homolog RhoA (Figure 2.1B).

Interestingly, when we sorted the modified cell lines for ALDH and observed RhoC expression as in Figure 2.1A, we found that RhoC expression was still enriched in the ALDH (+) population even within the genetically modified cell lines (Figure 2.1C-D). This was surprising, given that these cells were forcibly overexpressing (Figure 2.1C) or inhibiting (Figure 2.1D) RhoC. The fact that this

dichotomy in RhoC expression between the ALDH (+) and (-) populations persisted after genetic modification strengthened the case for an association between BCSCs and RhoC expression.

***Modifying RhoC expression alters the metastatic properties of CSCs* in vitro**

Upon observing a strong association between RhoC expression and BCSCs, we asked whether this relationship had a functional role in governing BCSC behavior. The acquisition of motility by otherwise stationary cells is a hallmark of cancer progression (86) and a process regulated across many cell lineages and cancer types by RhoC (51, 52, 87). Since CSCs have been linked to metastasis, albeit indirectly (84), we investigated RhoC effects on BCSC motility using time lapse microscopy.

We found that modulating RhoC expression significantly impacted cell velocity, even within the ALDH (+) CSC population in each cell line (Figure 2.2A). Inhibiting RhoC in highly motile SUM149 cells resulted in a significant reduction in cell speed, while overexpressing constitutively active RhoC in slow-moving MCF-10A cells significantly increased cell speed. Interestingly, we also observed significant changes in cell speed between ALDH (+) and (-) cells within each cell line that again paralleled RhoC expression. Decreased RhoC expression in SUM149 cells (either by shRNA inhibition, or within the ALDH (-) population) reduced cell motility to levels comparable to the non-tumorigenic MCF-10A

control cell line ("MCF-10A vec"). Even in the highly motile MCF-10A G14V cell line, ALDH (-) cells (which have lower RhoC G14V expression than ALDH (+) cells (Figure 2.1C)) moved significantly slower than ALDH (+) cells. The only cell line which did not show a significant difference in cell speed between the ALDH (+) and (-) populations was the MCF0-10A vec cell line. We note that this is not entirely unexpected, as this cell line is non-tumorigenic, slow-moving, and expresses low endogenous levels of RhoC (Figure 2.1B-C).

Three-dimensional Matrigel cell culture is frequently used as a tool to observe physiologically-relevant developmental, tumorigenic, and metastatic behaviors of mammary epithelial cells and breast cancer cells *in vitro* (88, 89). We employed this technique to broadly assess the cancerous properties of the RhoC-modified and ALDH-sorted cells. As has previously been observed for MCF-10A cells (88, 89), unsorted MCF-10A vec cells formed small, well-defined acinar structures (Figure 2.2B, first column, second row)—the *in vitro* representation of a normal, non-tumorigenic mammary gland. By contract, SUM149 scrambled cells grew as large, disorganized cell clusters that formed invasive protrusions into the surrounding matrix (Figure 2.2B, first column, third row)—growth characteristic of tumorigenic, metastatic breast cancer cells (89, 90).

Modifying RhoC expression had a significant and similar impact on the *in vitro* metastatic phenotype of both unsorted cell lines. MCF-10A G14V acinar-like structures were more disorganized than their vector control counterparts, with

cells invading outward from the central mass (Figure 2.2B, first column, first row), similar to SUM149 scrambled cells. Also of note was the slightly increased size of the MCF-10A G14V structures compared to the MCF-10A vec acini. Conversely, SUM149 shRhoC cells formed structures of comparable size to SUM149 scrambled cells; however, these structures had well-defined borders, showing minimal evidence of cell invasion into the matrix (Figure 2.2B, first column, fourth row).

The effects of sorting for ALDH once again mirrored RhoC expression within each cell line. The ALDH (+) population of each cell line (Figure 2.2B, second column) grew similarly to the unsorted population (Figure 2.2B, first column), whereas the ALDH (-) population appeared both non-tumorigenic and non-invasive in all cell lines (Figure 2.2B, third column). Of note, although some colonies in the SUM149 scrambled ALDH (-) population still formed large acinar-like structures, these structures had well-defined borders with no signs of invasive behavior (Figure 2.2B, third column, third row). Taken together, these data support a role for RhoC in mediating metastatic behaviors of the ALDH (+) BCSC population.

Modulating RhoC expression results in concurrent changes in CSC abundance

In the course of ALDH-sorting for our *in vitro* experiments we made a surprising observation: there appeared to be a RhoC-dependent change in BCSC

abundance in each cell line. To further investigate this observation, we compared the relative abundance of ALDH (+) BCSCs in each control cell line (SUM149 scrambled or MCF-10A vec) to the corresponding RhoC-modified cell line (SUM149 shRhoC or MCF-10A G14V). Surprisingly, we observed almost identical reciprocal differences between the two groups: a two-fold decrease in the ALDH (+) population of SUM149 shRhoC compared to scrambled, and a two-fold increase in the ALDH (+) population of MCF-10A G14V compared to vector (Figure 2.2C), suggesting that RhoC plays a role in determining the abundance of BCSCs within a population.

RhoC expression dictates metastasis of BCSCs

Based on our *in vitro* observations, we asked whether RhoC affects the behavior of BCSCs *in vivo*. To address this question we orthotopically xenografted NOD/SCID mice with either 50 ALDH-sorted SUM149 scrambled or shRhoC cells, or 5000 ALDH-sorted MCF-10A vec or G14V cells, and observed the incidence of tumorigenesis and metastasis.

Inhibiting RhoC in SUM149 cells caused a significant decrease in tumor incidence in the ALDH (+) population (see Table 2.1). 5 out of 9 (55.6%) SUM149 scrambled control mice developed tumors, whereas none of the eight mice injected with SUM149 shRhoC cells formed tumors (p = 0.029). There was no significant difference in tumor incidence between the ALDH (+) MCF-10A vec and G14V cell lines, although one MCF-10A G14V mouse did present with a

38

tumor (Table 2.1). At the limiting cell numbers used for this study none of the mice injected with ALDH (-) cells formed tumors.

Surprisingly, when we inspected the mice for evidence of metastasis we discovered large metastatic tumors completely filling the pleural cavity in many of the mice injected with ALDH (+) SUM149 scrambled and MCF-10A G14V cells (Figure 2.3Ai). We also observed one instance in the ALDH (+) SUM149 shRhoC cohort and two instances in the ALDH (-) MCF-10A G14V cohort (Figure 2.3B and Table 2.1). Histologic examination revealed these tumors to be poorly differentiated carcinomas, with remarkably similar appearance between the MCF-10A G14V and SUM149 scrambled metastases (Figure 2.3Aii). In all, 66.67% of mice injected with ALDH (+) SUM149 scrambled cells and 90% of mice injected with ALDH (+) MCF-10A G14V cells presented with metastases, compared to only 12.5% of ALDH (+) SUM149 shRhoC-injected and 33.33% of ALDH (-) MCF-10A G14V-injected mice (Table 2.1).

Even more surprising was the propensity for metastasis in mice that did not form primary tumors (Figure 2.3A-B). 35% of mice injected with ALDH (+) SUM149 scrambled cells, and a remarkable 80% of mice injected with ALDH (+) MCF-10A G14V cells had metastases independent of primary tumor formation (Figure 2.3B). Additionally, all of the ALDH (+) SUM149 shRhoC and ALDH (-) MCF-10A G14V mice presenting with metastases also lacked primary tumors (Figure 2.3B).

One central tenant of the CSC hypothesis is that CSCs can self-renew and generate heterogeneity within a tumor whereas non-CSCs cannot (83). Based on this assumption, we hypothesized that the dichotomy in RhoC expression between the ALDH (+) and (-) populations was maintained *in vivo*, since ALDH (-) cells should not be able to restore tumor heterogeneity. We used the SUM149 scrambled cell line to assay RhoC expression *in vivo*, as it is the only cell line in this study that expresses high levels of endogenous RhoC (Figure 2.1B).

Since none of the mice injected with 50 ALDH (-) SUM149 scrambled cells formed tumors we increased the injection to 5000 cells, at which point the ALDH (-) population also formed tumors. After allowing tumors to develop we euthanized the mice, extracted protein from the tumors, and assayed RhoC expression. The dichotomy of RhoC expression between ALDH (+) and ALDH (-) tumors persisted *in vivo*; ALDH (+) SUM149 scrambled tumors maintained RhoC expression during tumor growth, whereas ALDH (-) SUM149 scrambled tumors did not regain RhoC expression (Figure 2.2C). This data supports the assertion that ALDH (-) cells are indeed non-CSCs, and accordingly have a decreased ability to form tumors and/or metastasis (Figure 2.3B and Table 2.1) and are unable to restore tumor heterogeneity, as demonstrated by their inability to re-express RhoC after expansion *in vivo* (Figure 2.3C). Along with our previous findings illustrating the influence of RhoC on CSC abundance (Figure 2.2C), this data further supports the conclusion that RhoC expression is intimately linked to the BCSC phenotype.

RhoC and ALDH1 expression are highly correlated in clinical breast cancer samples

Expression of the ALDH1 protein has been shown to be a reliable marker for BCSCs in paraffin-embedded tissue (18). To extend our findings on the relationship between RhoC and BCSCs, we used Automated Quantitative Analysis (AQUA) of immunofluorescence signals for RhoC and ALDH1 in cytokeratin-positive cells from a breast cancer tissue microarray. Expression of RhoC and ALDH1 were strongly positively correlated in the 136 samples analyzed (Figure 2.3D), indicating that the tight association between RhoC and BCSCs uncovered *in vitro* and *in vivo* persists in breast cancer patients.

Discussion

CSCs have been shown to promote tumorigenesis in numerous cancer types (17, 91, 92), and recent work has begun to define a role for CSCs in cancer metastasis as well (23-26). Despite the established therapeutic importance of targeting metastasis and the growing understanding of the role of CSCs in metastasis, to date no functional molecular regulators have been identified that promote aggressive, metastatic behavior of BCSCs. Here we identify RhoC as such a promoter, one that is both necessary and sufficient for BCSC metastasis.

By approaching RhoC expression from two distinct angles—its necessity for metastasis of a breast cancer cell line (SUM149), and its sufficiency to induce metastasis of a non-tumorigenic mammary epithelial cell line (MCF-10A)—we were able to clearly elucidate a role for RhoC in BCSC metastasis. It is important to note that we used an orthotopic xenograft system rather than an intracardiac or tail vein injection assay to measure metastasis. As emphasized in a recent publication (23), the orthotopic xenograft model of spontaneous breast cancer metastasis is a more physiologically relevant model of breast cancer metastasis which more accurately recapitulates the microenvironmental obstacles metastatic cells encounter in human patients.

Modulating RhoC expression in either SUM149 or MCF-10A cells had a concordant effect on the metastatic potential of BCSCs from each cell line. Interestingly, not only did alterations in RhoC expression affect metastasis of the BCSCs, but RhoC was preferentially expressed by the BCSC fraction. We further found that RhoC expression and BCSC abundance are intertwined, as the abundance of BCSCs within a cell line was altered concurrently with modified RhoC expression. Further supporting the relationship between RhoC and BCSCs is our finding that expression of RhoC and the BCSC marker ALDH1 are strongly correlated in clinical breast cancer samples. Taken together, these data reveal a close association between RhoC and BCSCs; one in which RhoC expression determines BCSC metastatic potential and contributes to determining the frequency of BCSCs within a population. This evidence supports the theory that a

larger BCSC population (93)—and thus higher RhoC expression —may confer a worse prognosis (94).

It is interesting to note that a sizable fraction of mice injected with non-CSC ALDH (-) MCF-10A G14V still developed lung metastases (Table 2.1). That these cells were still capable of metastasizing further supports RhoC sufficiency to induce metastasis. Although the ALDH (-) fraction of the MCF-10A G14V cell line had lower RhoC expression, expression was not completely eliminated (Figure 2.1C), as is to be expected from a cell line forcibly overexpressing a transgene. Furthermore, the residual RhoC expression in the ALDH (-) population is predominately RhoC G14V—a constitutively active form of RhoC—thus amplifying the effect of even low levels of expression. Therefore, the fact that several of the ALDH (-) MCF-10A G14V developed metastases is not surprising, and is in agreement with the hypothesis that RhoC expression is capable of promoting metastasis independent of BCSC status—although under endogenous conditions RhoC expression is closely associated with the BCSC population.

In agreement with this assertion we also observed metastasis in one mouse injected with ALDH (+) SUM149 shRhoC cells. As we previously observed, RhoC is preferentially expressed by the ALDH (+) population (Figures 2.1A, C-D) and although we were able to achieve significant RhoC knockdown, RhoC expression was not completely eliminated from SUM149 shRhoC cells. Accordingly, the remaining RhoC was primarily confined to the ALDH (+) population (Figure 2.1D).

Again, though correlative, this evidence supports the hypothesis that RhoC expression is both necessary and sufficient for BCSC metastasis.

It is also important to emphasize that, although mice injected with ALDH (-) MCF-10A G14V developed metastases, they did not develop primary tumors (Table 2.1). Although RhoC has been shown to function in tumorigenic processes such as angiogenesis (95), its primary function, as illustrated by our work here and that of others (55), is in driving breast cancer metastasis. We note that IBC is metastatic from its inception; therefore the decrease in tumor formation of ALDH (+) SUM149 shRhoC compared to SUM149 scrambled cells may be attributable to both the early contributions of RhoC-mediated metastatic properties to IBC tumorigenesis (such as secretion of angiogenic factors), as well as the minor role that RhoC plays in tumorigenesis.

The work presented here provides strong rationale for therapeutically targeting RhoC. RhoC has previously been shown to be essential for metastasis in a transgenic breast cancer model (55) and is overexpressed in many different cancer types (52-54)—in particular IBC (85), which presently lacks effective therapies—yet this is the first work to relate RhoC to BCSCs. To this end, our lab has designed a small molecule RhoC inhibitor which has shown good *in vitro* and *in vivo* efficacy with no apparent toxicity (unpublished data). As therapies targeting CSCs emerge (96), it will be important to address which CSC

populations are being targeted—the tumorigenic or the metastatic population—in order to effectively combat the disease.

Materials and Methods

Reagents

shRNA was purchased from Open Biosystems through the University of Michigan Life Science Institute High Throughput Screening Core. For western blotting, the following antibodies were used: rabbit anti-RhoC (Cell Signaling), goat anti-actin, and mouse anti-RhoA (Santa Cruz Biotechnology). Matrigel and growth factor-reduced Matrigel were purchased from BD Biosciences. The ALDEFLUOR assay kit was purchased from StemCell Technologies.

Cell Culture

Untransfected cell lines were cultured in Ham's F12 (SUM149) supplemented with 5% fetal bovine serum, or DMEM/F12 (MCF-10A) supplemented with 10% horse serum. Selection media for shRNA-transfected cells consisted of standard cell line media containing 1µg/ml puromycin. Selection media for RhoC or RhoC G14V-transfected cells consisted of standard cell line media with 350µg/ml G418. MCF-10A cells were grown at 37°C in a humidified 5% CO_2 incubator, and SUM149 cells were grown at 37°C in a humidified 10% CO_2 incubator.

For 3D cell culture, cells were cultured as described by Lee et al. (89). Briefly, 4-well chamber slides (Lab-Tek) were coated with growth factor-reduced Matrigel (BD Biosciences). Cells were plated at a density of 2.1 x 10^4 cells/cm^2 in cell media containing 4% Matrigel and cultured for 7 days.

Time-Lapse Microscopy

DIC time-lapse videos were captured at 37°C using a Deltavision RT Live Cell Imaging System at the University of Michigan Microscopy and Image Analysis Lab. Images were acquired using SoftWoRx 3.5.1 software. Cell motility videos were analyzed using the MTrackJ plugin (http://www.imagescience.org/meijering/software/mtrackj/) for ImageJ (97), from which the average velocity of each cell line was calculated in µm/hour.

ALDEFLUOR Assay

The ALDEFLUOR assay was performed according to the manufacturer's instructions; see also (18).

Orthotopic Xenografts and Metastasis Analysis

All mouse work was performed in accordance with the University of Michigan's standards for animal use. After sorting into ALDH (+) and ALDH (-) populations with the ALDEFLUOR assay, cells were diluted 1:1 with Matrigel (BD Biosciences). NOD/SCID mice were anesthetized and 50 (SUM149 and variants) or 5000 (MCF-10A and variants) cells were injected directly into the fourth

mammary gland. Tumors were monitored weekly and mice were euthanized once tumor volume approached 2 cm^3 or mice showed signs of morbidity. Lungs were analyzed at the time of euthanization for macroscopic metastases. Tumors and lungs were then resected, fixed in 10% formalin, paraffin embedded, and stained with hematoxylin and eaosin.

In situ detection and quantification of protein expression

Tumors and Patients

Fresh and formalin-fixed, paraffin-embedded tissue blocks (FFPE) of breast cancer were obtained from the files of the Department of Pathology, University of Michigan Medical Center, Ann Arbor, MI. IRB approval was obtained and the diagnosis was confirmed by morphology. After pathological review, a tissue microarray was constructed from the most representative area using the methodology of Nocito et al. (98). Survival data was obtained from the Cancer Registry of The University of Michigan.

Immunohistochemical Staining and AQUA analysis.

Triple immunofluorescence staining was performed as previously described (99) and the AQUA system (HistoRx, New Haven, Connecticut) was used for the automated image acquisition and analysis. The detailed staining and imaging procedure can be found in the Supplemental Experimental Procedures.

Statistical Analysis

All p-values were calculated by Student's two-tailed t-test unless otherwise noted. Expression levels of ALDH1 and RhoC in TMA samples were compared using Spearman's rank coefficient.
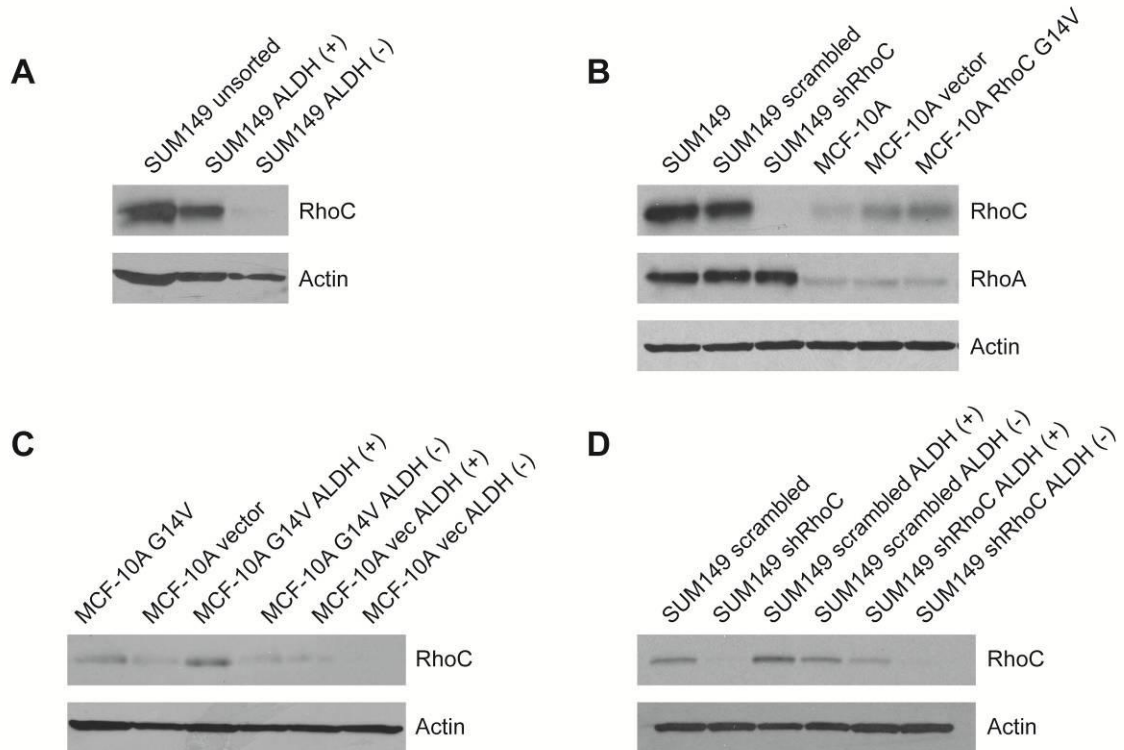
Figure 2.1 – RhoC expression is intimately linked to the ALDH (+) breast cancer stem cell population. (**A**) RhoC expression is directly related to breast cancer stem cell status in the highly aggressive, RhoC-overexpressing SUM149 IBC cell line. ALDH (+) SUM149 cells have high RhoC expression, whereas RhoC expression is significantly reduced in the ALDH (-) population. (**B**) To investigate the 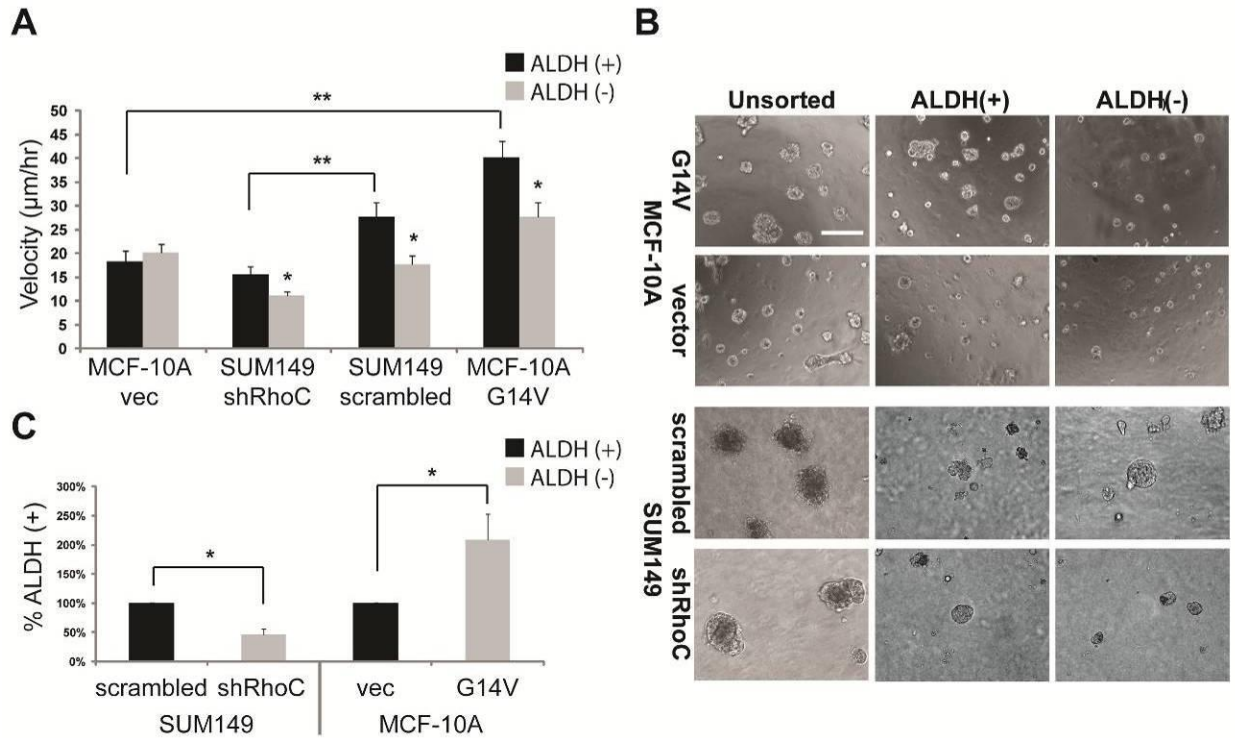effect of RhoC expression on breast cancer stem cell behavior we knocked down RhoC expression in SUM149 cells and, conversely, overexpressed a constitutively active form of RhoC (RhoC G14V) in the low RhoC-expressing normal-like mammary epithelial cell line MCF-10A. Importantly, modulating RhoC expression did not affect expression of the close homolog RhoA. (**C-D**) Interestingly, even when RhoC is exogenously expressed or inhibited in MCF-10A (**C**) or SUM149 cells (**D**), RhoC expression still segregates to the ALDH (+) population.

Figure 2.2 – RhoC dictates the behavior and abundance of breast cancer stem cells. (**A**) RhoC expression determines cell speed, even within the ALDH (+) population. Comparing the ALDH (+) populations of each cell line, modulating RhoC expression results in a corresponding change in cell speed (i.e. decreased cell speed in 149 shRhoC ALDH (+) compared to 149 scrambled ALDH (+)). Comparing between ALDH populations within a cell line, cell speed is decreased in the ALDH (-) population, concurrent with RhoC expression (Figure 2.1C-D). (**B**) Cell growth in 3D Matrigel culture reflects RhoC expression. Cells with high RhoC expression (149 scrambled and 10A G14V) exhibit aggressive, invasive growth in 3D culture, whereas cells with low RhoC expression (149 shRhoC and 10A vec) do not invade outward into the surrounding matrix (see "unsorted"). When sorted for ALDH, this invasive outgrowth is restricted to the ALDH (+) fraction of the high RhoC-expressing cell lines, suggesting that the aggressiveness of ALDH (+) breast cancer cells is reliant on RhoC (scale = 100 µm). (**C**) In addition to modifying the behavior of ALDH (+) cells, RhoC expression also alters the abundance of ALDH (+) BCSCs within a cell line. The percent of ALDH (+) cells is decreased by over 50% in 149 shRhoC compared to 149 scrambled cells, and is doubled in 10A G14V compared to 10A vector cells.

50
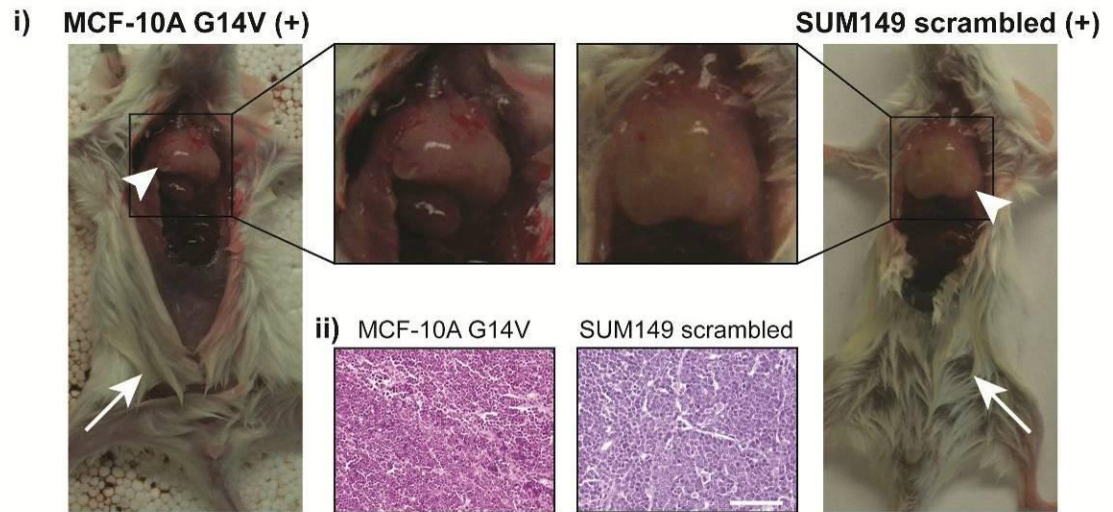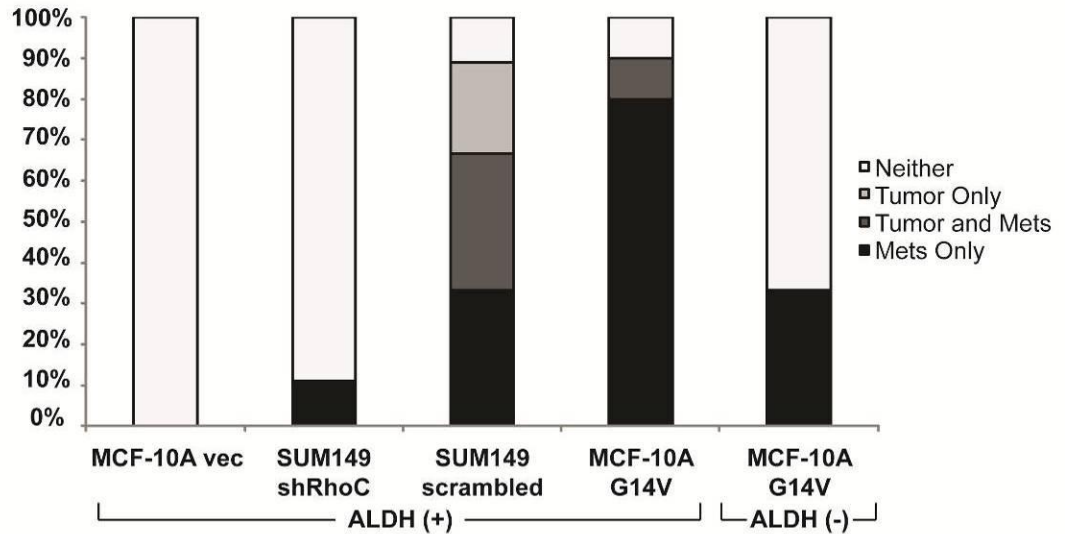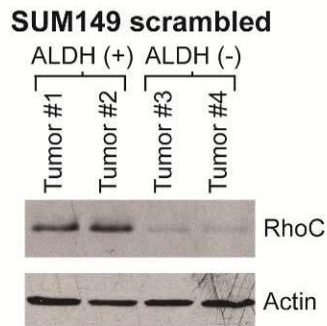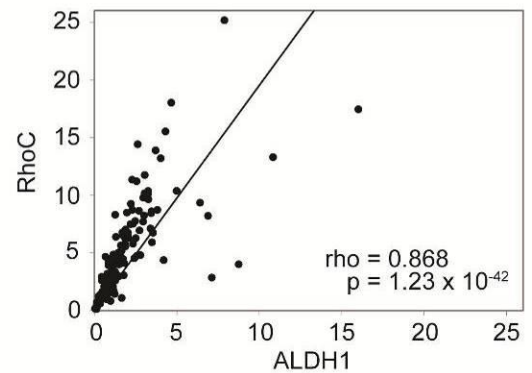
Figure 2.3 – RhoC expression determines the metastatic potential of ALDH (+) breast cancer stem cells. (**A**) NOD/SCID mice orthotopically xenografted with only 50 SUM149 or 5000 MCF-10A RhoC-expressing breast cancer stem

cells form large lung metastases, often independent of primary tumor formation. **i**) Arrows indicate injection sites lacking primary tumors, arrowheads indicate lung metastases. **ii**) H&E-staining shows that lung metastases from both MCF-10A G14V and SUM149 scrambled cells are poorly differentiated, invasive carcinomas (scale = 50 μm) (**B**) Quantitative analysis of xenografted mice establishes RhoC as a driving force behind ALDH (+) BCSC lung metastasis (also see Table 2.1). MCF-10A cells, which do not have the genetic mutations required to initiate primary tumor formation, instead metastasize independent of primary tumor formation when forced to overexpress active RhoC (RhoC G14V). Note that even ALDH (-) 10A G14V, which have reduced but not completely eliminated active RhoC expression, do not form primary tumors but can still metastasize, albeit less frequently, than ALDH (+) 10A G14V. Importantly, the incidence of cancer drops from greater than 85% in ALDH (+) 149 scrambled and 10A G14V mice to less than 13% in ALDH (+) 149 shRhoC and 10A vec mice, demonstrating the essential role RhoC plays in the aggressiveness of breast cancer stem cells *in vivo*. (**C**) Injecting mice with 5000 SUM149 scrambled cells—at which point both the ALDH (+) and ALDH (-) populations form tumors—reveals that reduced RhoC expression is maintained *in vivo* in ALDH (-) tumors. This provides mechanistic evidence for the inability of ALDH (-) cells to metastasize (their inability to reexpress RhoC), and speaks to the inability of the ALDH (-) population to reconstitute tumor heterogeneity. (**D**) RhoC and ALDH1 expression are highly correlated in clinical breast cancer samples (Spearman's rho = 0.868, p = 1.23 x 10^{-42}, df = 134).

Xenograft Analysis

Cell Line	ALDH	Total Mice	Tumors	Lung Metastases
MCF-10A vector	+	8	0	0
	-	7	0	0
MCF-10A G14V	+	10	1 (10%)	9 (90%)
	-	6	0	2 (33.33%)
SUM149 scrambled	+	9	5 (55.56%)	6 (66.67%)
	-	9	0	0
SUM149 shRhoC	+	8	0	1 (12.50%)
	-	8	0	0

Fisher's Exact Test

	Metastases	
		ALDH+
Cell Line	p-value for ALDH	p-value for RhoC
MCF-10A vector	n.s.	0.0002
MCF-10A G14V	0.035	
SUM149 scrambled	0.0045	0.0364
SUM149 shRhoC	n.s.	

Table 2.1 – Analysis of xenografted mice.

Supplemental Methods

Immunohistochemical Staining and AQUA analysis.

Briefly, after deparaffinization and rehydration, TMA slides were subjected to microwave epitope retrieval in 10 mM sodium citrate buffer, pH6. After rinsing several times in 10 mM Tris/HCl buffer, pH 8 containing 0.154 M NaCl and 0.05%(v/v) Tween-20 (TBST), endogenous peroxidase activity was blocked with 2.5% (v/v) H_2O_2 in methanol for 30 minutes. Non-specific binding of the antibodies was extinguished by a 30 minute incubation with 'Background Sniper" (BioCare Medical, Concord, CA). The TMA slide was then incubated with a combination of the tumor-specific antibody, cytokeratin (DAKO, Carpinteria, CA, rabbit polyclonal antibody, Z0622, 1:250) and ALDH1 (BD Biosciences, mouse monoclonal antibody, 611195, 1:100) overnight at 4C. The slides were then washed with TBST twice for 5 minutes. The slides were subsequently incubated with an antibody to RhoC (chicken IgY polyclonal antibody, 1:1000) for 60 minutes at room temperature. Slides were then washed as described above and incubated with a combination of goat anti rabbit IgG conjugated to AF555 (Molecular probes, Carpinteria, CA, A21428, 1:200) and goat anti chicken IgY conjugated to AF488 (Molecular probes, Carpinteria, CA, A11039, 1:200) in goat anti mouse Envision+ (DAKO, Carpinteria, CA, K4001) for 60 minutes at room temperature in a dark humidity tray. The slides were then washed as described above and the target image was developed by a CSA reaction of Cy5 labeled tyramide (PerkinElmer, Waltham, MA, 1:50). The slides were washed with 3 changes of water and stained with the DNA staining dye 4',6-diaminodo-2-

54

phenylindole (DAPI) in a non-fading mounting media (ProLong Gold, Molecular probes, Carpinteria, CA). The slides were allowed to dry overnight in a dark dry chamber and the edges were sealed.

For AQUA, images of each TMA core were captured with an Olympus BX51 microscope at 4 different extinction/emission wavelengths. Within each TMA spot, the area of tumor was distinguished from stromal and necrotic areas by creating a tumor specific mask from the anti-CK protein, which was visualized from Alexafluor 555 signal. The DAPI image was then used to differentiate between the cytoplasmic and nuclear staining within the tumor mask. The pixel intensity of the RhoC protein/antibody complex was determined from the AF488 signal, and finally, the fluorescence pixel intensity of the ALDH1 protein/antibody complex was obtained from the Cy5 signal and reported as pixel intensity.

This chapter represents a "manuscript in progress" and will be submitted for publication under the title "RhoC determines the metastatic potential and affects the abundance of breast cancer stem cells" by Devin T. Rosenthal, Jie Zhang, Liwei Bao, Lian Zhu, Kathy Toy, Zhifen Wu, Celina G. Kleer, and Sofia D. Merajver.

55

References

17.   Al-Hajj M, Wicha MS, Benito-Hernandez A, Morrison SJ, Clarke MF. Prospective identification of tumorigenic breast cancer cells. Proc Natl Acad Sci U S A. 2003;100:3983-8.

18.   Ginestier C, Hur MH, Charafe-Jauffret E, Monville F, Dutcher J, Brown M, et al. ALDH1 is a marker of normal and malignant human mammary stem cells and a predictor of poor clinical outcome. Cell Stem Cell. 2007;1:555-67.

19.   Dean M, Fojo T, Bates S. Tumour stem cells and drug resistance. Nat Rev Cancer. 2005;5:275-84.

21.   Mani SA, Guo W, Liao MJ, Eaton EN, Ayyanan A, Zhou AY, et al. The epithelial-mesenchymal transition generates cells with properties of stem cells. Cell. 2008;133:704-15.

22.   Liu R, Wang X, Chen GY, Dalerba P, Gurney A, Hoey T, et al. The prognostic role of a gene signature from tumorigenic breast-cancer cells. N Engl J Med. 2007;356:217-26.

23.   Liu H, Patel MR, Prescher JA, Patsialou A, Qian D, Lin J, et al. Cancer stem cells from human breast tumors are involved in spontaneous metastases in orthotopic mouse models. Proc Natl Acad Sci U S A. 2010;107:18115-20.

24.   Charafe-Jauffret E, Ginestier C, Iovino F, Tarpin C, Diebel M, Esterni B, et al. Aldehyde dehydrogenase 1-positive cancer stem cells mediate metastasis and poor clinical outcome in inflammatory breast cancer. Clin Cancer Res. 2010;16:45-55.

25.   Hermann PC, Huber SL, Herrler T, Aicher A, Ellwart JW, Guba M, et al. Distinct populations of cancer stem cells determine tumor growth and metastatic activity in human pancreatic cancer. Cell Stem Cell. 2007;1:313-23.

26.   Pang R, Law WL, Chu AC, Poon JT, Lam CS, Chow AK, et al. A subpopulation of CD26+ cancer stem cells with metastatic capacity in human colorectal cancer. Cell Stem Cell. 2010;6:603-15.

40.   Rosenthal DT, Brenner JC, Merajver SD. Rho Proteins in Cancer. In: van Golen KL, editor. The Rho GTPases in Cancer. New York: Springer New York; 2010. p. 29-42.

47.   Wheeler AP, Ridley AJ. Why three Rho proteins? RhoA, RhoB, RhoC, and cell motility. Exp Cell Res. 2004;301:43-9.

48.   Ridley AJ. The GTP-binding protein Rho. Int J Biochem Cell Biol. 1997;29:1225-9.

51.   van Golen KL, Wu ZF, Qiao XT, Bao LW, Merajver SD. RhoC GTPase, a novel transforming oncogene for human mammary epithelial cells that partially recapitulates the inflammatory breast cancer phenotype. Cancer Res. 2000;60:5832-8.

52.   Clark EA, Golub TR, Lander ES, Hynes RO. Genomic analysis of metastasis reveals an essential role for RhoC. Nature. 2000;406:532-5.

53.   Ikoma T, Takahashi T, Nagano S, Li YM, Ohno Y, Ando K, et al. A definitive role of RhoC in metastasis of orthotopic lung cancer in mice. Clin Cancer Res. 2004;10:1192-200.

54.   Islam M, Lin G, Brenner JC, Pan Q, Merajver SD, Hou Y, et al. RhoC expression and head and neck cancer metastasis. Mol Cancer Res. 2009;7:1771-80.

55.   Hakem A, Sanchez-Sweatman O, You-Ten A, Duncan G, Wakeham A, Khokha R, et al. RhoC is dispensable for embryogenesis and tumor initiation but essential for metastasis. Genes Dev. 2005;19:1974-9.

83.   Reya T, Morrison SJ, Clarke MF, Weissman IL. Stem cells, cancer, and cancer stem cells. Nature. 2001;414:105-11.

84.   Clevers H. The cancer stem cell: premises, promises and challenges. Nat Med. 2011;17:313-9.

85.   van Golen KL, Davies S, Wu ZF, Wang Y, Bucana CD, Root H, et al. A novel putative low-affinity insulin-like growth factor-binding protein, LIBC (lost in inflammatory breast cancer), and RhoC GTPase correlate with the inflammatory breast cancer phenotype. Clin Cancer Res. 1999;5:2511-9.

86.   Hanahan D, Weinberg RA. The hallmarks of cancer. Cell. 2000;100:57-70.

87.   Dietrich KA, Schwarz R, Liska M, Grass S, Menke A, Meister M, et al. Specific induction of migration and invasion of pancreatic carcinoma cells by RhoC, which differs from RhoA in its localisation and activity. Biol Chem. 2009;390:1063-77.

88.   Debnath J, Brugge JS. Modelling glandular epithelial cancers in three-dimensional cultures. Nat Rev Cancer. 2005;5:675-88.

89.   Lee GY, Kenny PA, Lee EH, Bissell MJ. Three-dimensional culture models of normal and malignant breast epithelial cells. Nat Methods. 2007;4:359-65.

90.   Kenny PA, Lee GY, Myers CA, Neve RM, Semeiks JR, Spellman PT, et al. The morphologies of breast cancer cell lines in three-dimensional assays correlate with their profiles of gene expression. Mol Oncol. 2007;1:84-96.

91.   Singh SK, Clarke ID, Terasaki M, Bonn VE, Hawkins C, Squire J, et al. Identification of a cancer stem cell in human brain tumors. Cancer Res. 2003;63:5821-8.

92.   Collins AT, Berry PA, Hyde C, Stower MJ, Maitland NJ. Prospective identification of tumorigenic prostate cancer stem cells. Cancer Res. 2005;65:10946-51.

93.   Korkaya H, Paulson A, Iovino F, Wicha MS. HER2 regulates the mammary stem/progenitor cell population driving tumorigenesis and invasion. Oncogene. 2008;27:6120-30.

94.   Kleer CG, Griffith KA, Sabel MS, Gallagher G, van Golen KL, Wu ZF, et al. RhoC-GTPase is a novel tissue biomarker associated with biologically aggressive carcinomas of the breast. Breast Cancer Res Treat. 2005;93:101-10.

95.   van Golen KL, Wu ZF, Qiao XT, Bao L, Merajver SD. RhoC GTPase overexpression modulates induction of angiogenic factors in breast cells. Neoplasia. 2000;2:418-25.

96.   Gupta PB, Onder TT, Jiang G, Tao K, Kuperwasser C, Weinberg RA, et al. Identification of selective inhibitors of cancer stem cells by high-throughput screening. Cell. 2009;138:645-59.

97.   Abramoff MD, Magelhaes PJ, Ram SJ. Image Processing with ImageJ. Biophotonics International. 2004;11:36-42.

98.	Nocito A, Kononen J, Kallioniemi OP, Sauter G. Tissue microarrays (TMAs) for high-throughput molecular pathology research. Int J Cancer. 2001;94:1-5.

99.	McCabe A, Dolled-Filhart M, Camp RL, Rimm DL. Automated quantitative analysis (AQUA) of in situ protein expression, antibody concentration, and prognosis. J Natl Cancer Inst. 2005;97:1808-15.

Chapter III

p38γ regulates breast cancer cell motility and metastasis through modulation of RhoC GTPase

Abstract

Understanding the molecular alterations that confer metastatic properties, such as increased motility, to otherwise benign breast cells is essential to controlling breast cancer and increasing patient survival. We show for the first time that p38γ MAPK regulates cell motility and metastasis of aggressive breast cancer cells and is associated with the basal breast cancer subtype. p38γ elicits its effects on cell motility by affecting expression of another metastasis-associated protein, RhoC, through a novel mode of regulation: modulation of RhoC ubiquitination. We uncover a mechanistic sequence of events whereby p38γ knockdown results in increased RhoC ubiquitination and a subsequent decrease in RhoC protein expression, as mediated by lysosomal degradation, ultimately resulting in decreased cell motility. The p38γ-RhoC relationship persists across multiple cell lines and in clinical breast cancer specimens. We find that p38γ has important clinical relevance, as high p38γ expression is associated with lower overall survival of breast cancer patients. The data presented here 1) provides a detailed characterization of how p38γ contributes to breast cancer progression,

2) identifies a novel mechanism for regulating RhoC expression, and 3) nominates p38γ as an important therapeutic target.

Introduction

Breast cancer presents as a hyperproliferative disease of mammary epithelial cells, which can grow uncontrollably for years yet remain confined within mammary ducts or lobules. If diagnosed at this early stage the disease responds well to therapeutic intervention (100). Breast cancer becomes much more severe once the cancer cells invade out of the mammary ducts and metastasize to vital organs. Understanding the molecular alterations that confer metastatic properties, such as motility and invasion, to otherwise benign cells is essential to controlling the disease and significantly improving patient survival.

p38 MAPK is a serine/threonine kinase responsible for integrating extracellular stimuli and translating them into cellular responses by phosphorylating a network of downstream effector proteins (57). The p38 arm of the MAPK pathway is effected by four closely related isoforms: p38 α, β, γ and δ. Despite their sequence similarity and shared upstream kinases, the p38 isoforms can have unrelated, and even antagonistic, roles in development and disease (59-63).

p38γ (also referred to as MAPK12, ERK6, or SAPK3) is expressed predominantly in muscle tissue where it promotes myoblast differentiation into myotubes (71-74). p38γ mRNA is overexpressed in several types of cancer (78, 79) and helps

increase Ras-induced cancer invasion (81, 82). Viewing the function of p38γ through the perspective of its developmental role led us to hypothesize that p38γ is involved in enabling mesenchymal-like behavior in breast cancer cells by controlling their motility properties.

Using p38γ-specific small hairpin RNA (shRNA), siRNA, and a dominant negative construct we reveal that p38γ is a crucial mediator of cellular motility and metastasis of aggressive breast cancer cells. p38γ elicits its effects at least in part through RhoC GTPase by affecting RhoC ubiquitination and degradation – a mechanism of regulation never before observed for RhoC. p38γ and RhoC expression are highly correlated in clinical breast cancer samples, and re-expressing RhoC restores motility to p38γ knockdown cells. Clinically, high p38γ expression in patient tissues is associated with the basal breast cancer subtype and confers a worse prognosis. The data presented here establish for the first time that p38γ is a metastasis-promoting gene responsible for enabling motility and metastasis of aggressive breast cancer cells through modulation of RhoC.

Results

p38γ phosphorylation is elevated in an aggressive breast cancer cell line

p38 is activated by dual phosphorylation on the Thr and Tyr residues of the conserved TGY motif (60, 101). To assess whether p38γ is functionally relevant in aggressive breast cancer, we assayed the levels of phospho-p38γ in a representative and widely used aggressive breast cancer cell line, MDA-MB-231

("231 cells"). Compared to the non-tumorigenic mammary epithelial cell line MCF-10A, 231 cells have increased levels of phosphorylated p38γ despite similar levels of total p38γ (Figure 3.1A).

To investigate the role of p38γ on the metastatic phenotypic features of 231 cells we used small hairpin RNA ("shRNA") to stably knock down p38γ expression (Figure 3.1B). Importantly, the shRNA did not affect expression of the other three p38 isoforms (data not shown). Since there is no p38γ-specific pharmacologic inhibitor we overexpressed dominant negative p38γ (102) ("DNp38γ") in MDA-MB-231 cells as an additional method to inhibit p38γ (See Supplementary Methods and Figure 3.S1).

Cell shape and cytoskeletal architecture are altered by p38γ knockdown

Immediately apparent in the p38γ knockdown cells ("shp38γ cells") was a change in cell morphology compared to scrambled control cells ("scrambled cells"). While scrambled cells exhibited the elongated morphology characteristic of 231 cells and mesenchymal cells in general, shp38γ cells adopted a more rounded cell shape (Figure 3.1C), as did DNp38γ cells (Figure 3.S1C). This change was shown quantitatively by measuring the cells' aspect ratio (see Methods). As depicted in Figure 3.1C (right), shp38γ cells are significantly less elongated than their scrambled counterparts (aspect ratio of scrambled = 4.27, shp38γ = 0.81, p-value = 7.82×10^{-7}).

Extending from this observation we asked whether the actin cytoskeleton was modified in shp38γ cells. Using immunofluorescent confocal microscopy we observed that shp38γ cells have a strikingly disorganized actin cytoskeleton (Figure 3.1D), as do DNp38γ cells (Figure 3.S1E). Scrambled cells form long actin stress fibers traversing the length of the cell characteristic of mesenchymal-like cells, well-aligned along the long axis (Figure 3.1D, left). shp38γ cells still have thick actin bundles resembling the stress fibers in the scrambled cells, but with a bimodal distribution and are primarily confined to the leading edge (Figure 3.1D, right). This cluster of actin bundles forms the lamellipodia-like structure present in shp38γ cells (Figures 3.1C-D) but shows little similarity to classic lamellipodia cytoskeletal architecture, which normally consists of thin branched actin filaments forming a protrusive meshwork (103).

p38γ knockdown dramatically alters cell motility

Elongated cell shape is one factor that can delineate the mode of motility used by a cell and distinguish metastatic from non-metastatic cancer cells *in vitro* (104, 105). To determine whether the rounded shape and modified cytoskeletal architecture of the shp38γ cells indicated a change in metastatic properties we first analyzed cell motility using time lapse microscopy.

p38γ knockdown had a profound effect on the quality of cell motility (Figure 3.2A) and on the velocity (Figure 3.2B). Scrambled control cells moved in a mesenchymal-like manner, consistent with their appearance and cytoskeletal

structure, forming long pseudopodial projections that adhered to the cell substrate and allowed the cells to "pull" themselves along in alternating cycles of protrusion and contraction (Figure 3.2A, top, and Video 1). shp38γ cells, however, appeared to have difficulty polarizing and were unable to form long pseudopodia (Figure 3.2A, bottom, and Video 1). The cells moved inefficiently using a broad lamellipodia-like structure and exhibited detachment anomalies at the rear of the cell.

To quantitatively assess the effect of p38γ knockdown on cell motility, cell tracks were generated and the resulting trajectories were measured (Figure 3.2B). shp38γ cells were less motile than scrambled control cells, as evidenced by significantly reduced cell speed (Figure 3.2B). Taken together, these data show that p38γ knockdown affects cell shape and inhibits efficient mesenchymal-like motion in a qualitative and quantitative manner.

p38γ knockdown impairs the in vitro metastatic behavior of 231 cells

Based on the reduced motility of the shp38γ cells we asked whether p38γ also affects other aspects of breast cancer metastasis. A crucial step in the metastatic process is invasion through the basement membrane that separates the epithelial ductal layers from the connective tissue parenchyma. When subjected to a Matrigel invasion assay shp38γ cells exhibited a 40% reduction in invasion compared to scrambled cells (Figure 3.2C), indicating that p38γ functions in this important early stage of metastasis.

64

To replicate *in vitro* the possible behavior *in vivo* we employed a three-dimensional cell culture system capable of promoting normal development of breast epithelial cells as well as illustrating the specific tumorigenic and metastatic properties of breast cancer cells (88, 89). Scrambled cells grown in 3D exhibited a stellate morphology characteristic of metastatic cells (Figure 3.2D, top) (89, 90). The cells were not organized into cohesive structures and invaded away from the central mass through the surrounding extracellular matrix. In contrast, shp38γ and DNp38γ cells formed non-invasive round acinar-like structures (Figure 3.2D, bottom, and Figure 3.S1D). Interestingly, shp38γ cells still did not form proper acini, as shown by an inability to apoptotically clear the lumen (Figure 3.2D, right). Taken together, these results strongly support a role for p38γ in the early steps of breast cancer metastasis.

Expression of the cytoskeletal remodeler and metastatic oncogene RhoC is decreased in shp38γ cells

The Rho-family GTPases (Rac, Rho, and cdc42) are the classic regulators of actin cytoskeletal dynamics driving cell motility (106). Based on the actin cytoskeletal changes and motility defects we observed we hypothesized that p38γ knockdown affected members of the Rho GTPase family. Interestingly, we found that RhoC GTPase protein levels were strongly downregulated in both shp38γ and DNp38γ cells (Figure 3.3A and S1F) with no change in the close homolog RhoA (data not shown). Surprisingly, RhoC mRNA levels were not

affected by p38γ knockdown (Figure 3.3B), suggesting that p38γ influences RhoC expression at the translational or post-translational level.

p38γ knockdown leads to increased RhoC ubiquitination and degradation

To determine whether p38γ affects RhoC expression at the translational or post-translational level we treated scrambled and shp38γ cells with the translation inhibitor cycloheximide and observed the effect on protein expression. Cycloheximide treatment caused a rapid decrease in RhoC protein levels in shp38γ cells with no corresponding decrease in scrambled cells (Figure 3.3C), indicating that RhoC protein is less stable in shp38γ cells.

Upon observing this change in RhoC protein stability we asked whether RhoC was ubiquitinated in shp38γ cells—a common marker of proteins slated for degradation. When we assayed RhoC ubiquitination we found that levels of ubiquitinated RhoC were increased in shp38γ cells compared to scrambled cells (Figure 3.3D).

To elucidate the mechanism by which RhoC is degraded we treated cells with either proteasome inhibitors (MG132 or lactacystin) or lysosome inhibitors (ammonium chloride or chloroquine) and observed the effect on RhoC protein levels. Inhibiting the lysosome led to an increase in RhoC protein (Figure 3.3E) whereas proteasome inhibitors had no effect on RhoC expression (data not shown), indicating that ubiquitinated RhoC is degraded by the lysosome. Taken

together, these data support the conclusion that p38γ affects RhoC expression by mediating RhoC protein stability through regulation of RhoC ubiquitination and lysosomal degradation.

Rescuing RhoC expression restores motility to shp38γ cells

Based on the established role that RhoC plays in cell motility (47) we hypothesized that decreased RhoC expression in shp38γ cells may directly contribute to the impaired motility of shp38γ cells. To test this hypothesis we stably transfected either RhoC or a constitutively active form of RhoC (RhoC G14V) into shp38γ cells to see if this could restore motility to these cells (Figure 3.4A). It is important to note that we selected two clones for each form of RhoC— one low expressing and one high expressing—to ensure that any effects we observed were not simply due to unrealistically high expression of the transfected gene.

When we observed the motility of the transfected clones we found that re-expressing RhoC significantly increased motility of the shp38γ cells to levels comparable to scrambled control cells (Figure 3.4B). Interestingly, the increase in cell speed seemed to have a near-linear relationship with RhoC expression/activity. Combined with our previous observations, these data establish a novel mechanistic link whereby p38γ directs cell motility through stabilization of RhoC protein.

p38γ and RhoC expression are highly correlated in human breast cancer tissues

We next asked whether the relationship between p38γ and RhoC persists in human breast cancer tissues. To address this question we assayed expression of p38γ and RhoC using AQUA of immunofluorescence signals for each marker in cytokeratin-positive cells from a breast cancer tissue microarray. Analysis of 177 breast cancer specimens revealed a strong positive correlation between p38γ and RhoC expression (Figure 3.4C). Taken together with our *in vitro* results, these data strongly support a relationship between p38γ and RhoC in breast cancer, one that likely involves p38γ regulation of RhoC expression.

p38γ affects the metastatic properties of other aggressive breast cancer cell lines

Because p38γ specifically alters the actomyosin contractile motility of MDA-MB-231 cells by affecting RhoC expression, we asked whether p38γ plays a similar role in other mesenchymal-like breast cancer cell lines. To address this question we used two additional widely studied breast cancer cell lines – Hs578t and BT549 – both of which have increased levels of phosphorylated p38γ compared to both MCF-10A and HME non-tumorigenic mammary epithelial cells (Figure 3.5A). Using siRNA, we transiently knocked down p38γ expression in these two cell lines (Figure 3.5B) and observed the effects on the actin cytoskeleton and cell motility.

siRNA knockdown of p38γ ("sip38γ") dramatically affected the actin cytoskeletal architecture and cell shape of both cell lines in a manner consistent with 231 shp38γ cells (Figure 3.5C-D). Accordingly, sip38γ cells moved significantly less than scrambled cells (Figure 3.5E-F). p38γ knockdown in these cell lines also reduced RhoC expression (Figure 3.5G). Taken together, these results support our conclusion that p38γ plays a crucial role in driving the motility of aggressive breast cancer cells by modulating RhoC expression.

p38γ is related to the basal breast cancer subtype

Having discovered that p38γ is associated with mesenchymal-like cell motility and is overactivated in three basal breast cancer cell lines, we hypothesized that p38γ is associated with the basal breast cancer subtype. To test this hypothesis we assayed p38γ expression in 43 breast cancer patient samples which were previously analyzed for molecular subtype by PAM50 (107). We found that the basal subtype is significantly enriched in the top quartile of p38γ-expressing tumors ($p = 0.018$, Figure 3.6A), whereas none of the other subtypes examined showed significant association with p38γ expression (data not shown). Taken together with our *in vitro* data on p38γ function in mesenchymal-like cell behavior, this clinical data strongly supports an association between high p38γ expression and the aggressive basal breast cancer subtype.

p38γ promotes breast cancer metastasis in vivo and is clinically associated with lower overall patient survival

Based on our *in vitro* observations we hypothesized that p38γ knockdown would reduce the metastatic potential of MDA-MB-231 breast cancer cells *in vivo*. To test this hypothesis we orthotopically xenografted athymic nude mice with 231 scrambled and shp38γ cells and allowed tumors to grow for 14 weeks, at which point we resected the tumors and analyzed the lymphatics for signs of tumor cell metastasis. Two-thirds of the mice injected with scrambled cells presented with lymphatic invasion and metastasis, compared to just over one-tenth of shp38γ-injected mice (Figure 3.6B-C). This *in vivo* data, combined with the extensive body of *in vitro* data presented here, strongly implicate p38γ as a metastatic oncogene that exerts its effects, at least in part, by driving cell motility through regulation of RhoC.

As a final means of determining the clinical relevance of p38γ expression we assayed p38γ expression in a cohort of 118 breast cancer cases containing patient survival data. Using the upper quartile of p38γ expression as a cutoff reveals a significant association between high p38γ expression and lower overall patient survival (p = 0.013, Figure 3.6D). This clinical data supports our *in vitro* and *in vivo* findings that p38γ is an important mediator of breast cancer cell aggressiveness, and establishes that p38γ expression has important implications for breast cancer patient outcome.

Discussion

As the breast is a non-vital organ, primary tumor burden is very rarely the direct cause of cancer-specific mortality. Instead, metastasis of cells from the primary tumor to vital organs results in patient death. Here we demonstrate that p38γ is a novel metastasis-modulating oncogene, deduce a mechanistic link between p38γ, its effect on RhoC, and the shp38γ phenotype, and reveal that this link has clinical relevance.

The importance of the p38 MAPK pathway in cancer has been appreciated (59, 108), but very diverse and sometimes contradictory roles have been described for p38 in cancer (79). In agreement with other recent findings (82, 109) we show that at least some of the heterogeneity of p38 functions may be attributed to the distinct contributions of specific p38 isoforms. Since the p38 MAPK pathway is a ubiquitously utilized stress-responsive pathway, it logically follows that metastasizing cancer cells, which encounter an ever-changing milieu of cellular stresses, may gain survival advantages under these stressed conditions upon modulation of the appropriate p38 MAPK isoforms; thus, dissecting the contributions of each p38 isoform would allow more precise targeting of specific subsets of cancer.

In support of this assertion we found that p38γ is more frequently associated with the basal breast cancer subtype – the most lethal molecular breast cancer

71

subtype. p38γ is thus an especially promising drug target as, in addition to the data presented here, it is a kinase, has restricted tissue expression (71, 73, 74), and lacks a phenotype when knocked out in mice (68)—possibly indicating that its inhibition may offer a differential detrimental effect on tumor versus normal cells.

Similarly to mediators of normal mesenchymal differentiation, such as twist and snail, which have been shown to also be important drivers of cancer progression (15, 110), so is the case for p38γ. p38γ functions in muscle cell differentiation, and thus it is consistent that it plays a role in aggressive, mesenchymal-like breast cancer cells. Interestingly, p38γ appears to exert its effects independent of classical cell differentiation markers, as p38γ knockdown does not alter expression of epithelial-to-mesenchymal transition markers such as vimentin or E-cadherin (data not shown) despite significantly reverting the mesenchymal-like phenotype of aggressive breast cancer cells. Although there are many other genes that have been shown to drive metastatic transition (111), based on the data presented here and in another recent publication (112) we propose that p38γ serves as a crucial regulator of the major cytoskeletal changes necessary for the switch to rapid, mesenchymal-like cell motility—independent of differentiation status—at least in part through its modulation of the major cytoskeletal modifier and metastatic oncogene RhoC.

RhoC is involved in stress fiber formation and actomyosin contraction (51, 113)—both of which are perturbed by p38γ knockdown—and has previously been linked to the p38 MAPK pathway (56). RhoC also promotes metastasis in several types of cancer, including breast (51-54), and plays a larger role in stress fiber formation and contraction than RhoA (49); thus we postulated that changes in RhoC expression influence the shp38γ phenotype. In support of this hypothesis we found that re-expressing RhoC alone was sufficient to restore motility to shp38γ cells—a surprising feat, given the multitude of proteins involved in cell motility (39, 40), which highlights the importance of RhoC in p38γ-mediated cell motility. Further supporting the link between p38γ and RhoC is our finding that expression of the two proteins is concurrently altered in clinical breast cancer specimens (Figure 3.4A), suggesting that the p38γ-RhoC axis may be functionally significant—and a potentially druggable target—in the clinic.

In our investigation of the interaction between p38γ and RhoC we discovered that p38γ regulates RhoC expression by preventing RhoC ubiquitination and subsequent lysosomal degradation. Ubiquitination and protein degradation have recently emerged as important mechanisms for regulating Rho GTPase expression (114), however this is the first demonstration of modulating RhoC ubiquitination as a relatively fast mechanism that can regulate RhoC action within a time domain relevant to cell motion. Further research into the specific proteins and mechanisms regulating ubiquitination of RhoC and other Rho GTPases

should have significant impact on our understanding how cell motility and metastasis are regulated.

We found that RhoC was degraded by the lysosome, rather than through the canonical proteasome degradation pathway. Although proteasomal degradation is by far the dominant mechanism for protein degradation under stress-free conditions, interestingly lysosomal degradation accounts for nearly 40% of protein degradation in muscle cells.

Research such as this may also be readily applicable to the clinic, specifically in the case of aggressive cancer subtypes—most notably inflammatory breast cancer (IBC)—which may rely on RhoC expression for metastasis. Targeting the proteins that regulate RhoC expression, in addition to or in place of targeting RhoC directly, should impact diseases such as IBC, which currently lacks effective treatments.

Materials and Methods

Reagents

shRNA was purchased from Open Biosystems through the University of Michigan Life Science Institute High Throughput Screening Core. A dominant negative p38γ plasmid (102) (Addgene plasmid 20354) was a kind gift from Roger Davis. FITC-labeled siRNA, cycloheximide, chloroquine, and ammonium chloride were purchased from Sigma Aldrich. For western blotting the following antibodies were

used: rabbit anti-p38α, anti-p38β, anti-p38γ, anti-p38δ, anti-RhoC, and mouse anti-phospho-p38 (Cell Signaling); goat anti-actin and mouse anti-ubiquitin (Santa Cruz Biotechnology); and mouse anti-hemagglutinin (Covance).

Cell Lines

Untransfected cell lines were cultured in RPMI 1640 (MDA-MB-231, BT549) or DMEM (Hs578t) supplemented with 10% fetal bovine serum, or DMEM/F12 (MCF-10A) supplemented with 10% horse serum. Selection media for shRNA-transfected cells consisted of standard cell line media containing 1μg/ml puromycin. MDA-MB-231 stably transfected with both shRNA and RhoC/RhoC G14V were cultured in standard cell line media containing 1μg/ml puromycin and 350μg/ml G418. All cell lines were grown at 37°C in a humidified 5% CO_2 incubator.

Transfections

2 μg of pGIPZ plasmid containing either scrambled or p38γ-specific shRNA were nucleofected into 50-70% confluent MDA-MB-231 cells according to the manufacturer's protocol (Lonza). Nucleofected cells were selected in puromycin and further isolated by FACS sorting for GFP. The same nucleofection process was used for RhoC/G14V plasmids (cDNA.org). Nucleofected cells were selected in G418 and positive clones were isolated.

3 nM siRNA was transfected into 50-70% confluent BT549 and Hs578t cells using Oligofectamine (Invitrogen) according to the manufacturer's protocol. Gene expression and cell behavior were observed 48 hours post transfection.

Phospho-p38γ Immunoprecipitation/Western Blot

Protein was extracted from 70% confluent cells with RIPA buffer. Total protein extracts were incubated with primary antibody (anti-p38γ or anti-phospho-p38) overnight at 4°C. The following morning protein-antibody complexes were captured by incubation with protein A/G beads (Santa Cruz Biotechnology). Immunoprecipitates were run on an SDS-PAGE gel, transferred to a nitrocellulose membrane, and probed with the appropriate reciprocal antibody (anti-p38γ or anti-phospho-p38).

Aspect Ratio Calculation

Images were acquired at room temperature using a Leica DM IRB microscope equipped with a Leica 20x/0.4 NA objective and Hamamatsu ORCA-03G camera with Metamorph software. Aspect ratio calculations were performed using ImageJ (97). The aspect ratio formula is length over width – length defined as the greatest distance perpendicular to the cell's leading edge (as determined by cytoskeletal architecture), and width as the longest distance between points measured perpendicular to the axis defining the length. Therefore a cell that is elongated in the direction of motion will have an aspect ratio greater than 1, while a cell that is rounder will have a value closer to, or lower than, 1.

3D Cell Culture

Cells were cultured as described by Lee et al. (89). Briefly, 4-well chamber slides (Lab-Tek) were coated with growth factor-reduced Matrigel (BD Biosciences). Cells were plated at a density of 2.1 x 10^4 cells/cm^2 in cell media containing 4% Matrigel and cultured for 4 days. The same microscope and imaging conditions were used as above.

Time-Lapse Microscopy

DIC time-lapse videos were captured at 37°C using a Deltavision RT Live Cell Imaging System equipped with UPlanApo 20x/0.7 NA and 40x/1.2 NA lenses at the University of Michigan Microscopy and Image Analysis Lab. Images were acquired using SoftWoRx 3.5.1 software. Cell motility videos were enhanced and analyzed using Imaris (Bitplane Scientific Software), from which the average speed of each cell line was calculated in µm/hour.

Actin Immunocytochemistry

50-70% confluent cells were fixed with 4% paraformaldehyde. Cells were then incubated in 1:50 AF568-phalloidin in PBS (Invitrogen) for 10 minutes, rinsed once in PBS for 5 minutes, and mounted with Prolong Gold anti-fade with DAPI. Images were acquired at room temperature using a Zeiss LSM 510 Meta laser-scanning microscope equipped with a C-Apochr 40x/1.2 NA and LSM 510

software. Each channel was imaged sequentially using multitrack recording before merging. Enhancements were performed using Photoshop (CS2; Adobe).

In situ detection and quantification of protein expression

Tumors and Patients

Fresh and formalin-fixed, paraffin-embedded tissue blocks (FFPE) of Breast Cancer were obtained from the files of the Department of Pathology, University of Michigan Medical Center, Ann Arbor, MI. IRB approval was obtained and the diagnosis was confirmed by morphology. After pathological review, a tissue microarray was constructed from the most representative area using the methodology of Nocito et al. (98). Survival data was obtained from the Cancer Registry of The University of Michigan.

Immunohistochemical Staining and AQUA analysis.

Triple immunofluorescence staining was performed as previously described (99) and the AQUA system (HistoRx, New Haven, Connecticut) was used for the automated image acquisition and analysis. The detailed staining and imaging procedure can be found in the Supplemental Methods.

Orthotopic Xenografts and Lymphatic Metastasis Analysis

All mouse work was performed in accordance with the University's standards for animal use. 231 scrambled and shp38γ cells were diluted 1:1 with Matrigel (BD Biosciences) to a final concentration of 3×10^6 cells/ml. Athymic nude mice were anesthetized and 1.5×10^5 cells (50 µl) were injected directly into the fourth

mammary gland. Tumors were monitored weekly and mice were euthanized once tumor volume approached 2 cm^3. Tumors were resected at the time of euthanization, fixed in 10% formalin, and were subsequently paraffin embedded. Hematoxylin and eaosin-stained tumor sections were scored for lymphatic metastasis in a single-blind manner by Dr. J. Erby Wilkinson at the ULAM Pathology Core. The number of mice presenting with lymphatic metastases were compared using Fisher's exact test. Images were captured at room temperature using an Olympus BX-51 upright light microscope with Olympus UPlanApo 10x/0.4 NA and 40x/0.85 NA objectives and an Olympus DP-70 high resolution digital camera with DP controller software.

Invasion and Bead Motility

Invasion (BD Biosciences) and bead motility (Thermo Scientific) assays were performed as previously described (56). Growth factor-reduced Matrigel was used for invasion assays. Images were taken at room temperature with a Leica MXFL III stereo microscope equipped with an Olympus DP-71 digital camera with DP controller software.

Statistical analyses

All p-values were calculated by Student's two-tailed t-test unless otherwise noted. Expression levels of p38γ and RhoC in TMA samples were compared using Spearman's rank coefficient. Association between p38γ and breast cancer subtype was determined by Fisher's exact test. The relationship between p38γ

expression and patient survival was calculated by Kaplan Meier analysis, with surviving patients censored. The log-rank test statistic for used to test for significance.
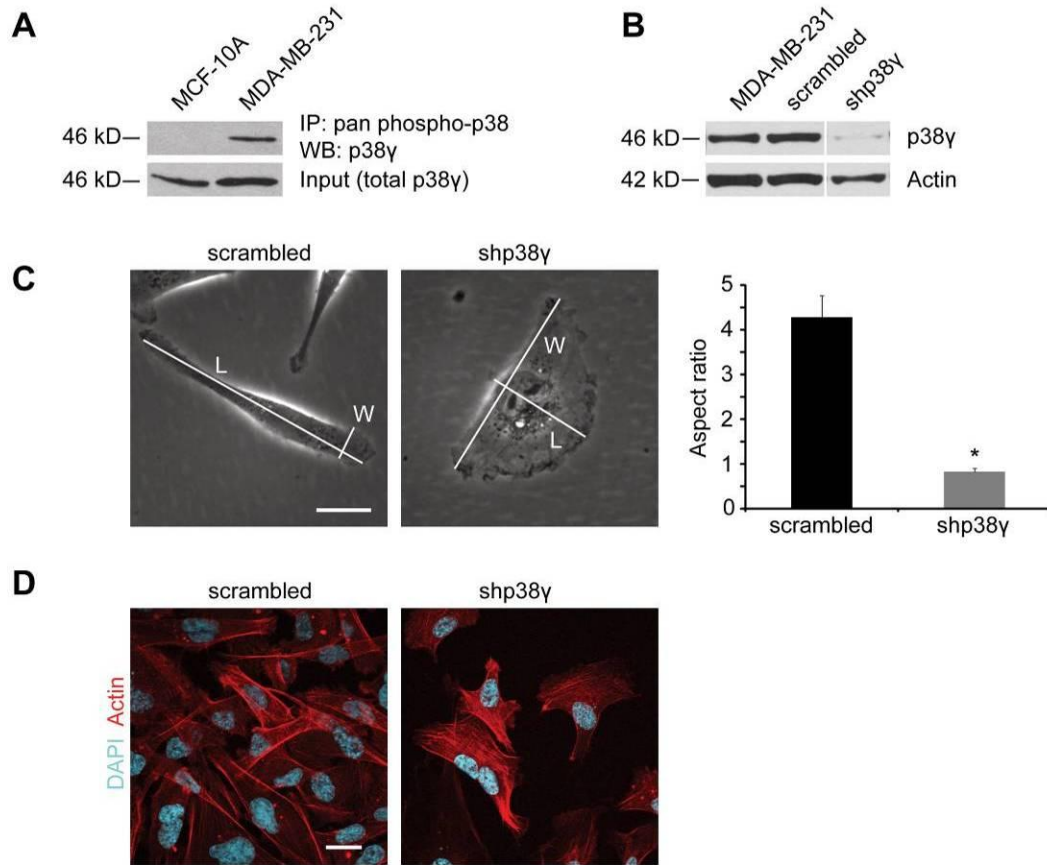
Figure 3.1 – p38γ governs MDA-MB-231 cell shape. (**A**) Phospho-p38γ levels
are elevated in the aggressive breast cancer cell line MDA-MB-231 compared to
non-tumorigenic MCF-10A mammary epithelial cells. (**B**) shRNA knockdown of
p38γ in MDA-MB-231 cells. (**C**) (left) Cell shape difference between scrambled
and shp38γ cells. (right) Quantification of cell shape difference by aspect ratio
measurement (length/width) (*p = 7.82 x 10^{-7}, n = 22 cells for scrambled, n = 27
cells for shp38γ, scale bar = 25 μm). Data are representative of three
independent experiments and are represented as ± s.e.m. (**D**) Actin cytoskeleton
of scrambled and shp38γ cells showing the lengthwise, parallel stress fibers in
scrambled cells (left) contrasting the bimodal fibers confined to the leading edge
of shp38γ cells (scale bar = 20 μm).
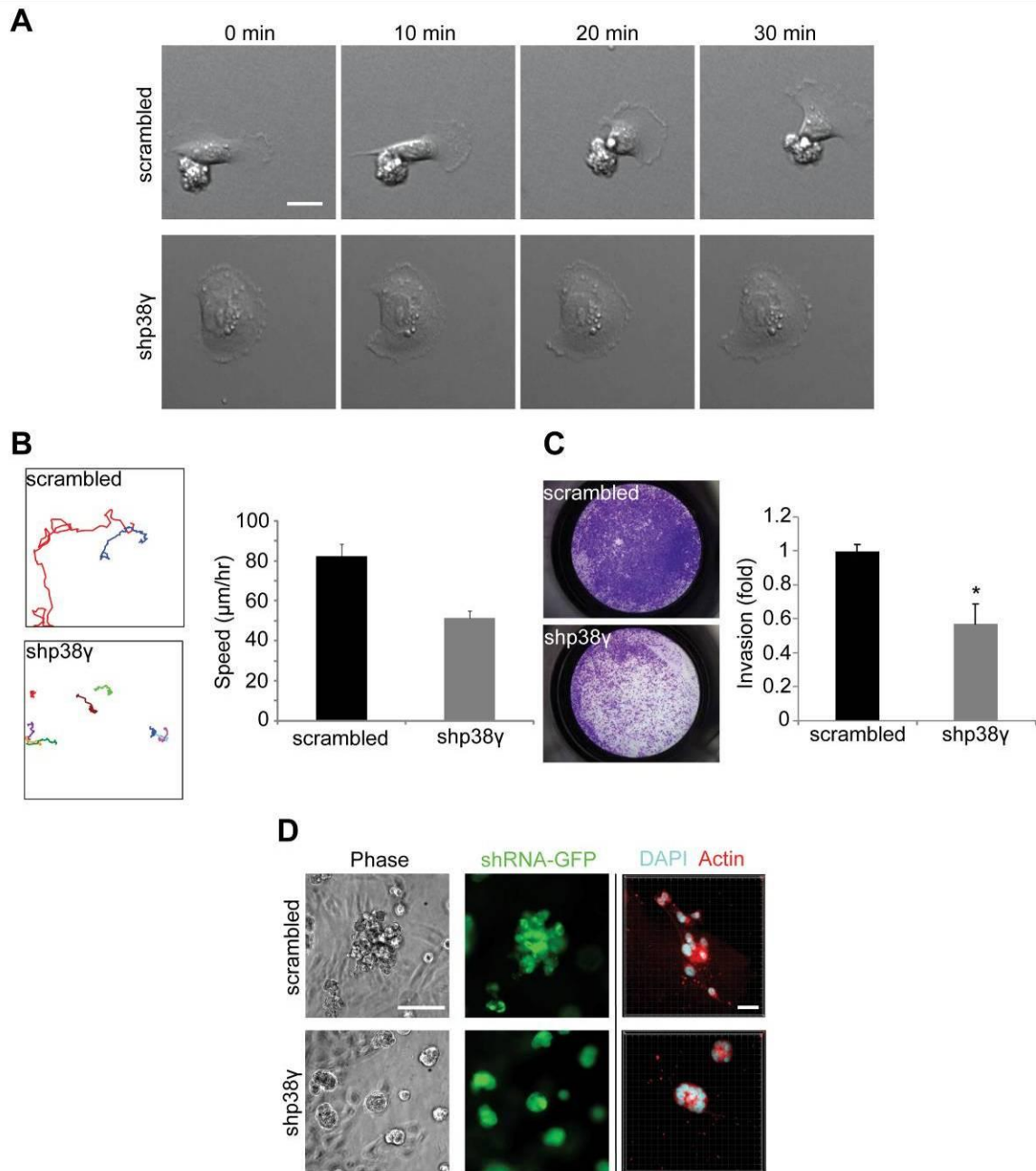
Figure 3.2 – p38γ knockdown impairs the metastatic properties of MDA-MB-231 cells. (**A**) Representative images from time lapse videos (see Video 1) of scrambled and shp38γ cells, demonstrating the characteristic mesenchymal-like motility of scrambled cells (top) and the non-productive crawling motion of shp38γ cells (bottom) (scale bar = 10 μm). (**B**) (left) Cell tracks from the videos in (**A**). (right) shp38γ cells are significantly slower than scrambled cells and accordingly travel less total distance (data not shown) (*p = 3.34 x 10^{-5}, n = 30 cells per cell line). (**C**) p38γ knockdown reduces MDA-MB-231 invasion through growth factor reduced Matrigel-coated transwell chambers. Representative wells are shown on the left, normalized OD readings from three independent experiments are represented on the right (*p = 0.022). Graphs in (**B**) and (**C**) are

represented as ± s.e.m. (**D**) Three-dimensional Matrigel culture of scrambled and shp38γ cells (right image is center slice of confocal stack, all others widefield) (left scale bar = 100 µm, right scale bar = 20 µm). All data are representative of three independent experiments.
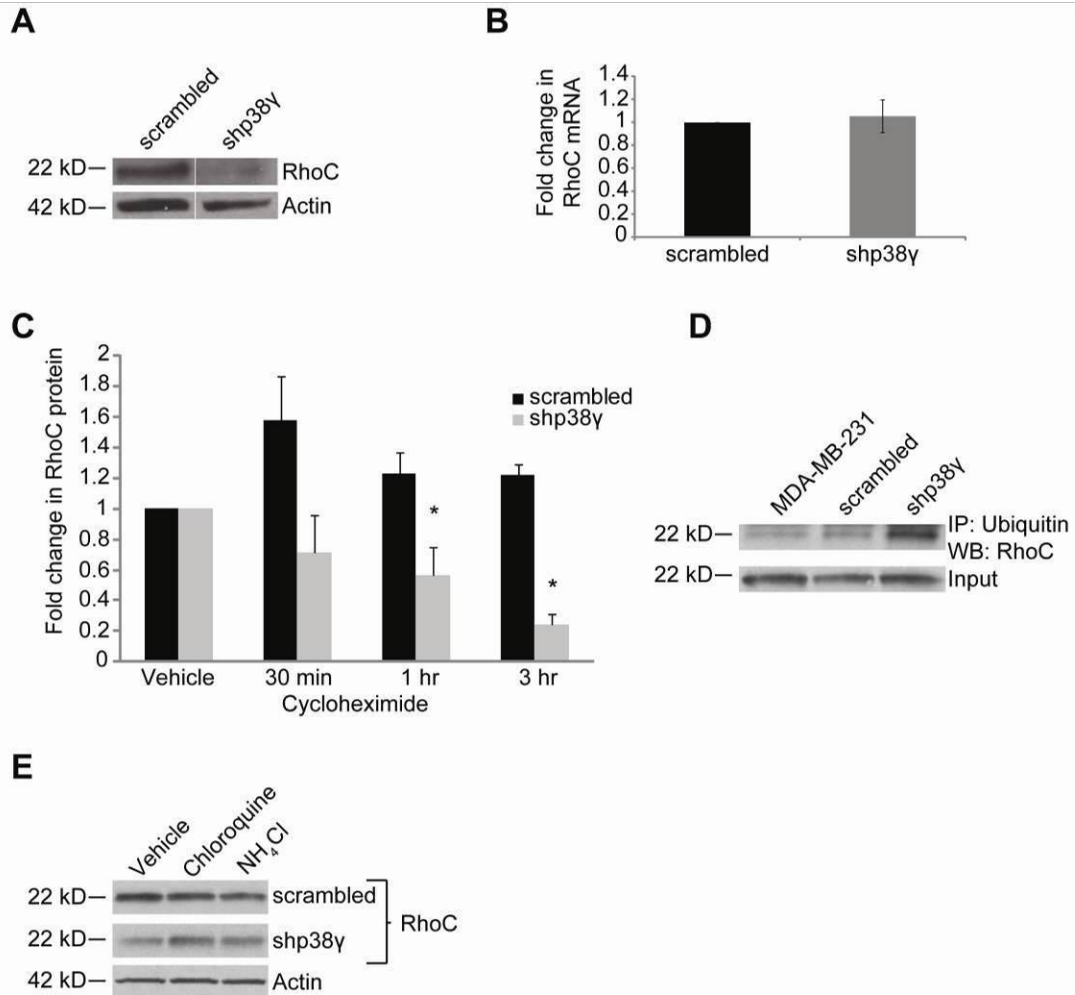
Figure 3.3 – p38γ affects RhoC expression by mediating RhoC ubiquitination and lysosomal degradation. Expression of RhoC GTPase protein (**A**) but not mRNA (**B**) is significantly reduced by p38γ knockdown. (**C**) Treating cells with the translation inhibitor cycloheximide reveals that RhoC protein is less stable in shp38γ cells. (**D**) RhoC ubiquitination is increased in shp38γ cells. (**E**) RhoC is degraded by the lysosome, as treatment with lysosome inhibitors leads to an increase in RhoC protein in shp38γ cells.
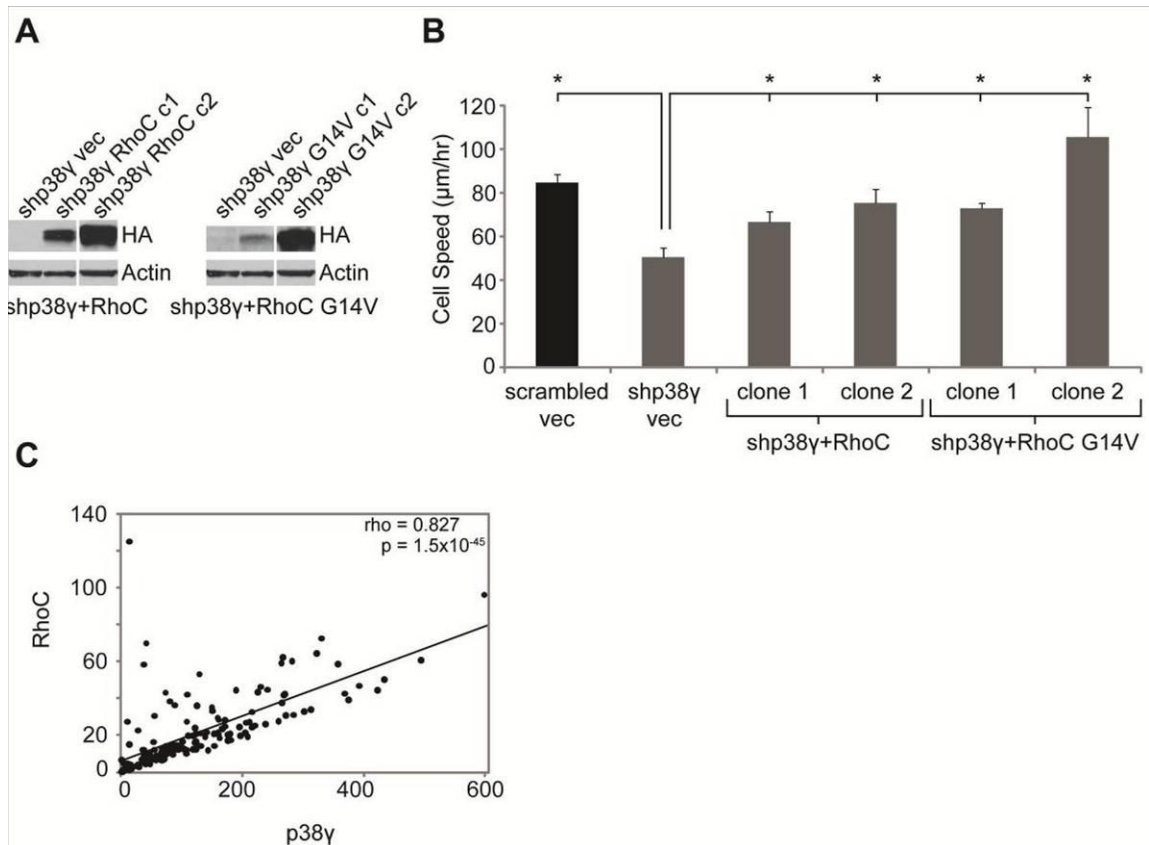
Figure 3.4 – p38γ and RhoC are functionally related and are co-expressed in clinical breast cancer samples. (**A**) shp38γ cells were stably transfected with either HA-tagged RhoC (left) or a constitutively active form of RhoC, RhoC G14V (right). Two clones—one high expressing and one low expressing—were selected for each construct. (**B**) The motility of stably transfected clones was analyzed by time lapse microscopy. Re-expressing RhoC in shp38γ cells significantly increases shp38γ cell speed to levels comparable to scrambled cells (*p<0.05). (**C**) p38γ and RhoC expression were quantified by AQUA from tissue microarrays of 177 breast cancer cases. Expression of the two proteins is strongly positively correlated in clinical breast cancer samples (rho = 0.827, p=1.5 x 10^{-45}).
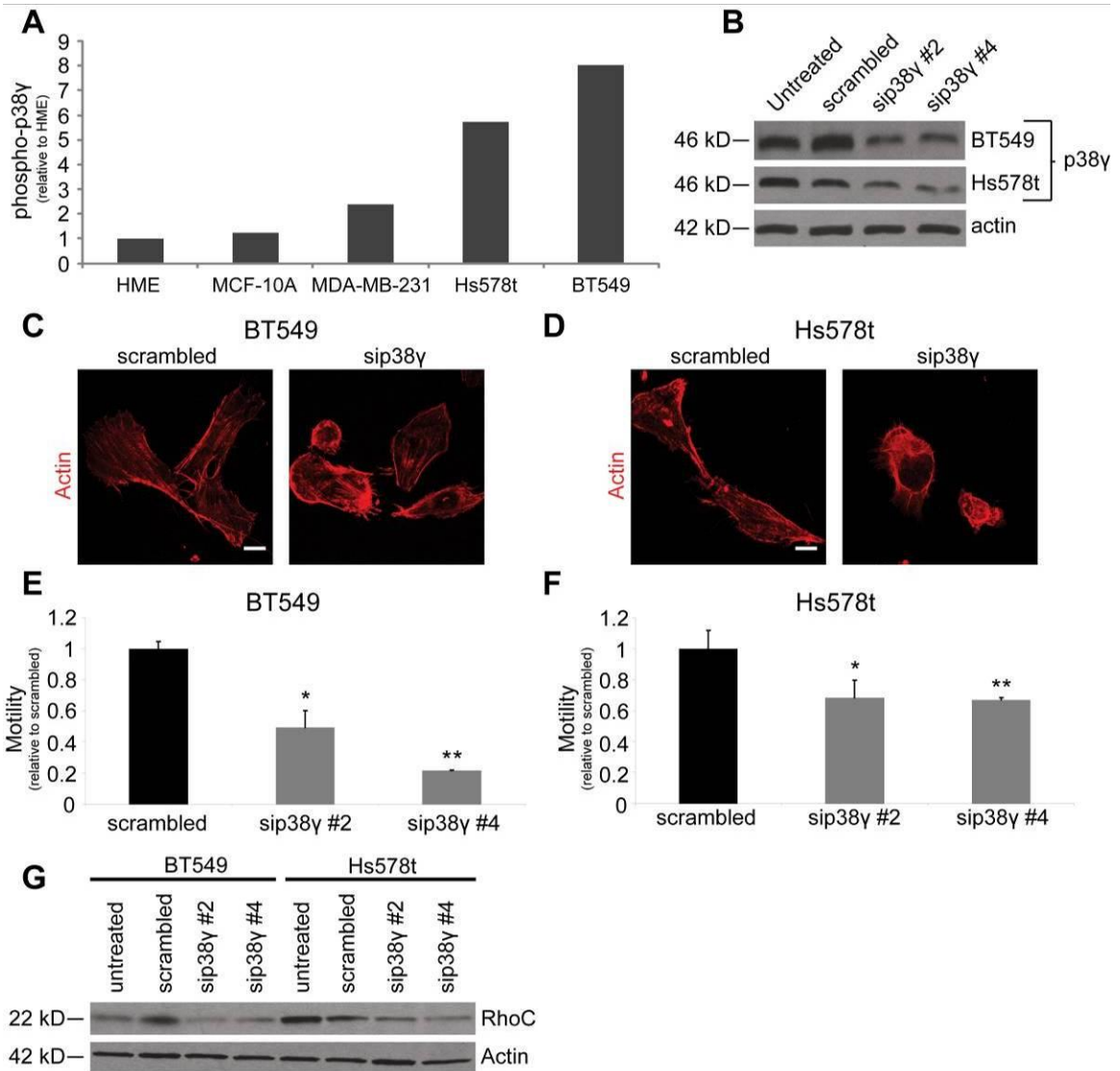
Figure 3.5 – p38γ functions similarly
cancer cell lines. (**A**) Levels of phospho-p38γ are elevated in the aggressive breast cancer cell lines MDA-MB-231, Hs578t, and BT549 compared to both HME and MCF-10A non-tumorigenic mammary epithelial cells. Graph shows IP/input (phospho-p38γ/total p38γ) quantification of a representative western blot. (**B**) Transient siRNA knockdown of p38γ in BT549 and Hs578t cells. The siRNA did not affect the other p38 isoforms (data not shown). (**C-D**) The actin cytoskeleton and cell shape of sip38γ BT549 (**C**) and Hs578t (**D**) cells are altered in a manner similar to 231 shp38γ cells (scale bar = 25 μm). Data are representative of three independent experiments. (**E-F**) p38γ knockdown reduces cell motility significantly, as measured by a bead motility assay in BT549 (**E**) and Hs578t (**F**) cells (For two BT549 siRNAs: *p = 0.0428, **p = 1.64 x 10^{-5}; for two Hs578t siRNAs: *p = 0.0001, **p = 0.0012. All data are represented as the average of three independent experiments ± s.e.m.). (**G**) RhoC expression is reduced in siRNA-transfected BT549 and Hs578t cells.

A

Subtype	High p38γ	Low p38γ	Total
Basal	6 (55%)	5 (16%)	11
Other	5 (45%)	27 (84%)	32
Total	11	32	43
			p=0.018

B

	Lymph Node Metastasis			
	Total Mice	Positive	Negative	% Mets
scrambled	6	4	2	66.7%
shp38γ	9	1	8	11.1%
				p=0.047

C

Ipsilateral | Contralateral Respective

D

Overall Survival

	Median Survival (years)	
Group	Estimate	95% CI
Low p38γ	10.85	(6.53-15.17)
High p38γ	5.89	(2.45-9.33)
p=0.013		
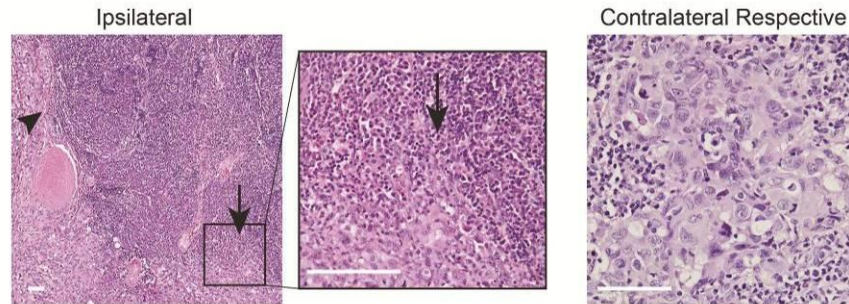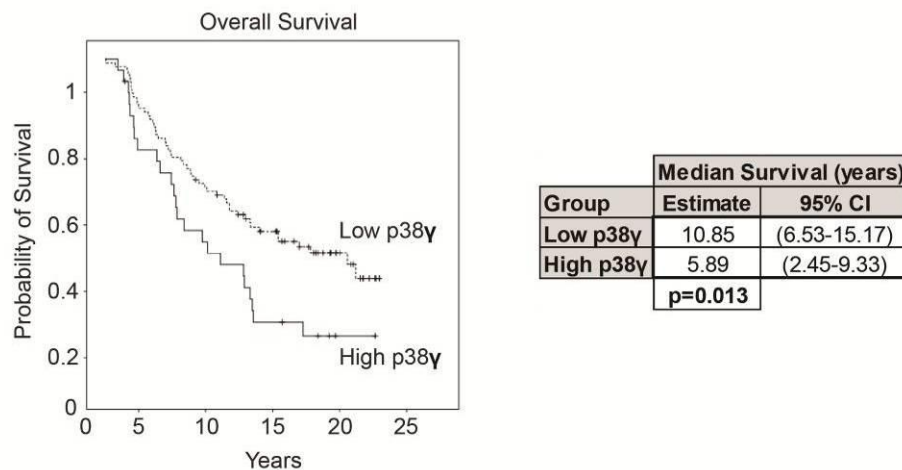
Figure 3.6 – p38γ is associated with the basal breast cancer subtype and affects metastasis and patient survival. (**A**) The basal breast cancer subtype is enriched in the top quartile of p38γ-expressing patient samples ("High p38γ") (p = 0.018). (**B**) Quantification of lymph node metastasis of orthotopically xenografted 231 scrambled and shp38γ cells. Scrambled cells had a significantly higher incidence of metastasis into lymph nodes in both the ipsilateral and contralateral mammary glands (p = 0.047), as measured by Fisher's exact test. (**C**) Representative tissues of 231 scrambled cells invading the ipsilateral lymph node (left) and a metastatic cluster in the contralateral respective mammary gland (right). The intact lymph node capsule is indicated by the arrowhead while invading scrambled cells are marked by the arrow and magnified in the inset (all scale bars = 100 µm). (**D**) High p38γ expression is associated with lower overall breast cancer patient survival as determined by Kaplan-Meier analysis (p = 0.013).

87

Supplemental Materials and Methods

Generation of dominant negative p38γ MDA-MB-231 cells

Selection media for cells transfected with dominant negative p38γ consisted of standard cell media containing 350μg/ml G418. For dominant negative p38γ cells, 1 μg of pcDNA-FLAG-p38γ agf was transfected into 50-70% confluent MDA-MB-231 cells using Genejammer transfection reagent (Stratagene) according to the manufacturer's instructions. Transfected cells were selected in G418 and positive clones were isolated.

Use of a dominant negative p38γ construct to validate shRNA results

As there is no p38γ-specific pharmacologic inhibitor we instead used a dominant negative p38γ construct (102) to validate our shRNA results. The dominant negative p38γ ("DNp38γ") has the Thr and Tyr residues of the TGY phosphorylation motif mutated to non-phosphorylatable Ala and Phe, and will thereby competitively inhibit endogenous p38γ binding to its activating kinases (102). However, p38γ shares its upstream kinases, MKK3 and MKK6, with the other p38 isoforms – therefore DNp38γ likely interferes to an extent with signaling through the other isoforms. To help minimize these off-target effects we selected clones with low levels of DNp38γ that were still able to reduce p38γ phosphorylation (Figure 3.S1A).

Immunohistochemical Staining and AQUA analysis

Briefly, after deparaffinization and rehydration, TMA slides were subjected to microwave epitope retrieval in 7.5 mM sodium citrate buffer, pH6. After rinsing several times in 10 mM Tris HCL buffer, pH 8 containing 0.154 M NaCl (TBS), endogenous peroxidase activity was blocked with 2.5% (v/v) H_2O_2 in methanol for 30 minutes. Non-specific binding of the antibodies was extinguished by 30 minute incubation with 'Background Sniper" (BioCare Medical, Concord, CA). The TMA slide was then incubated with the tumor-specific antibody, cytokeratin (AbD Serotec, Raleigh, NC, Mouse monoclonal antibody, MCA144HT, 1:50) overnight at 4C. The slides ere then washed with TBST twice for 5 minutes and then once with TBS for 5 minutes. The slides were then incubated with the antibodies to RhoC (chicken IgY polyclonal antibody, 1:1000, described in (115)) and p38γ (Abgent, rabbit polyclonal antibody, AP7224c, 1:50) for 60 minutes at room temperature. Slides were then washed as described above and incubated with a combination of goat anti mouse IgG conjugated to AF555 (Molecular probes, Carpinteria, CA, A21424, 1:200) and goat anti chicken IgY conjugated to AF488 (Molecular probes, Carpinteria, CA, A11039, 1:200) in goat anti rabbit Envision+ (DAKO, Carpinteria, CA) for 60 minutes at room temperature in a dark humidity tray. The slides were then washed as described above and the target image was developed by a CSA reaction of Cy5 labeled tyramide (PerkinElmer, Waltham, MA, 1:50). The slides were washed with 3 changes of TBS and stained with the DNA staining dye 4',6-diaminodo-2-phenylindole (DAPI) in a non-fading mounting media (ProLong Gold, Molecular probes, Carpinteria, CA). The slides were allowed to dry overnight in a dark dry chamber and the edges were sealed.

For AQUA, images of each TMA core were captured with an Olympus BX51 microscope at 4 different extinction/emission wavelengths. Within each TMA spot, the area of tumor was distinguished from stromal and necrotic areas by creating a tumor specific mask from the anti-CK protein, which was visualized from Alexafluor 555 signal. The DAPI image was then used to differentiate between the cytoplasmic and nuclear staining within the tumor mask. The pixel intensity of the RhoC protein/antibody complex was determined from the AF488 signal, and finally, the fluorescence pixel intensity of the p38γ protein/antibody complex was obtained from the Cy5 signal and reported as pixel intensity.

Figure 3.S1 – Creation and analysis of dominant negative p38γ clones. (**A**) Western blot showing FLAG-DNp38γ expression in stably transfected clones. (**B**) IP/western blot of phospho-p38γ levels in DNp38γ clones, indicating that p38γ phosphorylation is decreased by overexpression of DNp38γ. (**C**) Aspect ratio of DNp38γ clones is decreased compared to vector control cells (*p<0.05). Data are represented as ± s.e.m. (**D**) Three-dimensional Matrigel culture of vector control and DNp38γ cells, which show the same stellate (vector) and non-invasive (DNp38γ) phenotypes as scrambled and shp38γ cells, respectively (scale bar = 100 μm). (**E**) Actin cytoskeleton of vector and DNp38γ cells, showing a reorganization of the cytoskeleton and rounded cell shape (scale bar = 20 μm). (**F**) Expression of the cytoskeletal regulator and metastatic oncogene RhoC in vector and DNp38γ cells.

Video 1 – MDA-MB-231 shp38γ cells have impaired motility. MDA-MB-231 cells stably transfected with either a scrambled control shRNA (left) or shRNA targeting p38γ (right) were imaged by time lapse DIC microscopy (Deltavision RT). Frames were taken every 10 minutes for 18 hours. See Figure 3.2A for related stills.

References

15. Yang J, Mani SA, Donaher JL, Ramaswamy S, Itzykson RA, Come C, et al. Twist, a master regulator of morphogenesis, plays an essential role in tumor metastasis. Cell. 2004;117:927-39.

39. Ridley AJ. Rho GTPases and cell migration. J Cell Sci. 2001;114:2713-22.

40. Rosenthal DT, Brenner JC, Merajver SD. Rho Proteins in Cancer. In: van Golen KL, editor. The Rho GTPases in Cancer. New York: Springer New York; 2010. p. 29-42.

47. Wheeler AP, Ridley AJ. Why three Rho proteins? RhoA, RhoB, RhoC, and cell motility. Exp Cell Res. 2004;301:43-9.

49. Wu M, Wu ZF, Rosenthal DT, Rhee EM, Merajver SD. Characterization of the roles of RhoC and RhoA GTPases in invasion, motility, and matrix adhesion in inflammatory and aggressive breast cancers. Cancer. 2010;116:2768-82.

51. van Golen KL, Wu ZF, Qiao XT, Bao LW, Merajver SD. RhoC GTPase, a novel transforming oncogene for human mammary epithelial cells that partially recapitulates the inflammatory breast cancer phenotype. Cancer Res. 2000;60:5832-8.

52. Clark EA, Golub TR, Lander ES, Hynes RO. Genomic analysis of metastasis reveals an essential role for RhoC. Nature. 2000;406:532-5.

53. Ikoma T, Takahashi T, Nagano S, Li YM, Ohno Y, Ando K, et al. A definitive role of RhoC in metastasis of orthotopic lung cancer in mice. Clin Cancer Res. 2004;10:1192-200.

54. Islam M, Lin G, Brenner JC, Pan Q, Merajver SD, Hou Y, et al. RhoC expression and head and neck cancer metastasis. Mol Cancer Res. 2009;7:1771-80.

56. van Golen KL, Bao LW, Pan Q, Miller FR, Wu ZF, Merajver SD. Mitogen activated protein kinase pathway is involved in RhoC GTPase induced motility, invasion and angiogenesis in inflammatory breast cancer. Clin Exp Metastasis. 2002;19:301-11.

57. Chang L, Karin M. Mammalian MAP kinase signalling cascades. Nature. 2001;410:37-40.

59. Wagner EF, Nebreda AR. Signal integration by JNK and p38 MAPK pathways in cancer development. Nat Rev Cancer. 2009;9:537-49.

60. Cuenda A, Rousseau S. p38 MAP-kinases pathway regulation, function and role in human diseases. Biochim Biophys Acta. 2007;1773:1358-75.

61. Wang Y, Huang S, Sah VP, Ross J, Jr., Brown JH, Han J, et al. Cardiac muscle cell hypertrophy and apoptosis induced by distinct members of the p38 mitogen-activated protein kinase family. J Biol Chem. 1998;273:2161-8.

62. Platanias LC. Map kinase signaling pathways and hematologic malignancies. Blood. 2003;101:4667-79.

63. Qi X, Pohl NM, Loesch M, Hou S, Li R, Qin JZ, et al. p38alpha antagonizes p38gamma activity through c-Jun-dependent ubiquitin-proteasome pathways in regulating Ras transformation and stress response. J Biol Chem. 2007;282:31398-408.

68.   Sabio G, Arthur JS, Kuma Y, Peggie M, Carr J, Murray-Tait V, et al. p38gamma regulates the localisation of SAP97 in the cytoskeleton by modulating its interaction with GKAP. EMBO J. 2005;24:1134-45.

71.   Tortorella LL, Lin CB, Pilch PF. ERK6 is expressed in a developmentally regulated manner in rodent skeletal muscle. Biochem Biophys Res Commun. 2003;306:163-8.

72.   Cuenda A, Cohen P. Stress-activated protein kinase-2/p38 and a rapamycin-sensitive pathway are required for C2C12 myogenesis. J Biol Chem. 1999;274:4341-6.

73.   Wang XS, Diener K, Manthey CL, Wang S, Rosenzweig B, Bray J, et al. Molecular cloning and characterization of a novel p38 mitogen-activated protein kinase. J Biol Chem. 1997;272:23668-74.

74.   Li Z, Jiang Y, Ulevitch RJ, Han J. The primary structure of p38 gamma: a new member of p38 group of MAP kinases. Biochem Biophys Res Commun. 1996;228:334-40.

78.   Tang J, Qi X, Mercola D, Han J, Chen G. Essential role of p38gamma in K-Ras transformation independent of phosphorylation. J Biol Chem. 2005;280:23910-7.

79.   Loesch M, Chen G. The p38 MAPK stress pathway as a tumor suppressor or more? Front Biosci. 2008;13:3581-93.

81.   Qi X, Tang J, Loesch M, Pohl N, Alkan S, Chen G. p38gamma mitogen-activated protein kinase integrates signaling crosstalk between Ras and estrogen receptor to increase breast cancer invasion. Cancer Res. 2006;66:7540-7.

82.   Loesch M, Zhi HY, Hou SW, Qi XM, Li RS, Basir Z, et al. p38{gamma} MAPK cooperates with c-Jun in trans-activating matrix metalloproteinase 9. J Biol Chem. 2010.

88.   Debnath J, Brugge JS. Modelling glandular epithelial cancers in three-dimensional cultures. Nat Rev Cancer. 2005;5:675-88.

89.   Lee GY, Kenny PA, Lee EH, Bissell MJ. Three-dimensional culture models of normal and malignant breast epithelial cells. Nat Methods. 2007;4:359-65.

90.   Kenny PA, Lee GY, Myers CA, Neve RM, Semeiks JR, Spellman PT, et al. The morphologies of breast cancer cell lines in three-dimensional assays correlate with their profiles of gene expression. Mol Oncol. 2007;1:84-96.

97.   Abramoff MD, Magelhaes PJ, Ram SJ. Image Processing with ImageJ. Biophotonics International. 2004;11:36-42.

98.   Nocito A, Kononen J, Kallioniemi OP, Sauter G. Tissue microarrays (TMAs) for high-throughput molecular pathology research. Int J Cancer. 2001;94:1-5.

99.   McCabe A, Dolled-Filhart M, Camp RL, Rimm DL. Automated quantitative analysis (AQUA) of in situ protein expression, antibody concentration, and prognosis. J Natl Cancer Inst. 2005;97:1808-15.

100.   Burstein HJ, Polyak K, Wong JS, Lester SC, Kaelin CM. Ductal carcinoma in situ of the breast. N Engl J Med. 2004;350:1430-41.

101.   Cohen P. The search for physiological substrates of MAP and SAP kinases in mammalian cells. Trends Cell Biol. 1997;7:353-61.

102.   Enslen H, Raingeaud J, Davis RJ. Selective activation of p38 mitogen-activated protein (MAP) kinase isoforms by the MAP kinase kinases MKK3 and MKK6. J Biol Chem. 1998;273:1741-8.

103.   Ladwein M, Rottner K. On the Rho'd: the regulation of membrane protrusions by Rho-GTPases. FEBS Lett. 2008;582:2066-74.

104.   Rajah TT, Abidi SM, Rambo DJ, Dmytryk JJ, Pento JT. The motile behavior of human breast cancer cells characterized by time-lapse videomicroscopy. In Vitro Cell Dev Biol Anim. 1998;34:626-8.

105.   Partin AW, Schoeniger JS, Mohler JL, Coffey DS. Fourier analysis of cell motility: correlation of motility with metastatic potential. Proc Natl Acad Sci U S A. 1989;86:1254-8.

106.   Nobes CD, Hall A. Rho, rac, and cdc42 GTPases regulate the assembly of multimolecular focal complexes associated with actin stress fibers, lamellipodia, and filopodia. Cell. 1995;81:53-62.

107.   Nielsen TO, Parker JS, Leung S, Voduc D, Ebbert M, Vickery T, et al. A comparison of PAM50 intrinsic subtyping with immunohistochemistry and clinical prognostic factors in tamoxifen-treated estrogen receptor-positive breast cancer. Clin Cancer Res. 2010;16:5222-32.

108.   Simon C, Goepfert H, Boyd D. Inhibition of the p38 mitogen-activated protein kinase by SB 203580 blocks PMA-induced Mr 92,000 type IV collagenase secretion and in vitro invasion. Cancer Res. 1998;58:1135-9.

109.   Chen L, Mayer JA, Krisko TI, Speers CW, Wang T, Hilsenbeck SG, et al. Inhibition of the p38 kinase suppresses the proliferation of human ER-negative breast cancer cells. Cancer Res. 2009;69:8853-61.

110.   Cano A, Perez-Moreno MA, Rodrigo I, Locascio A, Blanco MJ, del Barrio MG, et al. The transcription factor snail controls epithelial-mesenchymal transitions by repressing E-cadherin expression. Nat Cell Biol. 2000;2:76-83.

111.   Chiang AC, Massague J. Molecular basis of metastasis. N Engl J Med. 2008;359:2814-23.

112.   Rosenthal DT, Iyer H, Escudero SE, Wu Z, Bao L, Garcia H, et al. Computational mechanical modeling reveals the role of p38γ in shaping the cytoskeleton and controlling locomotion of aggressive breast cancer cells. Cancer Research. 2011;Concurrent Submission.

113.   Wu M, Wu ZF, Merajver SD. Rho proteins and cell-matrix interactions in cancer. Cells Tissues Organs. 2007;185:100-3.

114.   Nethe M, Hordijk PL. The role of ubiquitylation and degradation in RhoGTPase signalling. J Cell Sci. 2010;123:4011-8.

115.   Kleer CG, van Golen KL, Zhang Y, Wu ZF, Rubin MA, Merajver SD. Characterization of RhoC expression in benign and malignant breast disease: a potential new marker for small breast carcinomas with metastatic ability. Am J Pathol. 2002;160:579-84.

Chapter IV

**Computational mechanical modeling reveals the role of p38γ in shaping the
cytoskeleton and controlling locomotion of aggressive breast cancer cells**

Abstract

Breast cancer lethality is primarily due to metastasis to distant vital organs. In the
multi-step process of dissemination cancer cells acquire pro-metastatic
properties, such as rapid motility. Understanding both the molecular alterations
and associated physical behaviors that confer effective and fast locomotion to
otherwise slow-moving breast cancer cells is therefore paramount to uncovering
a potentially modifiable determinant of metastases. We show for the first time
that p38γ MAPK controls cell motility specifically by regulating cytoskeletal
morphology. Using a computational mechanical model, which is based on the
finite element method, we demonstrate that p38γ-mediated cytoskeletal changes
are sufficient to control cell motility. The model predicted novel dynamics of
leading edge actin protrusions, which were verified experimentally, and which
proved to be closely related to cell shape and cytoskeletal morphology.

Major findings

By combining cell biology and computational mechanical modeling, we establish
p38γ as a metastatic oncogene responsible for controlling breast cancer cell

motility. Additionally, we demonstrate how p38γ specifically exerts this effect: we show that the dynamics of leading edge actin protrusion and trailing edge retraction by stress fibers determine the type of cell motility and locomotion, but they cannot act independently of cell shape and cytoskeletal architecture. We further deduce that p38γ is the key signaling link between cell shape, cytoskeletal structure, and the type of motion the cell exhibits.

Introduction

Cell motility involves the precise coordination of a broad array of signaling pathways, physical cues, and other environmental stimuli in order to generate coordinated mechanical forces that result in effective locomotion. Cells use different forms of motion; e.g., lamellipodial vs. filopodial; the latter commonly associated with mesenchymal-like cells. A mesenchymal cell makes linear progress in a given direction by coordinating (a) cell polarization by stress fiber formation in the direction of motion, (b) protrusion of the actin cytoskeleton at the cell's leading edge, (c) formation and adherence of focal adhesions at the leading edge, and (d) contraction of stress fibers by actomyosin-driven contractility, which causes retraction of the trailing edge by detachment and dissolution of focal adhesions there. These processes are triggered and sequentially regulated through an array of rapidly cycling signaling molecules, the most widely studied of them being the Rho GTPases: cdc42, Rac and Rho proteins, whose localization and activation are associated with the formation of filopodia, lamellipodia and stress fibers, respectively (116). The principles of mechanics

govern how the actions of these cytoskeletal structures produce motility and whole cell locomotion. The ability to properly shift from sessile to motile by exploiting mechanics is a hallmark of many developmental processes and is harnessed at the cellular and tissue levels in disease states such as cancer (117).

Cancer progression is broadly characterized by a shift from largely stationary, proliferative cells in the primary tumor to motile and invasive metastatic cells. In breast cancer and other epithelial cancers, this phenomenon is generally attributed to cells undergoing an epithelial-to-mesenchymal transition (EMT). During EMT cells shift from being coherent sheet-like epithelial cells to dynamically contractile, motile, mesenchymal-like cells. This change is evident even in culture in aggressive breast cancer cell lines such as MDA-MB-231, where cells appear fibroblast-like and move rapidly using a dynamic, contractility-based form of motility.

Coordination of motility to achieve effective locomotion requires the integration of inputs from broad-ranging environmental cues and stresses, and their translation into intracellular signaling for the proper orientation and turnover of the actin cytoskeleton, among other events. Although cytoskeletal remodeling that leads to motility generally runs through the Rho GTPase pathway (116), other upstream signaling molecules are responsible for translating extracellular stimuli into intracellular responses. Understanding the specific genetic alterations that lead to

a given motility phenotype is intrinsically difficult, as it is often a combination of heterogeneous genetic changes that contribute to a phenotype. Additionally, many signaling modifications—be they natural, or as a result of therapeutic intervention—are often compensated for by other signaling pathways or mechanisms, as pathways are not linear but rather interconnected information networks with extensive cross-talk.

Such a complex system can, in principle, be understood by using mathematics; in this case we adopted computational mechanical modeling as the tool to accomplish this. A full treatment of cell motility and locomotion as a complex system would include detailed models for sensing external stimuli, the signaling cascades that are generated, as well as the mechanical events of cytoskeletal remodeling and cell locomotion. Such an undertaking, however, presents daunting challenges in theory and computation, and indeed may not be entirely necessary: In this communication we have adopted a reduced representation in which only the mechanical events are modeled, while the external stimuli and cell signaling are taken as given. With this relatively simplified approach that nonetheless captures the crucial details of the internal mechanics of the cell, we are able to elucidate the central mechanical aspects of how cell shape, cytoskeletal morphology and actin dynamics give rise to motility, and ultimately to whole cell locomotion.

We have recently identified p38γ as a crucial regulator of breast cancer cell motility and metastasis (simultaneous submission) (118). Our findings indicate that a hallmark feature of modulating p38γ expression is the alteration of cytoskeletal orientation and architecture. Breast cancer cells that have p38γ knocked down by a small hairpin RNA (shRNA) have a dramatically modified cytoskeleton and significantly reduced cell speed compared to scrambled control cells (118); however, whether a functional link exists between these two observations has yet to be determined, and is the subject of this paper. To understand the role played by the p38γ-mediated cytoskeletal modifications, we developed a computational study of the mechanics of cell motility and locomotion.

Our computational study consists of a numerical, finite element treatment of the partial differential equations that govern the mechanics of cell structure and motion. Using this approach, we show that p38γ-mediated cytoskeletal changes are sufficient to account for the altered motility of cells lacking p38γ. In the course of this computational study we have discovered—and subsequently verified experimentally—a dynamic leading edge behavior in which motile cells develop oscillatory variations in the period and amplitude of actin filament protrusions depending upon their specific cytoskeletal architectures. Using input gathered from our cell biological experiments into the model, we were then able to derive a mechanistic sequence of events leading from p38γ knockdown to the observed motility defect. The study presented here (a) shows that p38γ is responsible for

driving the mesenchymal-like motility of aggressive breast cancer cells by regulating their cytoskeletal architecture, (b) uncovers a novel leading edge behavior used by motile cells, and (c) demonstrates the basic mechanical principles underlying the motion of live cells.

<u>Quick Guide to Equations and Assumptions</u>

The partial differential equation that governs the quasi-static balance of linear momentum of the cell is more amenable to computational solution when it is written in weak form. This form is an integral representation that exploits integration by parts to allow the use of less-smooth functions for numerical approximations:

Equation 1: Find *u* such that for all *w*,

$$\int \nabla^s \boldsymbol{w} \boldsymbol{:} \boldsymbol{\sigma}(\boldsymbol{\varepsilon}(\boldsymbol{u})) \, dV = 0,$$

where *u* is the displacement field vector, *w* is the weighting function vector, and *σ(ε(u))* is the stress tensor, here written to emphasize its dependence on the displacement field via the strain tensor *ε(u)*. The symbol ∇^s denotes the symmetric part of the gradient operator.

Major assumptions: At the typical speeds of cell motility, the effect of inertia is negligible, and the "dynamic" balance of linear momentum need not be considered.

Equation 2: The strain tensor is defined as

$$\boldsymbol{\varepsilon}(\boldsymbol{u}) = \nabla^s \boldsymbol{u}.$$

Major assumptions: The infinitesimal strain theory is assumed to hold, according to which nonlinear dependence of *ε* upon *u* can be neglected. This assumption makes for a simpler mathematical formulation and more rapid computations. The fully nonlinear theory leads to some quantitative differences in the computed stress, but does not alter the results in a qualitative manner.

Equation 3: The stress-strain response of the actin fibers and cell membrane is governed by the constitutive equation:

$$\boldsymbol{\sigma} = \lambda I tr(\boldsymbol{\varepsilon}) + 2\mu\boldsymbol{\varepsilon},$$

where λ and μ are Lamé parameters defined in terms of the more familiar Young's Modulus E and Poisson ratio v by

$$\lambda = vE/((1+v)(1-2v)) \text{ and } \mu = E/2(1+ v)$$

Major assumptions: The actin fibers and cell membrane are assumed to be elastic. This assumption implies that viscous effects associated with the kinetics of binding/unbinding of actin monomers with the cytoskeletal fibers and with the lipid bilayer will not be accounted for in the stress computations. We note, however, that the purpose of the *computational* model in this work is to represent the kinematics of cell motility and locomotion, and not to provide a precise computation of the stress. With more appropriate visco-elastic models for the actin fibers and cell membrane, the stress computed is more physically accurate, but the fundamental conclusions reached on cell motility and locomotion do not change. The viscoelastic models also result in a more complicated mathematical formulation, and slightly slower computations.

Equation 4: The matrix-vector version of the weak form (Equation 1) is:

$$Kd = F$$

where K is the finite element stiffness matrix, which includes the influence

of the mechanical properties, **d** is the vector of nodal displacements and **F** is the external force vector. The latter includes the effect of displacement boundary conditions that model the attachment of the cell to the substrate at focal adhesions.

Major assumptions: Our finite element implementation is based on the plane stress model of mechanics as explained in the text under "The *computational* cell model." Plane stress is an appropriate model for the two-dimensional shape adopted by cells on a substrate.

Cell structure	Young's Modulus, E (*GPa*)	Poisson's ratio, v	Thickness (nm)
Actin stress fiber	1.0	0.35	60—110
Cell membrane	0.00002	0.35	15

Table 4.1: Mechanical properties of sub-cellular structures in the computational cells. Typical numerical values from Phillips et al(119).

Computational cell type	Diameter of enclosing circle (µm)
Scrambled	46
Shp38γ	59

Table 4.2: Computational cell dimensions measured on live cells. For the scrambled cell, the reported diameter corresponds to the cell shape before it stretches, as shown in Figure 4.2C, top row, first panel.

Results

p38γ knockdown drastically alters actin cytoskeletal architecture

We previously observed that MDA-MB-231 breast cancer cells with p38γ knocked down ("shp38γ cells") have strikingly different cell shapes and disorganized actin cytoskeletons compared to MDA-MB-231 scrambled control cells ("scrambled cells") (118). Scrambled cells form long actin stress fibers traversing the length of the cell, well-aligned along the long axis. Furthermore, these cells develop leading edge filopodia, and the entire cell body is polarized in the direction of the stress fibers. In contrast, while shp38γ cells have thick actin bundles resembling the stress fibers in the scrambled cells, these fibers are primarily confined to the leading edge. The leading edge architecture is characterized by the formation of lamellipodia-like structures to which the actin bundles lie parallel. The cell shape is strikingly more rounded than the scrambled cells. To quantitatively address the cell shape and cytoskeletal differences between scrambled and shp38γ cells we measured aspect ratios of the cells, and the angle of the actin fibers relative to the leading edge in both cell lines.

Scrambled cells had aspect ratios (defined as the dimension perpendicular to the leading edge divided by the dimension parallel to the leading edge) of ~4, whereas the p38γ cells had aspect ratios < 1 (Figure 3.1A from Ref. 4).

The actin stress fibers are well-polarized in scrambled cells and oriented at $3.42^0 \pm 1.89^0$ (mean ± std. dev.) on either side of the normal to the leading edge (Figure 4.1B). This structure is consistent with the scrambled cell protrusive/contractile mode of motility (Movie 1). The actin bundles in the shp38γ cells, however, have a bimodal orientation distribution at $61.08° \pm 3.94^0$ (mean ± std. dev.) on either side of the normal to the leading edge, thus differing significantly from scrambled cell cytoskeletal architecture (Figure 4.1B). The lamellipodia-like structures associated with these actin bundles are observable during shp38γ cell motility (Movie 1), but show little similarity to classic lamellipodial cytoskeletal architecture, which normally consists of thin branched actin filaments forming a protrusive meshwork (103).

p38γ knockdown also had a profound effect on the modes (qualitative appearance) of cell motility and locomotion (Figure 4.2A), and on the speed (Figure 4.2B). Scrambled control cells moved in a mesenchymal manner, forming long filopodial projections that adhered to the substrate at the cells' leading edge. The cells then could "pull" themselves forward in alternating cycles of leading edge protrusion and trailing edge retraction—the latter presumably being facilitated by stress fiber contraction (Figure 4.4A, top, and Movie 1). shp38γ

106

cells, however, appeared to have difficulty polarizing and were unable to form long pseudopodia (Figure 4.4B, top, and Movie 1). The cells moved inefficiently, using a broad lamellipodia-like structure, with apparent oscillations of the whole cell body in the direction parallel to the leading edge, and exhibited failures of detachment at the rear of the cell.

Computational modeling reveals that p38γ-induced changes in cytoskeletal architecture influence cell motility

We observed that p38γ knockdown had functional (impaired motility and other metastatic properties) and structural (actin cytoskeleton and cell shape) effects on MDA-MB-231 cells (118). However, this left open the question of whether the change in actin cytoskeletal structure is sufficient to impair motility in the manner we observed. Since it remains inaccessible to experiments, this central question was addressed by computational modeling.

Our computational models use the finite element method to solve the partial differential equations that govern the mechanics of cell motility (see Materials and Methods for modeling details). We hypothesized that the strikingly different cytoskeletal architecture; i.e., polarized stress fibers in scrambled versus bimodal bundles of fibers in shp38γ cells, underlies the observed differences in motility.

To test this hypothesis we first created the computational model of scrambled cell motility. Using the typical dimensions of scrambled cells (Table 4.2/Figure 4.1A),

107

their observed cytoskeletal morphology of ±3.42⁰ (Figure 4.1B), and using the mechanical properties of actin stress fibers and cell membrane of mammalian cells (Table 4.1) we varied the rates of actin filament protrusion and retraction as inputs to the model to successfully recreate the observed motility and locomotion of live scrambled cells (Figure 4.2C, top panel, and Movie 2).

To determine whether actin cytoskeletal architecture is one of the defining features driving motility of the two MDA-MB-231 phenotypes, we next created the computational model of shp38γ cells with the cell dimensions reported in Table 4.2 and Figure 4.1A and cytoskeletal morphology of actin bundles at ±61.08⁰ reported in Figure 4.1B. The mechanical properties of the actin fibers and cell membrane were the same for shp38γ as for the scrambled cells (Table 4.1). Running the computational shp38γ cells exactly as the computational scrambled cell was unsuccessful. In particular, allowing the two families of stress fibers at ±61.08⁰ to extend and retract synchronously (in phase) produced computational shp38γ cell motion that was characterized by large leading edge ruffles but none of the oscillations in whole cell motion in the parallel direction to the leading edge that are evident in Movie 1. Since this computed motility bore little resemblance to the live shp38γ cells, we conjectured that the observed shp38γ motion was due mainly to the two families of actin bundles at +61.08⁰ and -61.08⁰ alternating (out of phase) in their protrusion and retraction. When incorporated, these dynamics, even without being precisely timed, produced a disjoint crawling motion with oscillations of the cell body in the direction parallel to the leading

edge of the computational shp38γ cell. This motility was remarkably similar to our live shp38γ cell motility (Figure 4.2C, bottom and Movie 2). These results suggested that actin cytoskeletal architecture is important for defining shp38γ cell motility, however further experiments were necessary to separate the influence of actin fiber orientation from actin protrusion/retraction dynamics.

Live scrambled and shp38γ cells have oscillating leading edge protrusions

The computational shp38γ cell motility thus revealed the possibility of a novel, previously unobserved aspect of cellular dynamics, namely waves of protrusion at the leading edge of a migrating cell that alternated between differentially-oriented families of actin fibers. Oscillations in retraction of the trailing edge of keratocytes have been previously observed (120) and regular, periodic changes in cell shape are important for productive cell movement (121). To our knowledge, however, such behavior has never been observed or characterized in the leading edge of motile cells, yet our computational study suggested that it is required for the observed shp38γ cell motility. To test this prediction of the model we studied in detail the dynamic behavior of the leading edge of scrambled and shp38γ cells stably transfected with RFP-actin.

Using time-lapse microscopy and standard imaging edge detection techniques (see Materials and Methods), we observed remarkable differences in leading edge protrusion between scrambled and shp38γ cells (Figure 4.3A and 4.3C). At first observation, scrambled cells appeared to protrude forward in one continuous

motion while shp38γ cells showed evidence of alternating left- and right-of-center protrusions corresponding to the two families of actin bundles at ±61.08⁰ (Figs. 3A and 3B). Upon closer analysis, leading edge protrusion in *both* cell lines actually manifested as alternating between left-of-center and right-of-center leading edge regions (Figs. 3B and 3C). (In the case of scrambled cells these regions correspond to the stress fibers at ±3.42⁰). The crucial difference between the cell lines was the time period between left and right protrusions; this period was much longer (4.83 ± 1.09 minutes) in shp38γ cells than in scrambled cells (1.75 ± 0.14 minutes) (Figure 4.3D). This periodicity is evident in the time lapse videos as the noticeably disjoint crawling motion of the shp38γ cells, contrasting the coordinated protrusion/retraction cycle of the scrambled cells (Movie 1). Also note the larger amplitudes of leading edge protrusions in shp38γ than in scrambled cells (Figure 4.3C).

These live cell results confirmed the prediction of the computational model. We repeated our computational cell motility studies with the mean left/right leading edge protrusion amplitudes and time periods of oscillation, and trailing edge retraction rates (Figure 4.3E), which we measured via time-lapse microscopy, now used as targets to be met by controlling the actin fiber extension/contraction rates in the model (see Materials and Methods). Thus incorporating these experimentally-observed leading edge dynamics further refined our computational models, showed good agreement between the live and computational cells, and importantly did not fundamentally alter the response of

the refined computational cell models from the initial models in a qualitative sense (Figure 4.4A-B; Movie 3).

Cytoskeletal architecture is a determinant factor of p38γ–mediated cell motility

In order to separate the effects of cytoskeletal architecture from the leading and trailing edge dynamics, we tried to "rescue" the phenotype of each computational cell by applying the protrusion dynamics (Figure 4.3C-D) of one phenotype to the other while maintaining their respective cytoskeletal architectures. Significantly, applying the scrambled cell leading and trailing edge behavior to the computational shp38γ cell did not restore wild type-like motility to the cell (Figure 4.5A). Correspondingly, the reverse situation—applying the shp38γ cell leading and trailing edge behavior to the computational scrambled cell—did not cause it to move like the shp38γ cell (Figure 4.5B), indicating that the leading and trailing edge dynamics of each cell type are not sufficient to enable their respective forms of motility independent of cytoskeletal architecture.

As a final means of separating the effects of cytoskeletal architecture from leading and trailing edge dynamics, we repeated our computational study by applying a synthesized motion (leading edge protrusion amplitude = 0.67 μm, period = 3 min., trailing edge retraction = 0.5 μm/min) to scrambled and shp38γ cells (Figure 4.5C-E). All of these parameters are approximately the means of the corresponding values for the live scrambled and shp38γ cells (Figure 4.3C-E).

111

The difference in cell speed between these computational scrambled and shp38γ cells, when normalized by computational scrambled cell speed, is remarkably similar to the difference between the live experiments in scrambled and shp38γ cells, after being similarly normalized by live scrambled cell speed (Figure 4.5C). The synthesized motility in the computational cells also is similar to actual motility of the live cells in a qualitative sense (Figure 4.5D and E), even though the actual speeds observed differ from the corresponding live cell speeds due to the synthetic nature of the imposed leading and trailing edge dynamics. This final study indicates that, when all other parameters remain the same, modifications in cytoskeletal architecture alone are sufficient to impair cell motility in the manner we observed experimentally: from creating effective locomotion in live scrambled cells to ineffective locomotion of shp38γ cells.

Discussion

Our models are based on the partial differential equations that govern motion of cells (and of all physical systems), and on the constitutive equations that specify how the forces (stresses) producing motion in cells are related to the details of that motion (strain) itself. These equations were posed in a numerical form suitable for efficient computation by the finite element method. This method uses a tessellation of the geometry of the cell, which is seen in Figure 4.S1. This framework constitutes our computational cell model.

Using the computational cell model in combination with our live cell microscopy studies, we showed that p38γ promotes breast cancer cell motility at least in part by mediating actin cytoskeletal remodeling, and thereby creating proper stress fiber orientation. Using the computational cell models, we first noted that whereas the observed whole cell locomotion could be produced by simultaneous action of all the observed stress fibers in scrambled cells, the experimentally observed ineffective locomotion of shp38γ cells was only possible if the action alternated between the two families of actin bundles seen in this cell phenotype. (We note that this question would prove difficult to address using cell biological techniques alone.)

The resulting mode of motility of the computational shp38γ cell model (Figure 4.2C and Movie 2) strongly resembled that of the corresponding live cells (Movie 1), suggesting that this computationally-inspired model of alternating action of the actin bundle families is representative of what is occurring in live cells. In live cell microscopy, prominent oscillations were observed at the leading edges of both cell types (Figure 4.3A), so we focused our analyses on this specific location in the cell. The method of normalizing leading edge protrusions explained in "Materials and Methods" (also Figure 4.3B-D) highlights the differences between the chosen regions, here called left- and right-of-center of the leading edge prompted by the distinct orientations of actin bundle families in the shp38γ cells (Figure 4.1B).

Leading edge protrusions are caused by actin filament polymerization (122-129). This is an inherently stochastic process due to the timing of arriving actin monomers, and is controlled also by upstream signaling events. Given this stochasticity, our method of normalization (Figure 4.3A-D and caption) is bound to yield out-of-phase oscillations of the left- and right-of-center protrusions. It is notable, however, that when shp38γ cells are compared with scrambled cells, the amplitude of these oscillations is larger by a factor of ~5, and the period by a factor of ~3 (with statistical significance), as seen in Figure 4.3C-D. The smaller amplitude and period of oscillations in the scrambled cells also serve to validate our initial model in which all stress fibers acted simultaneously in the computational model of these cells (Figure 4.2C). The association of left- and right-of-center leading edge regions with differentially-oriented families of actin fibers (Figure 4.1B and 3B) and the magnification of amplitude and period differences, with increased spread in orientation of these families suggests an important link between cytoskeletal morphology and actin protrusion dynamics.

While the computational model could be considered already validated by the confirmation of its prediction of alternating protrusions in shp38γ cells, we further tested it by incorporating the measured dynamics of leading edge protrusion and trailing edge retraction from Figure 4.3C-E. In these refined computations, the computational scrambled and shp38γ cells demonstrated motility and locomotion that were remarkably similar to the corresponding live cells (Figure 4.4A-B,

respectively). We consider this to be confirmation of the robustness and accuracy of our computational model of cell motility and locomotion.

Further investigation on the interaction of protrusion/retraction dynamics and cytoskeletal architecture (Figure 4.5) revealed that the measured leading edge dynamics cannot be divorced from the cytoskeletal morphology and cell shape, but rather they are interdependent. The leading edge dynamics reported in Figure 4.3C and 3D were obtained by averaging the protrusions at 8 points each along the left- and right-of-center leading edge regions of the respective cells. Since the leading edge shape and dimensions of scrambled and shp38γ cells are significantly different (see Figure 4.1A), the dynamics data obtained at points along their leading edges cannot be transposed from one cell type to the other in a consistent manner. These dynamics therefore seem inseparable from cell shape and cytoskeletal morphology. We note that this investigation of transposing dynamics with cell shape and cytoskeletal morphology is not possible without a computational model such as the one presented here, and is a powerful test of robustness of the predictions of the original model.

Our final computational investigation with synthetic motility further strengthens the idea that cell shape and cytoskeletal morphology have primacy in effecting motility and locomotion: With the same leading/trailing edge dynamics and mechanical properties but different cell shapes and cytoskeletal morphologies, the ratio of speed of scrambled and shp38γ cells is the same in the

computational cell models as in live cells. Since these synthetic dynamics were chosen so that the amplitude and period were each the average of the live scrambled and shp38γ cells, they did not bias the computational cell models toward either the scrambled or shp38γ phenotype. The actual speeds of the computational cells with these synthetic data therefore differed from the corresponding live cell speeds.

This finding of their inseparability sharpens the question of exactly how the leading edge actin dynamics are linked to cell shape and cytoskeletal morphology. While this is a subject for future investigation, we do speculate on the chain of events: p38γ knockdown → changes in cytoskeletal architecture → changes in cell shape → compensatory changes in leading edge protrusion periodicity → changes in cell motility.

Oscillation of other components of cell motility, such as cell shape (130) and trailing edge retraction (120), have already been shown to be essential for productive cell motility in *Dictyostelium* (130) and fish keratocytes (120). We expect that further investigation will uncover links between these processes and leading edge protrusion oscillations.

As explained in "Materials and Methods", we did not model the details of the leading edge actin filament network. Instead, we simplified cell motility into leading edge protrusion, adhesion, and trailing edge retraction. A more detailed

cytoskeletal model than this would be more faithful to sub-cellular morphology and result in some quantitative differences in computed whole cell movement, but would not change the fundamental conclusions reached by our computational study. By parametrizing the inputs to our computational cell models at just 8 points along each side (left and right) of the leading edge and 8 points along the trailing edge, the computations reproduce the dominant features of whole cell movement in quantitative and qualitative terms (Figure 4.4A and 4B). As argued above, this demonstrates the determining role played by cytoskeletal architecture in cell motility and whole cell locomotion.

The acquisition of motility properties by normally stationary epithelial cells is a defining characteristic of breast cancer metastatic progression (86). Motility itself is a product of an array of factors: intra-, inter-, and extracellular. Physical models integrate these diverse influences governing cell behavior by focusing on behavioral outputs (actin protrusion/retraction, whole cell movement, and the like), without necessarily concerning the specific genetic pathways dictating this behavior. This approach allows mechanistic interrogation of cell behavior or, as in the work presented here, mechanistic physical investigation of a specific genetic alteration; investigation that bridges the gap between signaling modifications (typically the subject of genetic and molecular biology studies) and cell behaviors (the focus of cell biology approaches). The fact that this broad incorporation of events yielded the discovery of a specific cellular behavior in our study reflects the utility of physical modeling in answering, and even creating,

specific mechanistic biological questions. Work such as this speaks to the power of physical cancer models to supplement, and even fuel, traditional genetic and molecular studies.

Materials and Methods

Reagents

shRNA was purchased from Open Biosystems through the University of Michigan Life Science Institute High Throughput Screening Core.

Cell Lines

Untransfected MDA-MB-231 were cultured in RPMI 1640 supplemented with 10% fetal bovine serum. Selection media for shRNA-transfected cells consisted of standard cell line media containing 1µg/ml puromycin. MDA-MB-231 stably transfected with both shRNA and RFP-actin were cultured in standard cell line media containing 1µg/ml puromycin and 350µg/ml G418. All cell lines were grown at 37°C in a humidified 5% CO_2 incubator.

Transfections

Two µg of pGIPZ plasmid containing either scrambled or p38γ-specific shRNA were nucleofected into 50-70% confluent MDA-MB-231 cells according to the manufacturer's protocol (Lonza). Nucleofected cells were selected in puromycin and further isolated by FACS sorting for GFP. RFP-actin was inserted into these

cells using the same technique, using G418 for selection followed by FACS sorting for RFP.

Time-Lapse Microscopy

DIC and RFP time-lapse videos were captured at 37°C using a Deltavision RT Live Cell Imaging System equipped with UPlanApo 20x/0.7 NA and 40x/1.2 NA lenses at the University of Michigan Microscopy and Image Analysis Lab. Images were acquired using SoftWoRx 3.5.1 software. For cell motility analysis images were captured every 10 minutes, and for leading edge protrusion analysis images were taken every 1 minute. Cell motility videos were enhanced and analyzed using Imaris (Bitplane Scientific Software), from which the average speed of each cell line was calculated in μm/hour, while leading edge protrusion videos were analyzed using ImageJ and Matlab (www.matlab.com).

Actin Immunocytochemistry

Fifty-70% confluent cells were fixed with 4% paraformaldehyde. Cells were then incubated in 1:50 AF568-phalloidin in PBS (Invitrogen) for 10 minutes, rinsed once in PBS for 5 minutes, and mounted with Prolong Gold anti-fade with DAPI. Images were acquired at room temperature using a Zeiss LSM 510 Meta laser-scanning microscope equipped with a C-Apochr 40x/1.2 NA and LSM 510 software. Each channel was imaged sequentially using multitrack recording before merging. Enhancements were performed using Photoshop (CS2; Adobe).

Actin Angle Analysis

The average stress fiber angles relative to the leading edge were measured using ImageJ. See Figure 4.1B.

Leading Edge Protrusion Analysis

Time-lapse videos of MDA-MB-231 scrambled and shp38γ cells expressing RFP-actin were generated for cell membrane protrusion analysis. Matlab's Image Processing tool box was used to convert the RGB images captured by the microscope to grayscale images of the same size (using the function rgb2gray). Each grayscale image was then converted into binary black/white images based on the threshold pixel intensity, which was determined using the image histogram (function imhist). After thresholding the intensity varied from 1 (white) for the cell to 0 (black) for the background. Comparison of the black and white images with the original RGB images showed no significant loss of accuracy in cell pixel area (imtool, pixel region comparison tool). The edge detection algorithm (edge) was applied to each binary image in order to create a one pixel-wide cell edge. We then created a new sequence of images, each containing the cell edges from two successive time points. These cell edge data were also used to compute cell centroids at each time instant.

The edge-detected images were next used to compute the distance between sections of the leading and trailing edge: A unit vector indicating the direction of cell motion was obtained by connecting the cell's centroids at two successive time instants. A number of pixels were selected on each section of the leading

and trailing edge and connected with the corresponding pixels on the edge at the next time instant using the unit vector for cell motion between these time instants. These pixel-to-pixel distances were tabulated, averaged and then converted to physical length units (microns), using the pixel:length ratio given for the microscope image. For microscope images with poor contrast, we used ImageJ software to manually choose pixels on the cell edge at each time instant. The subsequent steps remained the same.

Finally, we defined left- and right-of-center regions of the cell leading edge as demonstrated in Figure 4.3B. The motion of selected points on the left- or right-of-center regions was averaged over each time interval and subtracted from the motion of the center. These relative protrusions are shown in Figure 4.3C and the half-period of the resulting oscillations are plotted in Figure 4.3D.

The Computational Cell Model

A cell's motility is determined by its deformation in response to internal forces generated by actomyosin contractility. These phenomena are governed by the quasi-static balance of linear momentum, also referred to as the mechanical stress equilibrium equation. Our treatment of this partial differential equation is based on Equation 1 (see Quick Guide to Equations and Assumptions for all equations). The mechanical response of the cell and its sub-structures is described mathematically by the strain (Equation 2) in response to the mechanical stress. The stress-strain equation is expressed in Equation 3.

121

We have used two-dimensional models that represent the cells as seen on a planar substrate—the so-called plane stress approximation in continuum mechanics.(131) These models treat the cells as mechanical structures, with actin stress fibers having the mechanical behavior of thin beams, focal adhesions as fixed supports but allowed to change in time, and the cell wall as a thin membrane. Equations 1—3 are combined, and written in numerical form (Equation 4) suitable for computational solution by the finite element method (132).This is a mathematical technique for numerical solution of partial differential equations written in weak form, such as Equation 1. In the finite element method, Equation 1 is first approximated in a mathematically rigorous manner in terms of matrices and vectors (Equation 4) before solving it by using numerical techniques from linear algebra. The matrix-vector approximation is obtained by approximating the spatial domain of interest (in this case, the cell) as a mesh consisting of nodes and elements. The nodes are points on the cell and the elements are patches over which the mechanical response is averaged in a mathematically-rigorous manner. Using the commercial finite element package ABAQUS v6.8, we developed meshes for the scrambled and shp38γ cells. We use 3-noded continuum plane stress finite elements. The mesh of the scrambled cell used 1278 elements and that for the shp38γ cell used 2671 elements, respectively. See Figure 4.S1 for a detail of a typical finite element mesh. See Table 4.1 for thicknesses of actin fibers and cell membrane in the computational model, and Table 4.2 for computational cell dimensions.

The mechanics of motility and locomotion were recapitulated as follows: The sequence of actin polymerization, focal adhesion formation, and stress fiber retraction was imposed by prescribing the rates of extension/contraction of the mesh regions representing actin fibers by specifying the inelastic strains of these regions, and anchoring of the boundary points that represent stable focal adhesions.

In these exploratory computations we did not model the structural details of leading edge lamellipodial/filopodial protrusion due to polymerization of the leading edge actin filament network. Instead, leading edge protrusion as well as trailing edge retraction due to actomyosin stress fiber contractility were modeled as follows to recapitulate their roles in cell locomotion. The actin cytoskeleton was represented by generic fibers (Figure 4.2C, 4.4A, 4.4B, 4.5A, 4.5B, 4.5D, 4.5E). Each actin fiber was constrained to remain stationary at a chosen point along its length, which models a focal adhesion. The filament was thus divided into leading and trailing parts. The leading part could only extend, thus modeling cell leading edge lamellipodial/filopodial protrusion due to actin filament polymerization. The trailing part could only contract, thus modeling cell trailing edge retraction due to actomyosin contractility. Each such fiber was allowed to either extend while its trailing end was held stationary to model protrusion, or to contract while its leading end was held stationary to model retraction. We note that this combination of mechanisms has been proposed previously by Svitkina

et al. (133). Also see Ridley et al. (37) and Pollard et al. (134). In this work, we have proven that this mechanism leads to locomotion, if the laws of mechanics are used to model the cell and the cytoskeleton, as described above.
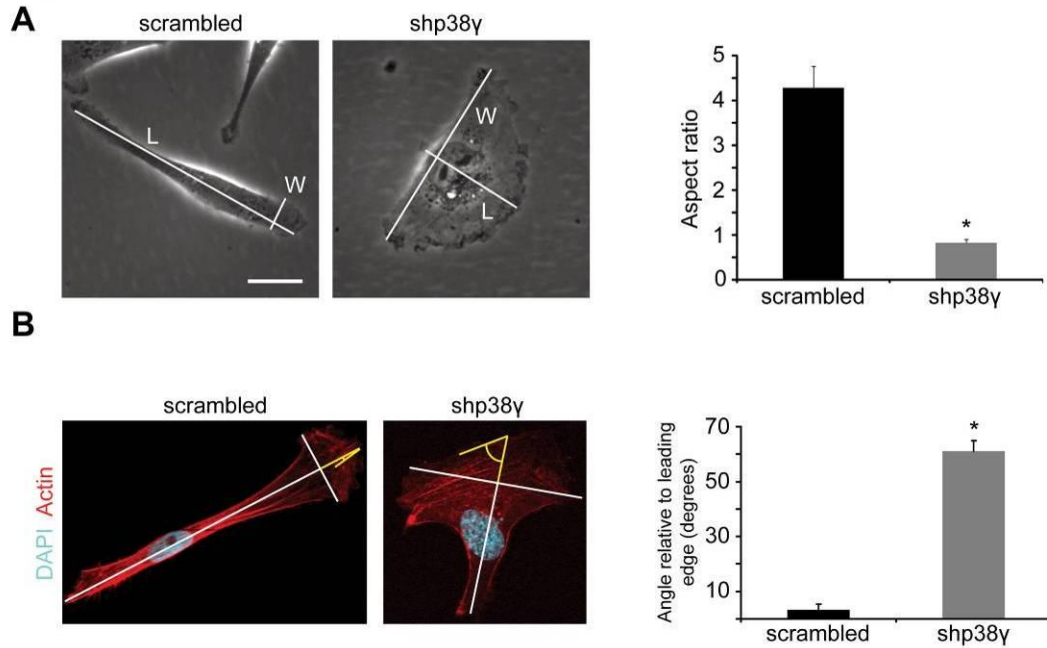
Figure 4.1 - p38γ knockdown alters cell shape and cytoskeletal architecture. (**A**) Cell shape difference by aspect ratio (L/W) (*p<0.05, n = 35 for scrambled and shp38γ, scale bar = 25 μm). Data are represented as ± SEM. This figure is from Ref. 4 (**B**) Scrambled cells have well-defined stress fibers and leading edge filopodia (top right corner of corresponding image). shp38γ cells have bimodally-oriented actin fibers that are parallel to leading edge lamellipodia (upper edge of corresponding image). Stress fiber angles are measured as shown (**p<0.01, n = 16 for scrambled, n = 22 for shp38γ).
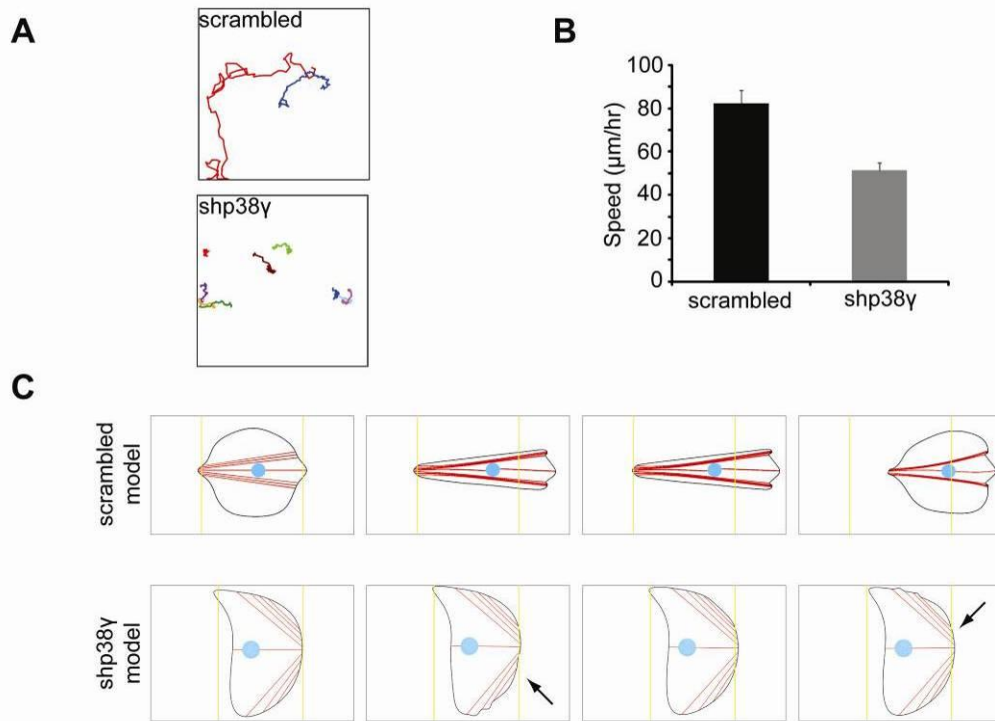
Figure 4.2 – Computational mathematical modeling nominates cytoskeletal architecture as the force driving p38γ-mediated cell motility. (**A**) p38γ knockdown impairs locomotion of MDA-MB-231 cells: Panels show the longer tracks made by scrambled control cells *versus* the shp38γ cells. (**B**) This is further supported by bar graphs on the right showing cell speeds in μm.hr^{-1}. The average speed of scrambled cells is twice that of shp38γ cells (*p<0.01, n = 19 cells for scrambled, n = 24 cells for shp38γ, data are ±SEM). Both (a) and (b) are from Ref. 4. (**C**) Preliminary computational models of scrambled and shp38γ cells using the observed cell-scale dynamics of leading or trailing edge protrusion or retraction, respectively. Note the development of a filopodium at the leading edge of the scrambled cell. Arrows point to out of phase lamellipodial oscillations arising from the two distributions of actin fibers in shp38γ cells. The actin fibers are in red and the nucleus is blue. The models successfully represent the coordinated locomotion of scrambled cells, and the oscillatory motility but ineffective locomotion of shp38γ cells.
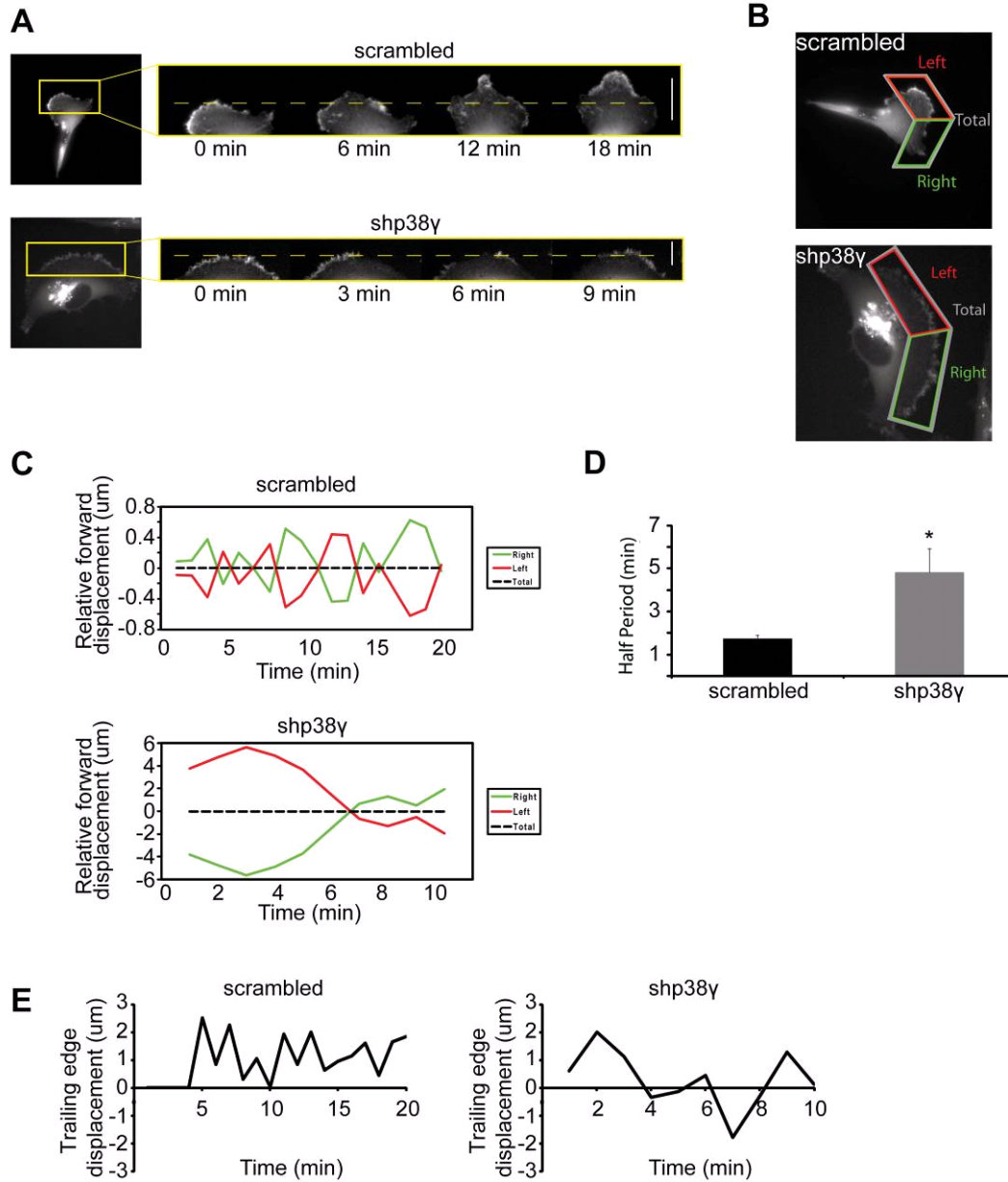
Figure 4.3 – The leading edge protrusion dynamics predicted by the *in silico* shp38γ model occur in live cells, and these behaviors differ between scrambled and shp38γ cells. (**A**) Kymographs of leading edge protrusion in scrambled and shp38γ cells. (**B**) Detail showing the "left-" and "right" sides of the leading edges of scrambled and shp38γ cells. (**C-D**) Dynamics of left and right sides of cell leading edges. Leading edge velocities from the highlighted regions in (**B**) are represented graphically (**C**). The reference velocity is set such that total forward displacement equals zero; thus, forward movement greater than the average of left and right appears positive, and forward movement less than the total average appears negative. (**D**) The half-period in (**C**) (average time between left-right intersections) is significantly longer for shp38γ cells than scrambled cells (*p<0.0072, n = 3 for each cell line). Data are representative of three

127

independent experiments and are represented as ± s.e.m. (**E**) Trailing edge motion of scrambled and shp38γ cells plotted as the incremental displacement between successive time instants. For scrambled cells the most rearward point was chosen. For shp38γ cells the positions were averaged over 8 points evenly spaced along the trailing edge.
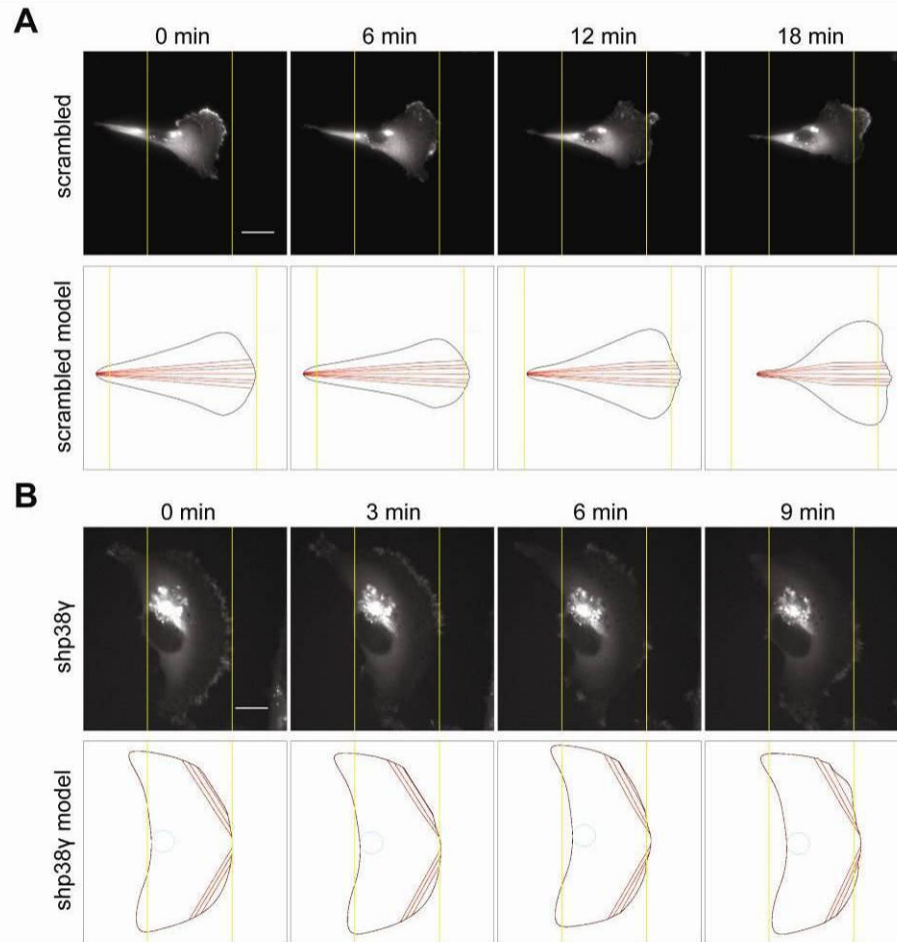
Figure 4.4 - Incorporating experimentally-derived leading edge protrusion dynamics into *in silico* scrambled and shp38γ cells more accurately represents, but does not change the fundamental behavior of, cell motility in the models. Time lapse images of RFP-actin-transfected scrambled (**A**) and shp38γ (**B**) cells (scale bar = 20 μm). Note the successful trailing edge retraction in scrambled, but not in shp38γ cells. Finite element computations for each cell type *computational*, shown below the corresponding live cell images, accurately model cell locomotion using only the morphology of the actin fibers (red) from Figure 4.3 to actuate the dynamics of actin filament protrusion at the cell leading edge (see Figure 4.5 for control experiments), and trailing edge retraction by actomyosin contractility. Together with the results of Figure 4.5, this validates the accuracy of our computational mechanical model in resolving whole cell locomotion from sub-cellular motility data.
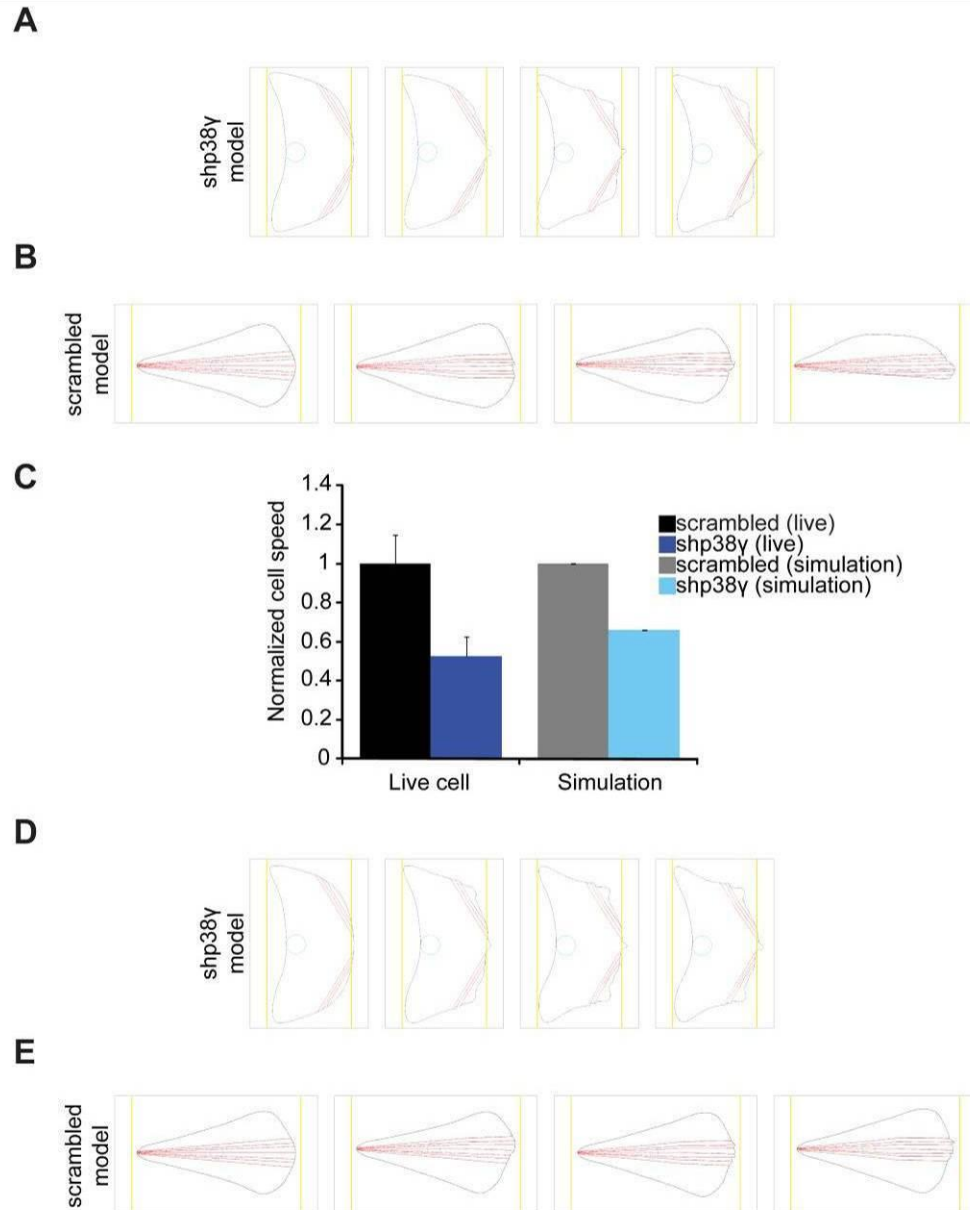
Figure 4.5 – Cytoskeletal architecture, not leading edge protrusion dynamics, defines cellular motility. (**A**) Motility of computational shp38γ cells obtained by transposing leading/trailing edge actin dynamics from scrambled cells does not rescue the ineffective locomotion of shp38γ cells. (**B**) Transposing leading/trailing edge dynamics of shp38γ cells on computational scrambled cells results in motility and locomotion that is unphysical. (**C**) Ratio of computational cell speeds from synthetic motion (see text for details) is the same as ratio of live cells. (**D-E**) Synthetic motility of computational shp38γ and scrambled cells is qualitatively similar to live cells.

Movie 1: The motility and locomotion of scrambled (left) and shp38γ (right) live cells.

Movie 2: The motility and locomotion of preliminary models of scrambled (left) and shp38γ (right) *in silico* cells.

Movie 3: The motility and locomotion of enhanced models of scrambled (left) and shp38γ (right) *in silico* cells, incorporating the leading edge protrusion and trailing edge retraction dynamics from Figure 4.3 in the main paper.
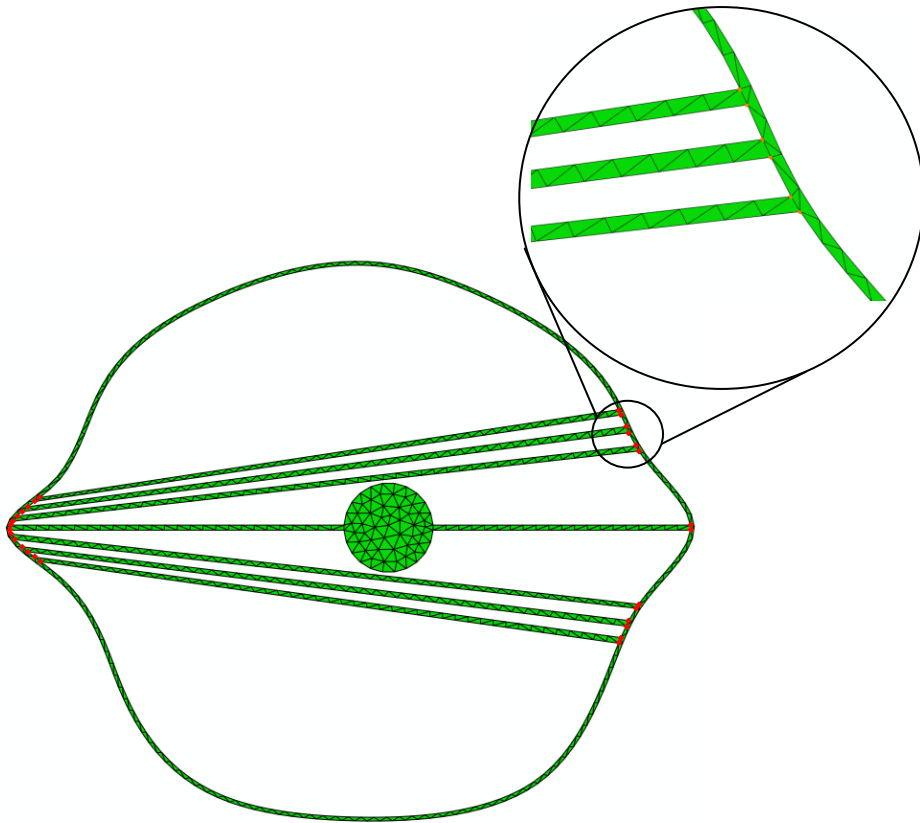
Figure 4.S1. Detail showing the finite element mesh with elements (triangles). The nodes are the vertices of the triangles.
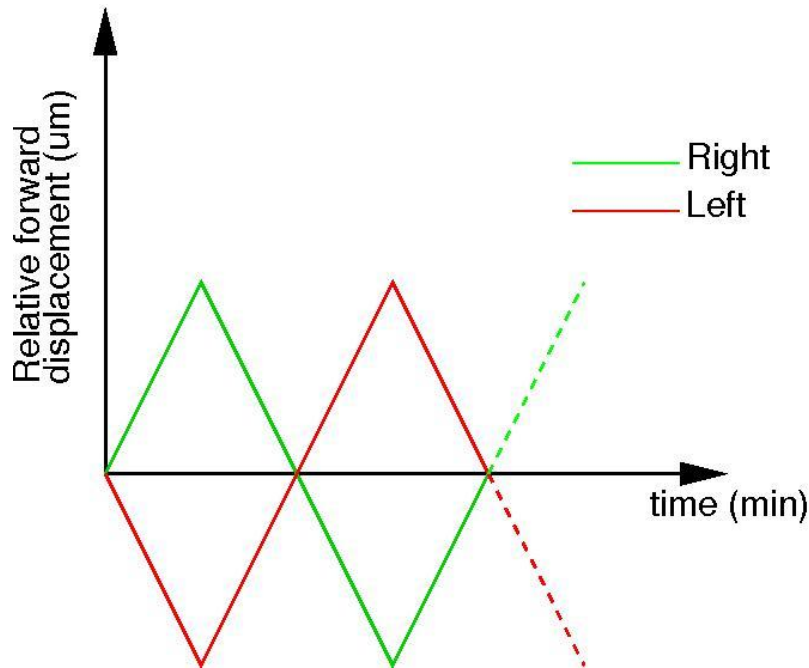
Figure 4.S2. Synthetic leading edge protrusion/retraction dynamics used to separate the effect of actin dynamics from cell shape and cytoskeletal morphology. The definition of left- and right-of-center regions and their displacements are as defined in Figure 4.3B in text.

References

37.   Ridley AJ, Schwartz MA, Burridge K, Firtel RA, Ginsberg MH, Borisy G, et al. Cell migration: integrating signals from front to back. Science. 2003;302:1704-9.

86.   Hanahan D, Weinberg RA. The hallmarks of cancer. Cell. 2000;100:57-70.

103.   Ladwein M, Rottner K. On the Rho'd: the regulation of membrane protrusions by Rho-GTPases. FEBS Lett. 2008;582:2066-74.

116.   Weinberg RA. The Biology of Cancer. 1 ed. New York, NY: Garland Science; 2007.

117.   Thiery JP. Epithelial-mesenchymal transitions in development and pathologies. Curr Opin Cell Biol. 2003;15:740-6.

118.   Rosenthal DT, Escudero SE, Bao L, Wu Z, Merajver SD. p38γ drives breast cancer cell motility and metastasis through regulation of RhoC GTPase. Cancer Research. 2011;Concurrent Submission.

119.   Phillips R, Kondev J, Theriot J. Physical biology of the cell. New York: Garland Science; 2009.

120.   Barnhart EL, Allen GM, Julicher F, Theriot JA. Bipedal locomotion in crawling cells. Biophys J. 2010;98:933-42.

121.   Ehrengruber MU, Coates TD, Deranleau DA. Shape oscillations: a fundamental response of human neutrophils stimulated by chemotactic peptides? FEBS Lett. 1995;359:229-32.

122.   Mogilner A. On the edge: modeling protrusion. Curr Opin Cell Biol. 2006;18:32-9.

123.   Peskin CS, Odell GM, Oster GF. Cellular motions and thermal fluctuations: the Brownian ratchet. Biophys J. 1993;65:316-24.

124.   Mogilner A, Oster G. Force generation by actin polymerization II: the elastic ratchet and tethered filaments. Biophys J. 2003;84:1591-605.

125.   Dickinson RB, Caro L, Purich DL. Force generation by cytoskeletal filament end-tracking proteins. Biophys J. 2004;87:2838-54.

126.   Dickinson RB, Purich DL. Clamped-filament elongation model for actin-based motors. Biophys J. 2002;82:605-17.

127.   Plastino J, Sykes C. The actin slingshot. Curr Opin Cell Biol. 2005;17:62-6.

128.   Gerbal F, Chaikin P, Rabin Y, Prost J. An elastic analysis of Listeria monocytogenes propulsion. Biophys J. 2000;79:2259-75.

129.   Bernheim-Groswasser A, Prost J, Sykes C. Mechanism of actin-based motility: a dynamic state diagram. Biophys J. 2005;89:1411-9.

130.   Del Alamo JC, Meili R, Alonso-Latorre B, Rodriguez-Rodriguez J, Aliseda A, Firtel RA, et al. Spatio-temporal analysis of eukaryotic cell motility by improved force cytometry. Proc Natl Acad Sci U S A. 2007;104:13343-8.

131.   Timoshenko S, Goodier J. Theory of Elasticity. New York: McGraw-Hill; 1951.

132.   Hughes TJR. Linear Static and Dynamic Finite Element Analysis Mineola, NY: Dover Publications; 2000.

133.	Svitkina TM, Verkhovsky AB, McQuade KM, Borisy GG. Analysis of the actin-myosin II system in fish epidermal keratocytes: mechanism of cell body translocation. J Cell Biol. 1997;139:397-415.

134.	Pollard TD, Cooper JA. Actin, a central player in cell shape and movement. Science. 2009;326:1208-12.

Chapter V

Conclusions and Future Directions

Conclusions

Cancer metastasis is a complex, multi-faceted process, and has accordingly been a tremendous obstacle for researchers and clinicians to fully understand and overcome. Despite its complexity, metastasis can be broken down into simple, overarching questions that address metastatic behavior. Here we interrogated the following two questions in an attempt to unravel metastatic complexity: What causes a cancer cell to become metastatic, and what then enables the metastatic behaviors of an already-metastasizing cancer cell?

Through our investigations we discovered that RhoC is an essential switch for determining whether or not a cancer cell is metastatic—even within the already aggressive cancer stem cell population. Once a breast cancer cell is metastatic, we found that p38γ mediates many of the mesenchymal-like metastatic properties of the metastasizing cell. Using a novel fusion of computational modeling and cell biology we dissected a physical mechanism by which p38γ regulates breast cancer cell motility, and in doing so discovered a new physical behavior of motile cells.

This work directly addresses the aforementioned questions and provides some answers; however, as with most scientific endeavors, the results yield more new research avenues and questions than they do concrete conclusions. Here we elaborate on the conclusions from this body of work and offer several perspectives on future research aimed at more deeply interrogating the questions raised by our current findings.

RhoC and breast cancer stem cells

We discovered that RhoC is both necessary and sufficient for breast cancer stem cell (BCSC) metastasis (Chapter 2). That RhoC contributes to breast cancer metastasis in general is neither surprising nor unprecedented—RhoC has previously been shown be necessary for breast cancer metastasis (55) and to induce metastatic properties *in vitro* in otherwise benign mammary epithelial cells (51, 95). The novelty of the current findings lies in the *sufficiency* for RhoC overexpression alone to induce metastasis, and the ability of RhoC to dictate metastasis of the BCSC population.

Until recently, the implicit assumption within the CSC field was that CSCs were a homogenous minority within an otherwise heterogeneous tumor. Though never directly stated as such, the majority of experiments focused on the CSC population as a whole—are CSCs tumorigenic, can CSCs be serially passaged, does the abundance of CSCs confer a worse prognosis—in effect neglecting any potential heterogeneity within the CSC population.

Recent studies identified subpopulations within the bulk CSC population that are required for metastasis (25, 26), suggesting that functional heterogeneity may exist within the CSC population. However, these studies identified subpopulations based on molecular markers and their *necessity* for metastasis, not molecular promoters that are *sufficient* for metastasis; therefore, the metastatic catalyst(s) remained undetermined. Although many genes are necessary for metastasis, few are sufficient, and likely even fewer are sufficient to alter the metastatic potential of a stringently selected population of cells such as CSCs. Here we identify RhoC as one such gene—to our knowledge the first identified molecular promoter of BCSC metastasis.

The work of Hakem et al. has been the defining *in vivo* work on RhoC in breast cancer metastasis for half a decade (55). Hakem and colleagues elegantly demonstrated that RhoC is dispensable for tumorigenesis but necessary for metastasis. The reciprocal experiment, however—determining RhoC sufficiency to induce breast cancer metastasis—has never been performed. Determining sufficiency separate from necessity is essential for understanding the switch to metastasis; a transition most clearly demonstrated by aggressive breast cancer subtypes, such as inflammatory breast cancer (IBC), that are metastatic from their inception.

Using IBC as a paradigm for metastatic progression, one can begin to grasp the importance of delineating sufficiency from necessity. IBC rarely presents with a cohesive primary tumor and therefore, as mentioned, is metastatic from its earliest stage. By defying the normal progression of epithelial cell→primary tumor→metastasis and instead sublimating from normal to metastatic, one would expect that the genes driving IBC are therefore sufficient to induce metastasis, irrespective of their tumorigenic potential.

As previously described (see Chapter 2), RhoC is necessary for breast cancer metastasis (52, 55), RhoC is overexpressed in IBC (85, 135), IBC has a high prevalence of BCSCs in lymphovascular emboli (136), and BCSCs mediate IBC metastasis (24). In light of these correlative connections, we hypothesized that RhoC may be sufficient to promote metastasis, and may function within the BCSC population.

Our experiments confirmed the previous findings that RhoC is necessary for breast cancer metastasis, as metastasis of IBC-derived SUM149 cells was significantly impaired following RhoC inhibition. RhoC sufficiency to promote metastasis was shown most clearly through ectopic overexpression in the non-tumorigenic, non-metastatic MCF-10A cell line. Ectopic RhoC overexpression was sufficient to promote MCF-10A metastasis *independent from primary tumor formation*, even within the ALDH (-) population. Taken together, these results strongly implicate RhoC as a <u>metastatic oncogene</u>; a gene that, when aberrantly

expressed, is capable of specifically inducing metastasis independent of primary tumor formation. We do not presume to support or challenge the central tenants of the CSC hypothesis here, but rather provide evidence suggesting that, while the metastatic potential of cancer cells may be enhanced by CSC identity, it is ultimately determined by expression of metastatic oncogenes, such as RhoC.

Interestingly, the relative abundance of BCSCs within both cell lines fluctuated according to RhoC expression. Links between RhoC and stem cell maintenance are limited and correlative at best—RhoC expression has been linked to glial progenitor cell populations (137) and RhoC is a downstream effector of Notch in cervical carcinoma cells (138)—therefore the connection between RhoC expression and BCSC population size must be further evaluated. One can speculate, though, that perhaps a certain percent of BCSCs within a tumor are inherently primed for metastasis. If these cells are metastatic BCSCs from inception, inhibiting RhoC as performed here may in effect eliminate that portion of the BCSC population and prevent early cancer cell dissemination. Such a concept is enticing, however much more research must be conducted to begin to test this hypothesis.

p38γ in breast cancer metastasis

In chapter 3 we investigated the role of p38γ in breast cancer metastasis. We discovered that p38γ is necessary for breast cancer metastasis, and is specifically involved in mediating mesenchymal-like behaviors such as motility

and invasion. This link between p38γ and mesenchymal-like behaviors was not entirely unexpected, as we originally hypothesized that p38γ may function in basal-like breast cancers based on its known role in muscle development (69, 71, 72, 74).

All cells within the body are united by a common set of genes. The differences between cell types thus lie not in their genomic blueprint, but in the utilization of their genetic material. For this reason one should not be surprised to find that, in order to behave like a muscle cell, a metastatic breast cancer cell usurps muscle-specific genes. As Gertrude Stein put it, "a rose is a rose is a rose"; in this case a non-muscle cell with the underlying genetic potential to behave like a muscle cell must utilize the genes used by muscle cells to behave like a muscle cell ("a muscle is a muscle is a muscle"). Data such as that presented here thus strongly supports the use of basic developmental research to inform and fuel translational cancer research.

p38 MAPK research has long been confounded by apparently conflicting results—is p38 pro-apoptotic, anti-apoptotic, pro-motility, or pro-differentiation (79)? Here we add to these discrepancies by demonstrating that p38γ overexpression and overactivation is an integral component of the basal-like breast cancer subtype. Interestingly, inhibiting either p38α or p38β individually had no effect on MDA-MB-231 cell behavior, whereas inhibiting either p38γ or p38δ had profound impacts (data not shown), indicating that the non-canonical

141

p38 isoforms may function independently in some cancer subtypes. This is especially relevant given that the vast majority of p38 research has focused on either the α or β isoforms, often without discriminating between the two. The data we present here strongly supports further research into the specific contributions of each p38 isoform—particularly the non-canonical γ and δ isoforms.

Interestingly, p38γ and RhoC expression are related, as changes in p38γ expression affect RhoC protein levels. This regulation is specifically due to changes in RhoC ubiquitination—a mechanism of regulation never before seen for RhoC. Although RhoC is overexpressed in many types of cancer (51-54), to date there is no identified mechanism for this upregulation. Preventing RhoC ubiquitination could serve as one such mechanism, and it also provides a mechanism for regulating RhoC expression on a short time scale compatible with the rapid turnover needed to regulate normal cell motility. Additional research into the proteins that regulate RhoC ubiquitination, as well as the biochemical details of RhoC ubiquitination, is therefore urgently needed.

p38γ and the cytoskeleton

Using a combination of cell biology and computational mechanical modeling we were able to determine a likely mechanistic link between the p38γ–mediated effects on cytoskeletal architecture and cell motility. By using computational modeling we also discovered, and subsequently experimentally verified, a novel physical behavior of motile cells—leading edge protrusion oscillations.

The computational models revealed that p38γ-mediated changes in cytoskeletal architecture were sufficient to alter MDA-MB-231 cell motility in both the qualitative and quantitative manners observed in live cells. Interestingly, this link was established in the absence of any genetics (other than p38γ knockdown), and was instead simply based on the physical properties of the motile cell—membrane and actin cytoskeleton rigidity, rates of protrusion and retraction, and the like. This work thus represents an alternative paradigm to the traditional "mechanistic" study. Rather than focusing on cellular signaling mechanisms—many of which can be compensated for by alternate signaling pathways—we focused on the physical, behavioral endpoint of these signaling networks; in essence accounting for all possible signaling inputs.

Although such a study does not immediately reveal specific, druggable targets, it does provide a systems-wide perspective on aberrant cell behavior (in this example, altered cell motility as a consequence of genetic manipulation) that can ultimately be used to identify new drug targets. Instead of trying to elucidate the individual signaling molecules that enable a phenotypic change, using computational mechanical modeling permits one to take a top-down approach. By understanding the basic physical properties that contribute to a given cellular behavior (here cytoskeletal architecture contributing to mesenchymal-like cell motility) one can work backwards; first identifying broad signaling networks that contribute to the physical behavior (i.e. cytoskeletal remodelers), narrowing that

143

down to protein families that govern the detailed physical properties underlying the cellular phenotype (i.e. Rho GTPases and stress fiber formation), and finally delineating the specific signaling molecules driving the observed phenotype (i.e. RhoC). Such an approach addresses issues such as crosstalk and compensation early on by implicitly incorporating them into the original mechanical model. Using signaling-based mathematical modeling and systems biology one could also aim to predict potential sources of compensation when therapeutically targeting the identified molecular driver (i.e. other Rho GTPases compensating for RhoC knockdown), and eventually determine optimal multi-target therapies aimed at disrupting a behavior, rather than a specific protein.

Future Directions

RhoC influence on BCSC population size

In the course of our analysis of RhoC influence on BCSCs we discovered that the abundance of BCSCs within a cell line changes concordant with RhoC expression (Chapter 2). These initial observations were made by using flow cytometry to compare the percent of ALDH (+) cells between our genetically-modified cell lines. This exciting and important initial result opens the door to more detailed studies investigating the RhoC-BCSC population size connection.

Although our initial flow results were intriguing, further studies need to be performed to accurately define the relationship between RhoC and BCSC population size. At present we have correlative evidence linking RhoC and BCSC

abundance; we now need to functionally evaluate this relationship. One standard functional measure of BCSC abundance is the mammosphere assay (139). In this assay, breast cancer cells are grown in a specialized suspension culture that selects for BCSC growth. Using this assay, we can evaluate whether the percent of cells capable of forming mammospheres differs between our RhoC-modified cell lines, thereby addressing the question "does modulating RhoC expression affect the abundance of functional BCSCs?"

If RhoC does affect BCSC population size, as preliminary data indicates is the case, the next logical question is "does RhoC affect BCSC self-renewal?" To address this question, mammospheres from the aforementioned experiment can be serially passaged. If BCSCs retain their self-renewal abilities regardless of RhoC expression, we would expect that the same percent of dissociated cells from primary mammospheres generated by each cell line will be able to form new mammospheres.

RhoC regulation of p38γ

We have shown that there is a strong, persistent relationship between p38γ and RhoC, and that p38γ can regulate RhoC expression by affecting RhoC ubiquitination (Chapter 3). Surprisingly, we have also observed that the reverse may be true as well—that RhoC may regulate p38γ expression.

We assayed p38γ mRNA levels in MCF-10A cells that overexpress constitutively active RhoC (10A G14V) compared to vector control MCF-10A (10A vec) and were surprised to find that p38γ expression was increased approximately two-fold in the 10A G14V cells—to nearly identical levels as MDA-MB-231 cells (Figure 5.1A).

The strongest evidence to date for RhoC regulating p38γ expression comes from a mammary-specific transgenic RhoC overexpression mouse model generated by our lab. This model uses the mouse mammary tumor virus (MMTV) promoter to drive constitutive mammary-specific overexpression of RhoC. We have also crossed this mouse with the tumorigenic and metastatic MMTV-driven Polyoma Middle-T (PyMt) mouse to create the PyMt-RhoC double transgenic.

When we assayed p38γ expression in mammary glands from the transgenic mouse strains (RhoC, PyMt, and PyMt-RhoC) compared to a control mouse (C57BL/6), we found that p38γ protein levels were elevated in all of the transgenic strains (Figure 5.1B). Interestingly though, p38γ levels were highest in the RhoC-overexpressing mice (RhoC and PyMt-RhoC), suggesting that RhoC overexpression is independently capable of increasing p38γ expression. Taken together with the cell line data, these findings strongly suggest that RhoC expression regulates p38γ expression.

To stringently test the hypothesis that RhoC regulates p38γ it is crucial to determine p38γ transcriptional, translational, and post-translational expression in each of the aforementioned systems (*in vitro* RhoC overexpression and transgenic mouse models). These experiments will allow us to deduce at which level of expression RhoC affects p38γ. From these data additional hypotheses regarding the RhoC mechanism of action for regulating p38γ can be generated.

If RhoC and p38γ do in fact regulate one another, two questions emerge: 1) do these two genes constantly regulate one another, or 2) does one initially activate the other (similar to the "Vogelgram" model of cancer progression (140)), which in turn maintains expression of the first? It is possible, for example, that during breast cancer progression RhoC is first overexpressed. RhoC overexpression may then increase p38γ expression, which in turn helps stabilize RhoC protein by preventing RhoC ubiquitination, thus maintaining a synergistic activation loop. Such a scenario fits with the previously described concept of RhoC as an initiator and p38γ as a maintainer of metastasis.

To begin to dissect this complex relationship we must first knock down RhoC in a RhoC- and p38γ-overexpressing breast cancer cell line, such as MDA-MB-231, and determine the effect on p38γ expression. If p38γ expression decreases in this cell line then the two are likely acting in synergy, which fits with example 1 from the previous paragraph. If p38γ expression is unaffected it is likely that RhoC no longer influences p38γ expression, as described in example 2. To

further examine the interrelationship between p38γ and RhoC, we will analyze expression of each protein in clinical breast cancer samples that span the stages of cancer progression—from normal breast to metastatic disease—and determine 1) expression of which, if either, protein increases first during breast cancer progression and 2) at which point(s) during breast cancer progression expression of the two proteins are highly correlated.

Regulation of p38γ activation

Phosphorylation is the standard mechanism for p38γ activation, and we demonstrated that p38γ phosphorylation is higher in breast cancer cells than non-tumorigenic mammary epithelial cells (Chapter 3). It is therefore pertinent to determine the upstream signaling events contributing to p38γ activation in breast cancer.

To address this question we analyzed mRNA levels of several p38 activators in MCF-10A vec, MCF-10A G14V, and MDA-MB-231 cells. We found that mRNA levels of the two major p38 activators, MKK3 and MKK6, are elevated in MDA-MB-231 cells compared to non-tumorigenic 10A vec cells (Figure 5.1C). When we assayed protein levels of these kinases in the transgenic RhoC models we observed that MKK6 expression varied concurrent with RhoC expression, while MKK3 expression was unaffected (Figure 5.1D). Interestingly, MKK3 and MKK6 mRNA levels were not increased in 10A G14V cells (Figure 5.1C), suggesting that RhoC may influence expression of MKK6 at the translational or post-

translational level. This may be mediated in part by affecting MKK3/6 phosphorylation, as phosphorylation of these two proteins is concomitantly increased with elevated RhoC expression (Figure 5.1D). Taken together, these data suggest that RhoC is influential on p38 signaling as a whole, and may specifically target the p38γ isoform.

Future experiments will assay the phosphorylation levels of MKK3 and MKK6 separately, as each isoform has been shown to have distinct effects on p38γ activation (141). Our experiments thus far suggest that p38γ activation in breast cancer cells is constitutive and occurs independent of external factors, which is consistent with cancer cells developing independence from extracellular signals (86). It is therefore imperative to determine where the upstream activation signals leading to constitutive p38γ activation in breast cancer come from, since p38γ activation likely stems from an intracellular source (rather than environmental stimuli, as is typically the case for p38 in non-tumorigenic cells). The source of p38γ activation should be a significant therapeutic target, as it is likely the driving force behind a broad array of aberrantly activated signaling pathways.

p38γ influence on focal adhesions and traction forces of migrating cells

In chapter 4 we analyzed in detail the aberrant motility of shp38γ cells and deduced the role of actin cytoskeletal architecture in p38γ-mediated cell motility, focusing specifically on stress fiber orientation. Although this study revealed an important role for the cytoskeleton in p38γ-mediated mesenchymal-like cell

motility, as discussed in Chapter 1, there are many other cellular components that contribute to mesenchymal-like cell motility.

Focal adhesions play an essential role in regulating actin stress fiber orientation, protrusion, retraction, and localization (31). Therefore, if cytoskeletal architecture and protrusion dynamics are affected by a genetic modification—as was shown to be the case following p38γ knockdown in chapter 4—focal adhesion distribution or dynamics are likely altered.

To investigate the role of focal adhesions in p38γ-mediated cell motility, we assayed focal adhesion protein expression levels and localization. Although overall levels of vinculin (a focal adhesion component) do not change between 231 scrambled and shp38γ cells (Figure 5.2A), focal adhesion distribution is dramatically altered (Figure 5.2B). In scrambled cells, focal adhesions are tightly clustered to the leading and trailing edges of the cell (Figure 5.2B, left), as is expected for mesenchymal-like cells (31, 142). By contrast, focal adhesions in shp38γ cells are indiscriminately dispersed around the cell periphery (Figure 5.2B, right), suggesting that shp38γ cells do not completely polarize to designate a leading and trailing edge.

Focal adhesions are the physical connections between a cell and its substrate, and accordingly are the sites of traction force during cell motility (31, 142); therefore, focal adhesions and traction force distribution are intimately intertwined

(142). While much research has centered on the genetic and molecular determinants of cancer cell motility, relatively little research has focused on the physical behaviors of moving cancer cell—specifically which forces characterize motile cells, and are consequently required for productive cell motility.

In collaboration with Dr. Jianping Fu we are employing a novel system for analyzing traction forces in scrambled and shp38γ cells, termed the micropost array device (mPAD) (143). Briefly, the mPAD is a dense array of polydimethylsiloxane (PDMS) pillars which cells are cultured on top of. By measuring post bending generated by cell-post interactions, the magnitude, distribution, and directionality of traction forces exerted by a cell can be calculated by a customized MATLAB program (143).

After optimizing the mPAD system for our scrambled and shp38γ cells, we were able to measure the traction forces exerted by both cell types. Though preliminary, our current data show that, as expected, distribution of traction forces in each cell type is roughly the same as focal adhesion distribution (Figure 5.2C – compare to Figure 5.2B). Interestingly, the overall force exerted by each cell type is not significantly different, nor is the vector sum force (Figure 5.2D). The differences in force instead lie with both the directionality of cell force, as well as the maximum force. The scrambled cell reaches peaks in both total force (143 nN) and vector sum force (35 nN) during contraction (Figure 5.2D). By contrast, the shp38γ cell total force peaks at 133 nN and the vector sum force

oscillates over time and only reaches a maximum of 23 nN, and the cell never undergoes rapid, contractile movement (Figure 5.2D). Taken together, these data suggest that directional, contractile cell motility requires polarized traction forces, and that these forces must be able to reach a certain force maximum.

To further probe this hypothesis, we will analyze additional cells during all phases of cell motility (protrusion, elongation, and contraction) to see if a force threshold value emerges. In addition, we will divide the forces in these cells into leading edge and trailing edge components and observe the specific forces required at each end of the cell for efficient cell elongation and contraction. To explore the genetic requirements for the observed traction forces and focal adhesion distribution, we will perform the same experiments using shp38γ cells that are forced to re-express RhoC (see Chapter 3). Since RhoC has been shown to be involved in stress fiber formation, contraction, and focal adhesion turnover (40, 47, 48), we expect that rescuing RhoC expression will redistribute focal adhesions in shp38γ cells to more closely resemble scrambled cells, potentially allowing shp38γ cells to generate sufficient polarized traction force to produce contractile movement. Lastly, these experiments will be extended to additional breast cancer cell lines that rely on p38γ for their motility (i.e. BT549 and Hs578t) to determine whether our results are broadly applicable.

Once detailed traction force data has been generated and analyzed, we can expand our studies into real-time, dynamic analysis of other motility related

processes—namely focal adhesion dynamics and cytoskeletal remodeling. By transfecting fluorescently-tagged actin and focal adhesion marker (such as vinculin or paxillin) expression plasmids into scrambled and shp38γ cells, we can observe the behavior of both motility components in real-time, with direct relation to whole cell movement and subcellular traction forces. Using these additional parameters, we can extend our initial cytoskeleton-based computational model of cell motility to begin generating a comprehensive, system-wide model of cell motility.

Proteomic and phospho-proteomic analysis of p38γ signaling in breast cancer

p38 is a well-established signaling hub capable of integrating wide-ranging inputs into diverse cellular responses (57); however, a systems biology view of p38 signaling in cancer—specifically p38γ signaling—has not been established. To address the diverse signaling roles of p38γ in breast cancer, we will determine quantitative proteomic and phospho-proteomic changes in MDA-MB-231 cells resulting from p38γ knockdown using Stable Isotope Labeling with Amino acids in Cell culture (SILAC) (144).

In brief, SILAC is a mass spectrometry (MS)-based technique for determining the relative abundance of isotopically-labeled proteins between two samples (in our case scrambled vs. shp38γ cells). By isotopcially-labeling the proteins in one sample (i.e. shp38γ) but not the other (i.e. scrambled), the MS peaks for identical

proteins from different samples will appear at slightly different retention times. By measuring the peak height for each sample the relative protein expression in one sample can be compared to the other. Phospho-SILAC is essentially identical to SILAC except that samples are enriched *a priori* for phosphopeptides by affinity purifying whole cell lysates on a phosphopeptide-binding TiO_2 column (145).

p38γ knockdown in MDA-MB-231 cells produces dramatic changes in cell behavior, from changes in cell shape and motility (Chapters 3 and 4) to changes in proliferation (data not shown). Since p38γ is a kinase and typically exerts its effects through phosphorylation of target proteins, we expect that many of its effects on cell behavior begin as changes in protein phosphorylation. To address this hypothesis, we will quantitatively determine differences in the phosphoproteome, and in the relative levels of phosphorylation of individual proteins, between scrambled and shp38γ cells using phospho-SILAC.

As exemplified by the changes in RhoC expression observed in Chapter 3, p38γ can also indirectly affect expression of important proteins, independent of phosphorylation. To gain a deeper understanding of p38γ effects on cell signaling we will analyze relative changes in total protein levels between scrambled and shp38γ cells using standard SILAC.

From these two datasets we can generate a systems-wide portrait of p38γ function in breast cancer cell behavior. By relating changes in signaling pathways

to the observed phenotypic effects of p38γ knockdown we can identify essential networks in the p38γ signaling cascade that govern the tumorigenic and metastatic properties of basal breast cancer cell behavior, and thus likely represent prime therapeutic targets. Understanding p38γ signaling at a systems-level will also fuel hypotheses regarding p38γ function in normal breast development, as well as in other cancer types.

Identify p38γ-specific inhibitors for therapeutic targeting

The work presented here provides strong rationale for therapeutically targeting p38γ as a means of preventing breast cancer metastasis, and previous work has shown that inhibiting p38γ also helps sensitize cancer cells to PARP inhibitors (146, 147). p38γ knockout mice have no adverse effects (68), suggesting that inhibiting p38γ may be minimally toxic. Additionally, inhibiting p38γ in breast cancer cells does not result in compensatory upregulation of other p38 isoforms, unlike inhibition of the other p38 isoforms—a trait attributed to the limited efficacy of p38 inhibitors in clinical trials (68, 148, 149). Unfortunately, at present there are no p38γ-specific pharmacologic inhibitors (BIRB-796 does inhibit p38γ at high doses, but also inhibits the other four p38 isoforms (150)).

Because of the high specificity required to inhibit p38γ independent of the other three p38 isoforms, it will be necessary to screen a large number of compounds. The University of Michigan Center for Chemical Genomics has over 174,000 chemical compounds and 20,000 natural compounds on hand, as well as high

throughput screening capabilities. By biochemically screening for compounds that inhibit p38γ interaction with a downstream effector (using a mammalian two-hybrid screen or a FRET-based screen), we can identify candidate p38γ-specific drugs, which can subsequently be validated in the lab through functional assays and comparison to shp38γ cells.
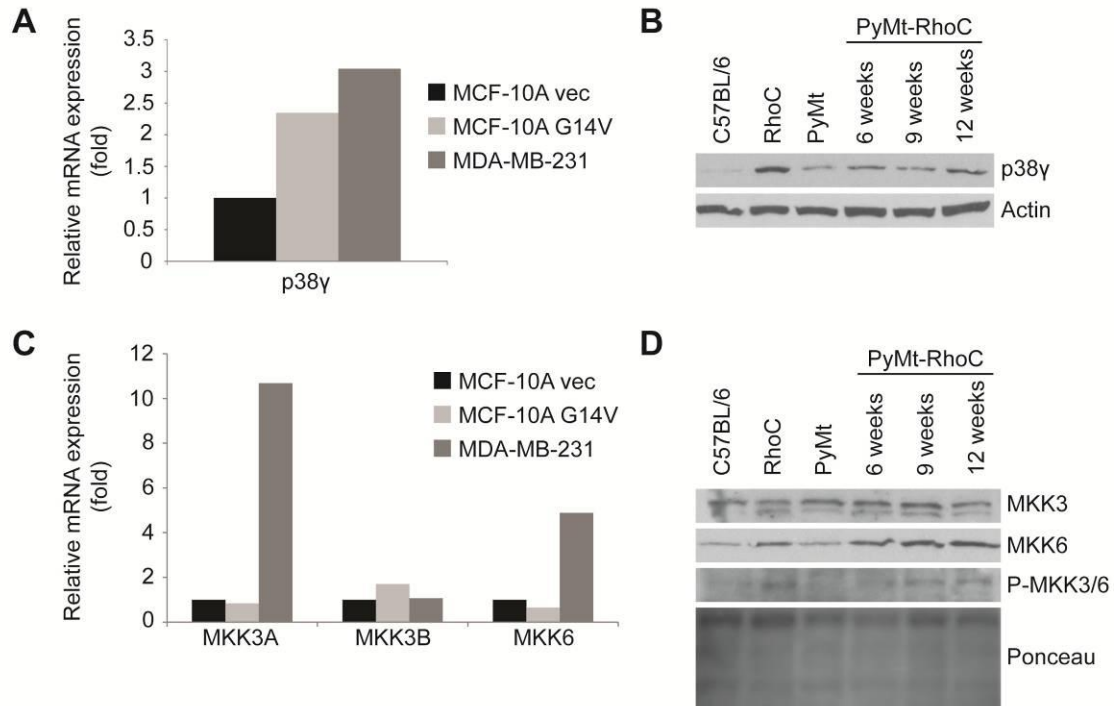
Figure 5.1 – RhoC regulates expression of p38γ and its upstream kinases.
(**A**) Ectopic RhoC expression in MCF-10A cells increases p38γ mRNA levels to levels comparable to MDA-MB-231 cells. (**B**) p38γ protein expression is increased in transgenic mice that overexpress either RhoC or PyMt and RhoC. (**C**) mRNA levels of MKK3 and MKK6, both upstream p38γ kinases, are increased in MDA-MB-231 cells but are not affected by RhoC G14V overexpression. (**D**) RhoC overexpression increases MKK6 expression and MKK3/6 phosphorylation, but not MKK3 expression, in both RhoC transgenic mouse models. Interestingly, although RhoC expression increases MKK6 protein levels it does not appear to affect MKK6 mRNA levels (**C**).
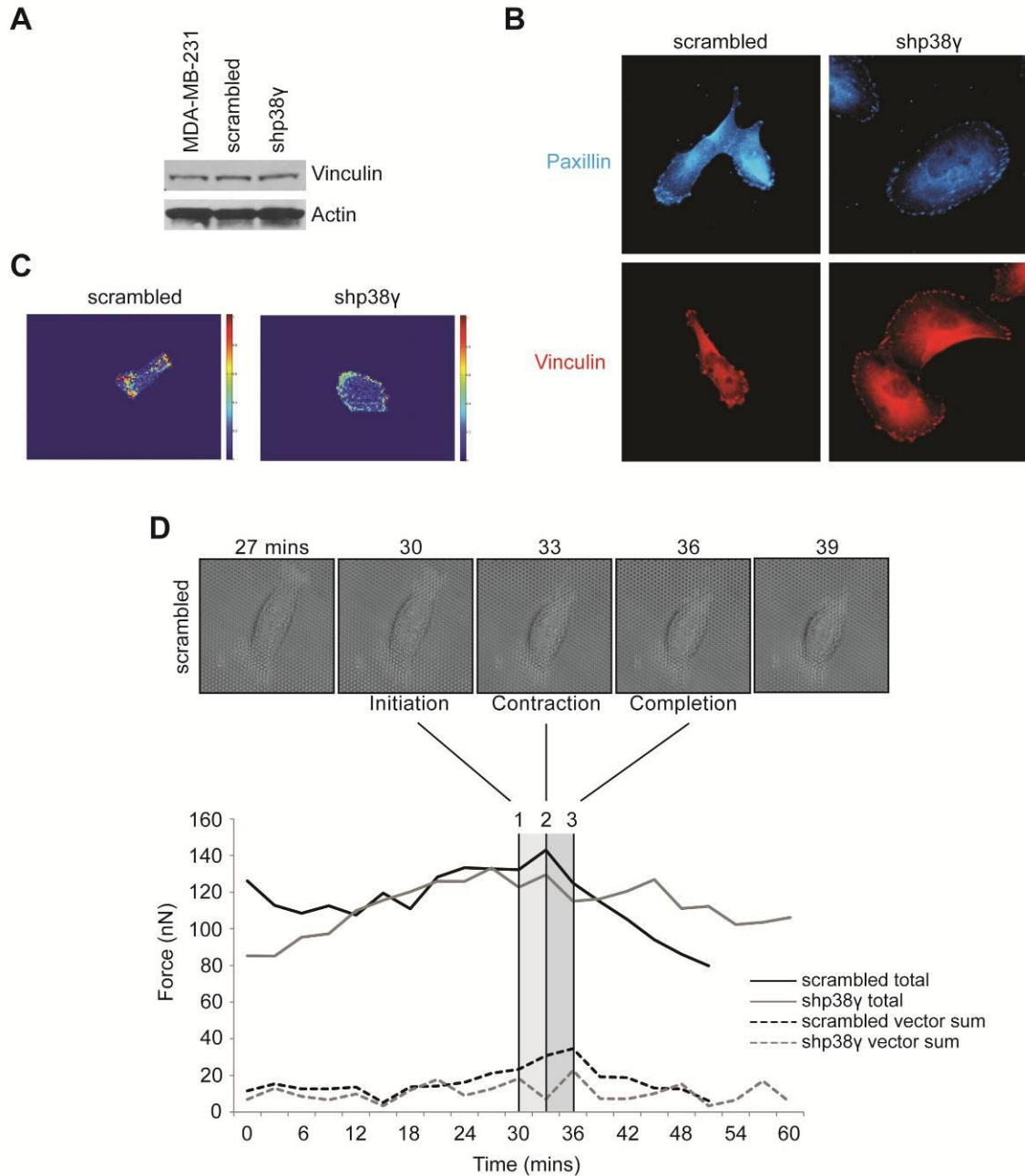
Figure 5.2 – Focal adhesions and traction forces differ between scrambled and shp38γ cells. (**A**) Total protein levels of the focal adhesion marker vinculin do not differ between scrambled and shp38γ cells, however focal adhesion distribution is significantly altered (**B**). (**C**) Traction force distribution generated by scrambled and shp38γ cells grown on mPADs mirrors focal adhesion distribution. (**D**) (top) Time lapse images of a scrambled cell on an mPAD undergoing a contractile event. The beginning and end of the contraction are labeled "Initiation" and "Completion", respectively. (bottom) Quantification of total (solid) and vector sum force (dashed) from time lapse images of both cell lines. Although both cell lines exert similar average force for both force measurements, shp38γ cells are

never able to exert the same maximum total force that scrambled cells reach during contraction (see point 2), suggesting that shp38γ cells cannot generate sufficient force to contract.

References

24. Charafe-Jauffret E, Ginestier C, Iovino F, Tarpin C, Diebel M, Esterni B, et al. Aldehyde dehydrogenase 1-positive cancer stem cells mediate metastasis and poor clinical outcome in inflammatory breast cancer. Clin Cancer Res. 2010;16:45-55.

25. Hermann PC, Huber SL, Herrler T, Aicher A, Ellwart JW, Guba M, et al. Distinct populations of cancer stem cells determine tumor growth and metastatic activity in human pancreatic cancer. Cell Stem Cell. 2007;1:313-23.

26. Pang R, Law WL, Chu AC, Poon JT, Lam CS, Chow AK, et al. A subpopulation of CD26+ cancer stem cells with metastatic capacity in human colorectal cancer. Cell Stem Cell. 2010;6:603-15.

31. Le Clainche C, Carlier MF. Regulation of actin assembly associated with protrusion and adhesion in cell migration. Physiol Rev. 2008;88:489-513.

40. Rosenthal DT, Brenner JC, Merajver SD. Rho Proteins in Cancer. In: van Golen KL, editor. The Rho GTPases in Cancer. New York: Springer New York; 2010. p. 29-42.

47. Wheeler AP, Ridley AJ. Why three Rho proteins? RhoA, RhoB, RhoC, and cell motility. Exp Cell Res. 2004;301:43-9.

48. Ridley AJ. The GTP-binding protein Rho. Int J Biochem Cell Biol. 1997;29:1225-9.

51. van Golen KL, Wu ZF, Qiao XT, Bao LW, Merajver SD. RhoC GTPase, a novel transforming oncogene for human mammary epithelial cells that partially recapitulates the inflammatory breast cancer phenotype. Cancer Res. 2000;60:5832-8.

52. Clark EA, Golub TR, Lander ES, Hynes RO. Genomic analysis of metastasis reveals an essential role for RhoC. Nature. 2000;406:532-5.

53. Ikoma T, Takahashi T, Nagano S, Li YM, Ohno Y, Ando K, et al. A definitive role of RhoC in metastasis of orthotopic lung cancer in mice. Clin Cancer Res. 2004;10:1192-200.

54. Islam M, Lin G, Brenner JC, Pan Q, Merajver SD, Hou Y, et al. RhoC expression and head and neck cancer metastasis. Mol Cancer Res. 2009;7:1771-80.

55. Hakem A, Sanchez-Sweatman O, You-Ten A, Duncan G, Wakeham A, Khokha R, et al. RhoC is dispensable for embryogenesis and tumor initiation but essential for metastasis. Genes Dev. 2005;19:1974-9.

57. Chang L, Karin M. Mammalian MAP kinase signalling cascades. Nature. 2001;410:37-40.

68. Sabio G, Arthur JS, Kuma Y, Peggie M, Carr J, Murray-Tait V, et al. p38gamma regulates the localisation of SAP97 in the cytoskeleton by modulating its interaction with GKAP. EMBO J. 2005;24:1134-45.

69. Gillespie MA, Le Grand F, Scime A, Kuang S, von Maltzahn J, Seale V, et al. p38-{gamma}-dependent gene silencing restricts entry into the myogenic differentiation program. J Cell Biol. 2009;187:991-1005.

71.   Tortorella LL, Lin CB, Pilch PF. ERK6 is expressed in a developmentally regulated manner in rodent skeletal muscle. Biochem Biophys Res Commun. 2003;306:163-8.

72.   Cuenda A, Cohen P. Stress-activated protein kinase-2/p38 and a rapamycin-sensitive pathway are required for C2C12 myogenesis. J Biol Chem. 1999;274:4341-6.

74.   Li Z, Jiang Y, Ulevitch RJ, Han J. The primary structure of p38 gamma: a new member of p38 group of MAP kinases. Biochem Biophys Res Commun. 1996;228:334-40.

79.   Loesch M, Chen G. The p38 MAPK stress pathway as a tumor suppressor or more? Front Biosci. 2008;13:3581-93.

85.   van Golen KL, Davies S, Wu ZF, Wang Y, Bucana CD, Root H, et al. A novel putative low-affinity insulin-like growth factor-binding protein, LIBC (lost in inflammatory breast cancer), and RhoC GTPase correlate with the inflammatory breast cancer phenotype. Clin Cancer Res. 1999;5:2511-9.

86.   Hanahan D, Weinberg RA. The hallmarks of cancer. Cell. 2000;100:57-70.

95.   van Golen KL, Wu ZF, Qiao XT, Bao L, Merajver SD. RhoC GTPase overexpression modulates induction of angiogenic factors in breast cells. Neoplasia. 2000;2:418-25.

135.   Kleer CG, Zhang Y, Pan Q, Gallagher G, Wu M, Wu ZF, et al. WISP3 and RhoC guanosine triphosphatase cooperate in the development of inflammatory breast cancer. Breast Cancer Res. 2004;6:R110-5.

136.   Xiao Y, Ye Y, Yearsley K, Jones S, Barsky SH. The lymphovascular embolus of inflammatory breast cancer expresses a stem cell-like phenotype. Am J Pathol. 2008;173:561-74.

137.   Debeb BG, Zhang X, Krishnamurthy S, Gao H, Cohen E, Li L, et al. Characterizing cancer cells with cancer stem cell-like features in 293T human embryonic kidney cells. Mol Cancer. 2010;9:180.

138.   Srivastava S, Ramdass B, Nagarajan S, Rehman M, Mukherjee G, Krishna S. Notch1 regulates the functional contribution of RhoC to cervical carcinoma progression. Br J Cancer. 2010;102:196-205.

139.   Dontu G, Abdallah WM, Foley JM, Jackson KW, Clarke MF, Kawamura MJ, et al. In vitro propagation and transcriptional profiling of human mammary stem/progenitor cells. Genes Dev. 2003;17:1253-70.

140.   Fearon ER, Vogelstein B. A genetic model for colorectal tumorigenesis. Cell. 1990;61:759-67.

141.   Remy G, Risco AM, Inesta-Vaquera FA, Gonzalez-Teran B, Sabio G, Davis RJ, et al. Differential activation of p38MAPK isoforms by MKK6 and MKK3. Cell Signal. 2010;22:660-7.

142.   Balaban NQ, Schwarz US, Riveline D, Goichberg P, Tzur G, Sabanay I, et al. Force and focal adhesion assembly: a close relationship studied using elastic micropatterned substrates. Nat Cell Biol. 2001;3:466-72.

143.   Fu J, Wang YK, Yang MT, Desai RA, Yu X, Liu Z, et al. Mechanical regulation of cell function with geometrically modulated elastomeric substrates. Nat Methods. 2010;7:733-6.

144.   Ong SE, Blagoev B, Kratchmarova I, Kristensen DB, Steen H, Pandey A, et al. Stable isotope labeling by amino acids in cell culture, SILAC, as a simple and accurate approach to expression proteomics. Mol Cell Proteomics. 2002;1:376-86.

145.   Thingholm TE, Jorgensen TJ, Jensen ON, Larsen MR. Highly selective enrichment of phosphorylated peptides using titanium dioxide. Nat Protoc. 2006;1:1929-35.

146.   Meng F, Zhang H, Liu G, Kreike B, Chen W, Sethi S, et al. p38gamma Mitogen-Activated Protein Kinase Contributes to Oncogenic Properties Maintenance and Resistance to Poly (ADP-Ribose)-Polymerase-1 Inhibition in Breast Cancer. Neoplasia. 2011;13:472-82.

147.   Turner NC, Lord CJ, Iorns E, Brough R, Swift S, Elliott R, et al. A synthetic lethal siRNA screen identifying genes mediating sensitivity to a PARP inhibitor. EMBO J. 2008;27:1368-77.

148.   Zhang J, Shen B, Lin A. Novel strategies for inhibition of the p38 MAPK pathway. Trends Pharmacol Sci. 2007;28:286-95.

149.   O'Keefe SJ, Mudgett JS, Cupo S, Parsons JN, Chartrain NA, Fitzgerald C, et al. Chemical genetics define the roles of p38alpha and p38beta in acute and chronic inflammation. J Biol Chem. 2007;282:34663-71.

150.   Kuma Y, Sabio G, Bain J, Shpiro N, Marquez R, Cuenda A. BIRB796 inhibits all p38 MAPK isoforms in vitro and in vivo. J Biol Chem. 2005;280:19472-9.

Full Reference List

1.   Howlader N NA, Krapcho M, Neyman N, Aminou R, Waldron W, Altekruse SF, Kosary CL, Ruhl J, Tatalovich Z, Cho H, Mariotto A, Eisner MP, Lewis DR, Chen HS, Feuer EJ, Cronin KA, Edwards BK. SEER Cancer Statistics Review, 1975-2008. Bethesda, MD: National Cancer Institute; 2011.
2.   Pandey PR, Saidou J, Watabe K. Role of myoepithelial cells in breast tumor progression. Front Biosci. 2010;15:226-36.
3.   Polyak K, Hu M. Do myoepithelial cells hold the key for breast tumor progression? J Mammary Gland Biol Neoplasia. 2005;10:231-47.
4.   Martin GR, Timpl R. Laminin and other basement membrane components. Annu Rev Cell Biol. 1987;3:57-85.
5.   Wiseman BS, Werb Z. Stromal effects on mammary gland development and breast cancer. Science. 2002;296:1046-9.
6.   Condeelis J, Pollard JW. Macrophages: obligate partners for tumor cell migration, invasion, and metastasis. Cell. 2006;124:263-6.
7.   Bockhorn M, Jain RK, Munn LL. Active versus passive mechanisms in metastasis: do cancer cells crawl into vessels, or are they pushed? Lancet Oncol. 2007;8:444-8.
8.   Racila E, Euhus D, Weiss AJ, Rao C, McConnell J, Terstappen LW, et al. Detection and characterization of carcinoma cells in the blood. Proc Natl Acad Sci U S A. 1998;95:4589-94.
9.   Gaforio JJ, Serrano MJ, Sanchez-Rovira P, Sirvent A, Delgado-Rodriguez M, Campos M, et al. Detection of breast cancer cells in the peripheral blood is positively correlated with estrogen-receptor status and predicts for poor prognosis. Int J Cancer. 2003;107:984-90.
10.   Cristofanilli M, Budd GT, Ellis MJ, Stopeck A, Matera J, Miller MC, et al. Circulating tumor cells, disease progression, and survival in metastatic breast cancer. N Engl J Med. 2004;351:781-91.
11.   Yang J, Weinberg RA. Epithelial-mesenchymal transition: at the crossroads of development and tumor metastasis. Dev Cell. 2008;14:818-29.
12.   Thiery JP, Acloque H, Huang RY, Nieto MA. Epithelial-mesenchymal transitions in development and disease. Cell. 2009;139:871-90.
13.   Thiery JP. Epithelial-mesenchymal transitions in tumour progression. Nat Rev Cancer. 2002;2:442-54.
14.   Lee JM, Dedhar S, Kalluri R, Thompson EW. The epithelial-mesenchymal transition: new insights in signaling, development, and disease. J Cell Biol. 2006;172:973-81.
15.   Yang J, Mani SA, Donaher JL, Ramaswamy S, Itzykson RA, Come C, et al. Twist, a master regulator of morphogenesis, plays an essential role in tumor metastasis. Cell. 2004;117:927-39.
16.   Perou CM, Sorlie T, Eisen MB, van de Rijn M, Jeffrey SS, Rees CA, et al. Molecular portraits of human breast tumours. Nature. 2000;406:747-52.
17.   Al-Hajj M, Wicha MS, Benito-Hernandez A, Morrison SJ, Clarke MF. Prospective identification of tumorigenic breast cancer cells. Proc Natl Acad Sci U S A. 2003;100:3983-8.

18.   Ginestier C, Hur MH, Charafe-Jauffret E, Monville F, Dutcher J, Brown M, et al. ALDH1 is a marker of normal and malignant human mammary stem cells and a predictor of poor clinical outcome. Cell Stem Cell. 2007;1:555-67.

19.   Dean M, Fojo T, Bates S. Tumour stem cells and drug resistance. Nat Rev Cancer. 2005;5:275-84.

20.   McDermott SP, Wicha MS. Targeting breast cancer stem cells. Mol Oncol. 2010;4:404-19.

21.   Mani SA, Guo W, Liao MJ, Eaton EN, Ayyanan A, Zhou AY, et al. The epithelial-mesenchymal transition generates cells with properties of stem cells. Cell. 2008;133:704-15.

22.   Liu R, Wang X, Chen GY, Dalerba P, Gurney A, Hoey T, et al. The prognostic role of a gene signature from tumorigenic breast-cancer cells. N Engl J Med. 2007;356:217-26.

23.   Liu H, Patel MR, Prescher JA, Patsialou A, Qian D, Lin J, et al. Cancer stem cells from human breast tumors are involved in spontaneous metastases in orthotopic mouse models. Proc Natl Acad Sci U S A. 2010;107:18115-20.

24.   Charafe-Jauffret E, Ginestier C, Iovino F, Tarpin C, Diebel M, Esterni B, et al. Aldehyde dehydrogenase 1-positive cancer stem cells mediate metastasis and poor clinical outcome in inflammatory breast cancer. Clin Cancer Res. 2010;16:45-55.

25.   Hermann PC, Huber SL, Herrler T, Aicher A, Ellwart JW, Guba M, et al. Distinct populations of cancer stem cells determine tumor growth and metastatic activity in human pancreatic cancer. Cell Stem Cell. 2007;1:313-23.

26.   Pang R, Law WL, Chu AC, Poon JT, Lam CS, Chow AK, et al. A subpopulation of CD26+ cancer stem cells with metastatic capacity in human colorectal cancer. Cell Stem Cell. 2010;6:603-15.

27.   Lewis AK, Bridgman PC. Nerve growth cone lamellipodia contain two populations of actin filaments that differ in organization and polarity. J Cell Biol. 1992;119:1219-43.

28.   Machesky LM. Lamellipodia and filopodia in metastasis and invasion. FEBS Lett. 2008;582:2102-11.

29.   Ponti A, Machacek M, Gupton SL, Waterman-Storer CM, Danuser G. Two distinct actin networks drive the protrusion of migrating cells. Science. 2004;305:1782-6.

30.   Gupton SL, Anderson KL, Kole TP, Fischer RS, Ponti A, Hitchcock-DeGregori SE, et al. Cell migration without a lamellipodium: translation of actin dynamics into cell movement mediated by tropomyosin. J Cell Biol. 2005;168:619-31.

31.   Le Clainche C, Carlier MF. Regulation of actin assembly associated with protrusion and adhesion in cell migration. Physiol Rev. 2008;88:489-513.

32.   Zamir E, Geiger B. Components of cell-matrix adhesions. J Cell Sci. 2001;114:3577-9.

33.   Burridge K, Fath K, Kelly T, Nuckolls G, Turner C. Focal adhesions: transmembrane junctions between the extracellular matrix and the cytoskeleton. Annu Rev Cell Biol. 1988;4:487-525.

34.   Burridge K, Chrzanowska-Wodnicka M. Focal adhesions, contractility, and signaling. Annu Rev Cell Dev Biol. 1996;12:463-518.

35.   Webb DJ, Parsons JT, Horwitz AF. Adhesion assembly, disassembly and turnover in migrating cells -- over and over and over again. Nat Cell Biol. 2002;4:E97-100.

36.   Ezratty EJ, Partridge MA, Gundersen GG. Microtubule-induced focal adhesion disassembly is mediated by dynamin and focal adhesion kinase. Nat Cell Biol. 2005;7:581-90.

37.   Ridley AJ, Schwartz MA, Burridge K, Firtel RA, Ginsberg MH, Borisy G, et al. Cell migration: integrating signals from front to back. Science. 2003;302:1704-9.

38.   Lauffenburger DA, Horwitz AF. Cell migration: a physically integrated molecular process. Cell. 1996;84:359-69.

39.   Ridley AJ. Rho GTPases and cell migration. J Cell Sci. 2001;114:2713-22.

40.   Rosenthal DT, Brenner JC, Merajver SD. Rho Proteins in Cancer. In: van Golen KL, editor. The Rho GTPases in Cancer. New York: Springer New York; 2010. p. 29-42.

41.   Ridley AJ, Paterson HF, Johnston CL, Diekmann D, Hall A. The small GTP-binding protein rac regulates growth factor-induced membrane ruffling. Cell. 1992;70:401-10.

42.   Ridley AJ, Hall A. The small GTP-binding protein rho regulates the assembly of focal adhesions and actin stress fibers in response to growth factors. Cell. 1992;70:389-99.

43.   Chimini G, Chavrier P. Function of Rho family proteins in actin dynamics during phagocytosis and engulfment. Nat Cell Biol. 2000;2:E191-6.

44.   Etienne-Manneville S, Hall A. Rho GTPases in cell biology. Nature. 2002;420:629-35.

45.   Evers EE, Zondag GC, Malliri A, Price LS, ten Klooster JP, van der Kammen RA, et al. Rho family proteins in cell adhesion and cell migration. Eur J Cancer. 2000;36:1269-74.

46.   Raftopoulou M, Hall A. Cell migration: Rho GTPases lead the way. Dev Biol. 2004;265:23-32.

47.   Wheeler AP, Ridley AJ. Why three Rho proteins? RhoA, RhoB, RhoC, and cell motility. Exp Cell Res. 2004;301:43-9.

48.   Ridley AJ. The GTP-binding protein Rho. Int J Biochem Cell Biol. 1997;29:1225-9.

49.   Wu M, Wu ZF, Rosenthal DT, Rhee EM, Merajver SD. Characterization of the roles of RhoC and RhoA GTPases in invasion, motility, and matrix adhesion in inflammatory and aggressive breast cancers. Cancer. 2010;116:2768-82.

50.   Bellovin DI, Simpson KJ, Danilov T, Maynard E, Rimm DL, Oettgen P, et al. Reciprocal regulation of RhoA and RhoC characterizes the EMT and identifies RhoC as a prognostic marker of colon carcinoma. Oncogene. 2006;25:6959-67.

51.   van Golen KL, Wu ZF, Qiao XT, Bao LW, Merajver SD. RhoC GTPase, a novel transforming oncogene for human mammary epithelial cells that partially recapitulates the inflammatory breast cancer phenotype. Cancer Res. 2000;60:5832-8.

52.   Clark EA, Golub TR, Lander ES, Hynes RO. Genomic analysis of metastasis reveals an essential role for RhoC. Nature. 2000;406:532-5.

53.   Ikoma T, Takahashi T, Nagano S, Li YM, Ohno Y, Ando K, et al. A definitive role of RhoC in metastasis of orthotopic lung cancer in mice. Clin Cancer Res. 2004;10:1192-200.

54.   Islam M, Lin G, Brenner JC, Pan Q, Merajver SD, Hou Y, et al. RhoC expression and head and neck cancer metastasis. Mol Cancer Res. 2009;7:1771-80.

55.   Hakem A, Sanchez-Sweatman O, You-Ten A, Duncan G, Wakeham A, Khokha R, et al. RhoC is dispensable for embryogenesis and tumor initiation but essential for metastasis. Genes Dev. 2005;19:1974-9.

56.   van Golen KL, Bao LW, Pan Q, Miller FR, Wu ZF, Merajver SD. Mitogen activated protein kinase pathway is involved in RhoC GTPase induced motility, invasion and angiogenesis in inflammatory breast cancer. Clin Exp Metastasis. 2002;19:301-11.

57.   Chang L, Karin M. Mammalian MAP kinase signalling cascades. Nature. 2001;410:37-40.

58.   Raman M, Chen W, Cobb MH. Differential regulation and properties of MAPKs. Oncogene. 2007;26:3100-12.

59.   Wagner EF, Nebreda AR. Signal integration by JNK and p38 MAPK pathways in cancer development. Nat Rev Cancer. 2009;9:537-49.

60.   Cuenda A, Rousseau S. p38 MAP-kinases pathway regulation, function and role in human diseases. Biochim Biophys Acta. 2007;1773:1358-75.

61.   Wang Y, Huang S, Sah VP, Ross J, Jr., Brown JH, Han J, et al. Cardiac muscle cell hypertrophy and apoptosis induced by distinct members of the p38 mitogen-activated protein kinase family. J Biol Chem. 1998;273:2161-8.

62.   Platanias LC. Map kinase signaling pathways and hematologic malignancies. Blood. 2003;101:4667-79.

63.   Qi X, Pohl NM, Loesch M, Hou S, Li R, Qin JZ, et al. p38alpha antagonizes p38gamma activity through c-Jun-dependent ubiquitin-proteasome pathways in regulating Ras transformation and stress response. J Biol Chem. 2007;282:31398-408.

64.   English JM, Cobb MH. Pharmacological inhibitors of MAPK pathways. Trends Pharmacol Sci. 2002;23:40-5.

65.   Schindler EM, Hindes A, Gribben EL, Burns CJ, Yin Y, Lin MH, et al. p38delta Mitogen-activated protein kinase is essential for skin tumor development in mice. Cancer Res. 2009;69:4648-55.

66.   Junttila MR, Ala-Aho R, Jokilehto T, Peltonen J, Kallajoki M, Grenman R, et al. p38alpha and p38delta mitogen-activated protein kinase isoforms regulate invasion and growth of head and neck squamous carcinoma cells. Oncogene. 2007;26:5267-79.

67.   Efimova T. p38delta mitogen-activated protein kinase regulates skin homeostasis and tumorigenesis. Cell Cycle. 2010;9:498-05.

68.   Sabio G, Arthur JS, Kuma Y, Peggie M, Carr J, Murray-Tait V, et al. p38gamma regulates the localisation of SAP97 in the cytoskeleton by modulating its interaction with GKAP. EMBO J. 2005;24:1134-45.

69.   Gillespie MA, Le Grand F, Scime A, Kuang S, von Maltzahn J, Seale V, et al. p38-{gamma}-dependent gene silencing restricts entry into the myogenic differentiation program. J Cell Biol. 2009;187:991-1005.

70.   Cuenda A, Cohen P, Buee-Scherrer V, Goedert M. Activation of stress-activated protein kinase-3 (SAPK3) by cytokines and cellular stresses is mediated via SAPKK3 (MKK6); comparison of the specificities of SAPK3 and SAPK2 (RK/p38). EMBO J. 1997;16:295-305.

71.   Tortorella LL, Lin CB, Pilch PF. ERK6 is expressed in a developmentally regulated manner in rodent skeletal muscle. Biochem Biophys Res Commun. 2003;306:163-8.

72.   Cuenda A, Cohen P. Stress-activated protein kinase-2/p38 and a rapamycin-sensitive pathway are required for C2C12 myogenesis. J Biol Chem. 1999;274:4341-6.

73.   Wang XS, Diener K, Manthey CL, Wang S, Rosenzweig B, Bray J, et al. Molecular cloning and characterization of a novel p38 mitogen-activated protein kinase. J Biol Chem. 1997;272:23668-74.

74.   Li Z, Jiang Y, Ulevitch RJ, Han J. The primary structure of p38 gamma: a new member of p38 group of MAP kinases. Biochem Biophys Res Commun. 1996;228:334-40.

75.   Sabio G, Reuver S, Feijoo C, Hasegawa M, Thomas GM, Centeno F, et al. Stress- and mitogen-induced phosphorylation of the synapse-associated protein SAP90/PSD-95 by activation of SAPK3/p38gamma and ERK1/ERK2. Biochem J. 2004;380:19-30.

76.   Sabio G, Cerezo-Guisado MI, Del Reino P, Inesta-Vaquera FA, Rousseau S, Arthur JS, et al. p38gamma regulates interaction of nuclear PSF and RNA with the tumour-suppressor hDlg in response to osmotic shock. J Cell Sci. 2010;123:2596-604.

77.   Hasegawa M, Cuenda A, Spillantini MG, Thomas GM, Buee-Scherrer V, Cohen P, et al. Stress-activated protein kinase-3 interacts with the PDZ domain of alpha1-syntrophin. A mechanism for specific substrate recognition. J Biol Chem. 1999;274:12626-31.

78.   Tang J, Qi X, Mercola D, Han J, Chen G. Essential role of p38gamma in K-Ras transformation independent of phosphorylation. J Biol Chem. 2005;280:23910-7.

79.   Loesch M, Chen G. The p38 MAPK stress pathway as a tumor suppressor or more? Front Biosci. 2008;13:3581-93.

80.   Hou SW, Zhi HY, Pohl N, Loesch M, Qi XM, Li RS, et al. PTPH1 dephosphorylates and cooperates with p38gamma MAPK to increase ras oncogenesis through PDZ-mediated interaction. Cancer Res. 2010;70:2901-10.

81.   Qi X, Tang J, Loesch M, Pohl N, Alkan S, Chen G. p38gamma mitogen-activated protein kinase integrates signaling crosstalk between Ras and estrogen receptor to increase breast cancer invasion. Cancer Res. 2006;66:7540-7.

82.   Loesch M, Zhi HY, Hou SW, Qi XM, Li RS, Basir Z, et al. p38{gamma} MAPK cooperates with c-Jun in trans-activating matrix metalloproteinase 9. J Biol Chem. 2010.

83.   Reya T, Morrison SJ, Clarke MF, Weissman IL. Stem cells, cancer, and cancer stem cells. Nature. 2001;414:105-11.

84.   Clevers H. The cancer stem cell: premises, promises and challenges. Nat Med. 2011;17:313-9.

85.   van Golen KL, Davies S, Wu ZF, Wang Y, Bucana CD, Root H, et al. A novel putative low-affinity insulin-like growth factor-binding protein, LIBC (lost in inflammatory breast cancer), and RhoC GTPase correlate with the inflammatory breast cancer phenotype. Clin Cancer Res. 1999;5:2511-9.

86.   Hanahan D, Weinberg RA. The hallmarks of cancer. Cell. 2000;100:57-70.

87.   Dietrich KA, Schwarz R, Liska M, Grass S, Menke A, Meister M, et al. Specific induction of migration and invasion of pancreatic carcinoma cells by RhoC, which differs from RhoA in its localisation and activity. Biol Chem. 2009;390:1063-77.

88.   Debnath J, Brugge JS. Modelling glandular epithelial cancers in three-dimensional cultures. Nat Rev Cancer. 2005;5:675-88.

89.   Lee GY, Kenny PA, Lee EH, Bissell MJ. Three-dimensional culture models of normal and malignant breast epithelial cells. Nat Methods. 2007;4:359-65.

90.   Kenny PA, Lee GY, Myers CA, Neve RM, Semeiks JR, Spellman PT, et al. The morphologies of breast cancer cell lines in three-dimensional assays correlate with their profiles of gene expression. Mol Oncol. 2007;1:84-96.

91.   Singh SK, Clarke ID, Terasaki M, Bonn VE, Hawkins C, Squire J, et al. Identification of a cancer stem cell in human brain tumors. Cancer Res. 2003;63:5821-8.

92.   Collins AT, Berry PA, Hyde C, Stower MJ, Maitland NJ. Prospective identification of tumorigenic prostate cancer stem cells. Cancer Res. 2005;65:10946-51.

93.   Korkaya H, Paulson A, Iovino F, Wicha MS. HER2 regulates the mammary stem/progenitor cell population driving tumorigenesis and invasion. Oncogene. 2008;27:6120-30.

94.   Kleer CG, Griffith KA, Sabel MS, Gallagher G, van Golen KL, Wu ZF, et al. RhoC-GTPase is a novel tissue biomarker associated with biologically aggressive carcinomas of the breast. Breast Cancer Res Treat. 2005;93:101-10.

95.   van Golen KL, Wu ZF, Qiao XT, Bao L, Merajver SD. RhoC GTPase overexpression modulates induction of angiogenic factors in breast cells. Neoplasia. 2000;2:418-25.

96.   Gupta PB, Onder TT, Jiang G, Tao K, Kuperwasser C, Weinberg RA, et al. Identification of selective inhibitors of cancer stem cells by high-throughput screening. Cell. 2009;138:645-59.

97.   Abramoff MD, Magelhaes PJ, Ram SJ. Image Processing with ImageJ. Biophotonics International. 2004;11:36-42.

98.   Nocito A, Kononen J, Kallioniemi OP, Sauter G. Tissue microarrays (TMAs) for high-throughput molecular pathology research. Int J Cancer. 2001;94:1-5.

99.   McCabe A, Dolled-Filhart M, Camp RL, Rimm DL. Automated quantitative analysis (AQUA) of in situ protein expression, antibody concentration, and prognosis. J Natl Cancer Inst. 2005;97:1808-15.

100. Burstein HJ, Polyak K, Wong JS, Lester SC, Kaelin CM. Ductal carcinoma in situ of the breast. N Engl J Med. 2004;350:1430-41.

101. Cohen P. The search for physiological substrates of MAP and SAP kinases in mammalian cells. Trends Cell Biol. 1997;7:353-61.

102. Enslen H, Raingeaud J, Davis RJ. Selective activation of p38 mitogen-activated protein (MAP) kinase isoforms by the MAP kinase kinases MKK3 and MKK6. J Biol Chem. 1998;273:1741-8.

103. Ladwein M, Rottner K. On the Rho'd: the regulation of membrane protrusions by Rho-GTPases. FEBS Lett. 2008;582:2066-74.

104. Rajah TT, Abidi SM, Rambo DJ, Dmytryk JJ, Pento JT. The motile behavior of human breast cancer cells characterized by time-lapse videomicroscopy. In Vitro Cell Dev Biol Anim. 1998;34:626-8.

105. Partin AW, Schoeniger JS, Mohler JL, Coffey DS. Fourier analysis of cell motility: correlation of motility with metastatic potential. Proc Natl Acad Sci U S A. 1989;86:1254-8.

106. Nobes CD, Hall A. Rho, rac, and cdc42 GTPases regulate the assembly of multimolecular focal complexes associated with actin stress fibers, lamellipodia, and filopodia. Cell. 1995;81:53-62.

107. Nielsen TO, Parker JS, Leung S, Voduc D, Ebbert M, Vickery T, et al. A comparison of PAM50 intrinsic subtyping with immunohistochemistry and clinical prognostic factors in tamoxifen-treated estrogen receptor-positive breast cancer. Clin Cancer Res. 2010;16:5222-32.

108. Simon C, Goepfert H, Boyd D. Inhibition of the p38 mitogen-activated protein kinase by SB 203580 blocks PMA-induced Mr 92,000 type IV collagenase secretion and in vitro invasion. Cancer Res. 1998;58:1135-9.

109. Chen L, Mayer JA, Krisko TI, Speers CW, Wang T, Hilsenbeck SG, et al. Inhibition of the p38 kinase suppresses the proliferation of human ER-negative breast cancer cells. Cancer Res. 2009;69:8853-61.

110. Cano A, Perez-Moreno MA, Rodrigo I, Locascio A, Blanco MJ, del Barrio MG, et al. The transcription factor snail controls epithelial-mesenchymal transitions by repressing E-cadherin expression. Nat Cell Biol. 2000;2:76-83.

111. Chiang AC, Massague J. Molecular basis of metastasis. N Engl J Med. 2008;359:2814-23.

112. Rosenthal DT, Iyer H, Escudero SE, Wu Z, Bao L, Garcia H, et al. Computational mechanical modeling reveals the role of p38γ in shaping the cytoskeleton and controlling locomotion of aggressive breast cancer cells. Cancer Research. 2011;Concurrent Submission.

113. Wu M, Wu ZF, Merajver SD. Rho proteins and cell-matrix interactions in cancer. Cells Tissues Organs. 2007;185:100-3.

114. Nethe M, Hordijk PL. The role of ubiquitylation and degradation in RhoGTPase signalling. J Cell Sci. 2010;123:4011-8.

115. Kleer CG, van Golen KL, Zhang Y, Wu ZF, Rubin MA, Merajver SD. Characterization of RhoC expression in benign and malignant breast disease: a potential new marker for small breast carcinomas with metastatic ability. Am J Pathol. 2002;160:579-84.

116.	Weinberg RA. The Biology of Cancer. 1 ed. New York, NY: Garland Science; 2007.

117.	Thiery JP. Epithelial-mesenchymal transitions in development and pathologies. Curr Opin Cell Biol. 2003;15:740-6.

118.	Rosenthal DT, Escudero SE, Bao L, Wu Z, Merajver SD. p38γ drives breast cancer cell motility and metastasis through regulation of RhoC GTPase. Cancer Research. 2011;Concurrent Submission.

119.	Phillips R, Kondev J, Theriot J. Physical biology of the cell. New York: Garland Science; 2009.

120.	Barnhart EL, Allen GM, Julicher F, Theriot JA. Bipedal locomotion in crawling cells. Biophys J. 2010;98:933-42.

121.	Ehrengruber MU, Coates TD, Deranleau DA. Shape oscillations: a fundamental response of human neutrophils stimulated by chemotactic peptides? FEBS Lett. 1995;359:229-32.

122.	Mogilner A. On the edge: modeling protrusion. Curr Opin Cell Biol. 2006;18:32-9.

123.	Peskin CS, Odell GM, Oster GF. Cellular motions and thermal fluctuations: the Brownian ratchet. Biophys J. 1993;65:316-24.

124.	Mogilner A, Oster G. Force generation by actin polymerization II: the elastic ratchet and tethered filaments. Biophys J. 2003;84:1591-605.

125.	Dickinson RB, Caro L, Purich DL. Force generation by cytoskeletal filament end-tracking proteins. Biophys J. 2004;87:2838-54.

126.	Dickinson RB, Purich DL. Clamped-filament elongation model for actin-based motors. Biophys J. 2002;82:605-17.

127.	Plastino J, Sykes C. The actin slingshot. Curr Opin Cell Biol. 2005;17:62-6.

128.	Gerbal F, Chaikin P, Rabin Y, Prost J. An elastic analysis of Listeria monocytogenes propulsion. Biophys J. 2000;79:2259-75.

129.	Bernheim-Groswasser A, Prost J, Sykes C. Mechanism of actin-based motility: a dynamic state diagram. Biophys J. 2005;89:1411-9.

130.	Del Alamo JC, Meili R, Alonso-Latorre B, Rodriguez-Rodriguez J, Aliseda A, Firtel RA, et al. Spatio-temporal analysis of eukaryotic cell motility by improved force cytometry. Proc Natl Acad Sci U S A. 2007;104:13343-8.

131.	Timoshenko S, Goodier J. Theory of Elasticity. New York: McGraw-Hill; 1951.

132.	Hughes TJR. Linear Static and Dynamic Finite Element Analysis Mineola, NY: Dover Publications; 2000.

133.	Svitkina TM, Verkhovsky AB, McQuade KM, Borisy GG. Analysis of the actin-myosin II system in fish epidermal keratocytes: mechanism of cell body translocation. J Cell Biol. 1997;139:397-415.

134.	Pollard TD, Cooper JA. Actin, a central player in cell shape and movement. Science. 2009;326:1208-12.

135.	Kleer CG, Zhang Y, Pan Q, Gallagher G, Wu M, Wu ZF, et al. WISP3 and RhoC guanosine triphosphatase cooperate in the development of inflammatory breast cancer. Breast Cancer Res. 2004;6:R110-5.

136. Xiao Y, Ye Y, Yearsley K, Jones S, Barsky SH. The lymphovascular embolus of inflammatory breast cancer expresses a stem cell-like phenotype. Am J Pathol. 2008;173:561-74.

137. Debeb BG, Zhang X, Krishnamurthy S, Gao H, Cohen E, Li L, et al. Characterizing cancer cells with cancer stem cell-like features in 293T human embryonic kidney cells. Mol Cancer. 2010;9:180.

138. Srivastava S, Ramdass B, Nagarajan S, Rehman M, Mukherjee G, Krishna S. Notch1 regulates the functional contribution of RhoC to cervical carcinoma progression. Br J Cancer. 2010;102:196-205.

139. Dontu G, Abdallah WM, Foley JM, Jackson KW, Clarke MF, Kawamura MJ, et al. In vitro propagation and transcriptional profiling of human mammary stem/progenitor cells. Genes Dev. 2003;17:1253-70.

140. Fearon ER, Vogelstein B. A genetic model for colorectal tumorigenesis. Cell. 1990;61:759-67.

141. Remy G, Risco AM, Inesta-Vaquera FA, Gonzalez-Teran B, Sabio G, Davis RJ, et al. Differential activation of p38MAPK isoforms by MKK6 and MKK3. Cell Signal. 2010;22:660-7.

142. Balaban NQ, Schwarz US, Riveline D, Goichberg P, Tzur G, Sabanay I, et al. Force and focal adhesion assembly: a close relationship studied using elastic micropatterned substrates. Nat Cell Biol. 2001;3:466-72.

143. Fu J, Wang YK, Yang MT, Desai RA, Yu X, Liu Z, et al. Mechanical regulation of cell function with geometrically modulated elastomeric substrates. Nat Methods. 2010;7:733-6.

144. Ong SE, Blagoev B, Kratchmarova I, Kristensen DB, Steen H, Pandey A, et al. Stable isotope labeling by amino acids in cell culture, SILAC, as a simple and accurate approach to expression proteomics. Mol Cell Proteomics. 2002;1:376-86.

145. Thingholm TE, Jorgensen TJ, Jensen ON, Larsen MR. Highly selective enrichment of phosphorylated peptides using titanium dioxide. Nat Protoc. 2006;1:1929-35.

146. Meng F, Zhang H, Liu G, Kreike B, Chen W, Sethi S, et al. p38gamma Mitogen-Activated Protein Kinase Contributes to Oncogenic Properties Maintenance and Resistance to Poly (ADP-Ribose)-Polymerase-1 Inhibition in Breast Cancer. Neoplasia. 2011;13:472-82.

147. Turner NC, Lord CJ, Iorns E, Brough R, Swift S, Elliott R, et al. A synthetic lethal siRNA screen identifying genes mediating sensitivity to a PARP inhibitor. EMBO J. 2008;27:1368-77.

148. Zhang J, Shen B, Lin A. Novel strategies for inhibition of the p38 MAPK pathway. Trends Pharmacol Sci. 2007;28:286-95.

149. O'Keefe SJ, Mudgett JS, Cupo S, Parsons JN, Chartrain NA, Fitzgerald C, et al. Chemical genetics define the roles of p38alpha and p38beta in acute and chronic inflammation. J Biol Chem. 2007;282:34663-71.

150. Kuma Y, Sabio G, Bain J, Shpiro N, Marquez R, Cuenda A. BIRB796 inhibits all p38 MAPK isoforms in vitro and in vivo. J Biol Chem. 2005;280:19472-9.